

# DYNAMIC BEHAVIOR OF MULTI-LEGGED PINNED AND RIGID STRUCTURAL JOINTS

by

Ronald L. Frink

Bachelor of Science Ocean Engineering  
Florida Institute of Technology (1984)

Submitted to the Department of Ocean Engineering  
in Partial Fulfillment of the Requirements  
for the Degrees of

MASTER OF SCIENCE  
IN OCEAN ENGINEERING

and

MASTER OF SCIENCE  
IN MECHANICAL ENGINEERING

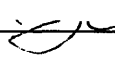
at the

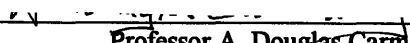
MASSACHUSETTS INSTITUTE OF TECHNOLOGY  
August, 1995

© Massachusetts Institute of Technology 1995. All rights reserved.

Signature of Author   
Department of Ocean Engineering  
August, 1995

Certified by   
Assistant Professor J. Robert Fricke  
Department of Ocean Engineering, Thesis Supervisor

Certified by   
Assistant Professor Zaichun Feng  
Department of Mechanical Engineering, Thesis Reader

Accepted by   
MASSACHUSETTS INSTITUTE OF TECHNOLOGY  
Professor A. Douglas Carmichael, Chairman  
Department Graduate Committee, Department of Ocean Engineering

FEB 20 1997

LIBRARIES

# **DYNAMIC BEHAVIOR OF MULTI-LEGGED PINNED AND RIGID STRUCTURAL JOINTS**

by

Ronald L. Frink

Submitted to the Department of Ocean Engineering on August 1, 1995  
in partial fulfillment of the requirements for the degrees of  
Master of Science in Ocean Engineering  
and Master of Science in Mechanical Engineering

## **Abstract**

The objective of this thesis is to explore the dynamic response of three-legged structural joints to longitudinal impulse excitation. Three joints have been analyzed in the experimentation. One joint is pinned with spherical male legs whose surfaces are coated with Teflon. The spherical male legs of the second pinned-joint are coated with a visco-elastic interface. The third joint is rigid. The intent of the Teflon-coated joint is to model a frictionless pinned-joint and the intent of the joint with the visco-elastic interface is to gain insight into joint damping behavior.

A scattering matrix whose elements are transfer functions is introduced to assist in understanding wave type coupling that occurs when an incident longitudinal wave scatters at each joint. Reciprocity has been used to determine other scattering matrix elements that could not be determined directly from experimentation. The experimental data has then been compared to analytical solutions from two-dimensional models; a two-dimensional analytical solution was used since generalized three-dimensional analytical solutions are not available.

The rigid joint exhibited relatively high levels of transmission for each wave type. Average transmission efficiency ranged between -7 to -34 dB. The rigid joint exhibited significant longitudinal transmission. The predicted transmission efficiency was, on the average, 30 dB lower than the experimental results. Three mechanisms are proposed which explain the failure of the analytical model to accurately predict the transmission efficiency. The Teflon-coated spherical pinned-joint offered significant transmission reduction when compared to the rigid joint. It is only for narrow frequency bands and for few wave types where the rigid joint exhibits lower levels of transmission when compared to the Teflon-coated spherical pinned-joint. The spherical pinned-joint with the visco-elastic interface offered minimal overall transmission for all wave types. It is only for very narrow frequency bands and few wave types where either the rigid joint or the Teflon-coated joint exhibited lower levels of transmission. Flexural-to-longitudinal and longitudinal-to-flexural transmission efficiencies of -60 to -70 dB were observed for this joint at frequencies above 7.5 kHz. Longitudinal-to-longitudinal transmission efficiencies as low as -55 dB were also observed for the joint with the visco-elastic interface demonstrating a clear advantage for incorporating damping material into the design of a joint.

Thesis Supervisor: Dr. J. R. Fricke  
Title: Assistant Professor

## Acknowledgments

I wish to extend my appreciation to Professor J. Robert Fricke and Professor Ira Dyer. Without the funding and support you graciously provided, this wonderful experience of being in academia once again would have been less pleasant and less possible. I wish to thank the entire acoustics group administrative staff. Sabina, Taci and Isela, I thank you for everything and truly appreciate the job that you so superbly perform. I also thank Hua He for his thoughtful discussions and recommendations that often kept me on the right path.

Most importantly, I thank my wonderful family. Mom, Pat, Ann, Mike, and Keith. You are everything a son and brother could ask for. You have always been there supporting and encouraging me and I thank you for letting me do the same for you. To all my critters, Chris, Beth, Tim, Nathan and Ann Marie; I can only hope that I have been as much an inspiration in your lives as you have been in mine. Your uncle loves you. I pray that you will aspire to be honest, loving and giving. One day I will look up to all of you in out-stretched arms and say, "Thank you God for bringing me to this summit." I will not get there alone! Be specific and committed to the vision of your dreams. Make them so.

*At certain levels, our life is not our own. If you choose to live in a community, have friends, if you have loved ones and you are loved, then you have entered an implicit and binding agreement. This agreement represents a willingness to take responsible precautions to protect your life and therefore uphold the commitment to those who help give your life meaning and structure - the commitment to be here tomorrow, the next day and the following so to allow the project of growth and community to continue, develop and move forward for the sake of future generations.*

# Table of Contents

Abstract .....	2
Acknowledgments .....	3
Table of Contents .....	4
List of Figures .....	6
List of Tables .....	9
List of Symbols .....	11
Chapter 1    Introduction .....	14
1.1    Previous Research .....	16
1.2    Objective .....	16
1.3    Approach .....	17
Chapter 2    Apparatus .....	18
2.1    Joint Descriptions .....	18
2.2    Experimental Configuration .....	21
2.3    Data Acquisition Equipment .....	24
Chapter 3    Experimental Execution .....	27
3.1    Impulse Excitation .....	27
3.2    Windowing .....	27
Chapter 4    Scattering Matrix .....	31
4.1    Principle .....	31
4.2    Joint Scattering Matrices .....	32
4.2.1    Joint ‘A’ Scattering Matrices .....	33
4.2.2    Joint ‘B’ Scattering Matrices .....	34
4.2.3    Joint ‘C’ Scattering Matrices .....	35
4.3    Determination of Joint Scattering Matrices .....	36

	4.3.1 Transmission Function Derivation using the Concept of Reciprocity .....	37
Chapter 5	Analytical Models and Predictions .....	41
	5.1 Transmission from Flexural Wave Excitation .....	41
	5.2 Transmission from Longitudinal Wave Excitation ...	44
Chapter 6	Experimental Results .....	46
	6.1 Experimentally Determined Data .....	46
	6.2 Data Determined by Reciprocity .....	51
	6.3 Relative Joint Response .....	52
	6.4 Scattering Matrix Elements Determined Experimentally .....	59
	6.5 Scattering Matrix Elements Determined by Reciprocity .....	72
Chapter 7	Conclusion .....	82
	7.1 Discussion of Results .....	82
	7.2 Recommendations for Future Research .....	83
Appendix A	Joint 'A' Design .....	86
Appendix B	Joint 'B' Design .....	91
Appendix C	Joint 'C' Design .....	105
Appendix D	Matlab Code .....	107
Appendix E	Data Collection and Organization .....	114
Bibliography	.....	118

## List of Figures

2-1	Joint ‘A’ (Rigid Joint) .....	19
2-2	Joint ‘B’ (Spherical Pinned-Joint, Teflon coated contact surfaces) .	20
2-3	Joint ‘B’ (top section, bottom section, and spherical male leg) .....	20
2-4	Laboratory experimental configuration .....	22
2-5	Static compressive loading configuration .....	23
2-6	Coordinate System .....	23
2-7	Accelerometer Configuration .....	25
2-8	Orientation of an accelerometer pair in a typical cross-section to measure wave types .....	25
2-9	Data acquisition equipment .....	26
3-1	Example of the windowing process for a typical incident longitudinal waveform (Leg 1) .....	29
3-2	Example of the windowing process for a typical transmitted longitudinal waveform (Leg 3) .....	30
5-1	Two-dimensional structural joint .....	41
5-2	Model of two-dimensional joint with stiffness, dissipation and mass .....	42
6-1	Cross-section of the leg/joint interaction demonstrating radial oscillatory expansion and contraction .....	49
6-2	Cross-section of the leg/joint interaction demonstrating translational oscillatory behavior .....	49
6-3	Rigid Joint Scattering Matrix Elements b14 and b24 .....	60
6-4	Rigid Joint Scattering Matrix Elements b34 and b44 .....	61
6-5	Rigid Joint Scattering Matrix Elements c14 and c24 .....	62
6-6	Rigid Joint Scattering Matrix Elements c34 and c44 .....	63
6-7	Teflon Joint Scattering Matrix Elements e14 and e24 .....	64
6-8	Teflon Joint Scattering Matrix Elements e34 and e44 .....	65
6-9	Teflon Joint Scattering Matrix Elements f14 and f24 .....	66

6-10	Teflon Joint Scattering Matrix Elements f34 and f44 .....	67
6-11	Visco-Elastic Joint Scattering Matrix Elements h14 and h24 .....	68
6-12	Visco-Elastic Joint Scattering Matrix Elements h34 and h44 .....	69
6-13	Visco-Elastic Joint Scattering Matrix Elements k14 and k24 .....	70
6-14	Visco-Elastic Joint Scattering Matrix Elements k34 and k44 .....	71
6-15	Rigid Joint Scattering Matrix Elements b41 and b42 determined by Reciprocity .....	73
6-16	Rigid Joint Scattering Matrix Elements b43 and c41 determined by Reciprocity .....	74
6-17	Rigid Joint Scattering Matrix Elements c42 and c43 determined by Reciprocity .....	75
6-18	Teflon Joint Scattering Matrix Elements e41 and e42 determined by Reciprocity .....	76
6-19	Teflon Joint Scattering Matrix Elements e43 and f41 determined by Reciprocity .....	77
6-20	Teflon Joint Scattering Matrix Elements f42 and f43 determined by Reciprocity .....	78
6-21	Visco-Elastic Joint Scattering Matrix Elements h41 and h42 determined by Reciprocity .....	79
6-22	Visco-Elastic Joint Scattering Matrix Elements h43 and k41 determined by Reciprocity .....	80
6-23	Visco-Elastic Joint Scattering Matrix Elements k42 and k43 determined by Reciprocity .....	81
A-1	Joint 'A' (Oblique View) .....	86
A-2	Joint 'A' (Top View) .....	87
A-3	Joint 'A' (Side View) .....	88
A-4	Joint 'A' Body .....	89
A-5	Joint 'A' Leg Penetrations (see-through view) .....	90
B-1	Joint 'B' Body (Oblique View) .....	92
B-2	Joint 'B' Top Section Upright (Oblique View) .....	93

<b>B-3</b>	<b>Joint 'B' Top Section Inverted (Oblique View)</b> .....	<b>94</b>
<b>B-4</b>	<b>Joint 'B' Top Section (Top View)</b> .....	<b>95</b>
<b>B-5</b>	<b>Joint 'B' Top Section (Side View)</b> .....	<b>96</b>
<b>B-6</b>	<b>Joint 'B' Top Section (Plane Cut View)</b> .....	<b>97</b>
<b>B-7</b>	<b>Joint 'B' Bottom Section Upright (Oblique View)</b> .....	<b>98</b>
<b>B-8</b>	<b>Joint 'B' Bottom Section Inverted (Oblique View)</b> .....	<b>99</b>
<b>B-9</b>	<b>Joint 'B' Bottom Section (Top View)</b> .....	<b>100</b>
<b>B-10</b>	<b>Joint 'B' Bottom Section (Side View)</b> .....	<b>101</b>
<b>B-11</b>	<b>Joint 'B' Spherical Male Leg (Oblique View)</b> .....	<b>102</b>
<b>B-12</b>	<b>Joint 'B' Spherical Male Leg (Side View)</b> .....	<b>103</b>
<b>B-13</b>	<b>Joint 'B' Spherical Male Leg (Top View)</b> .....	<b>104</b>
<b>C-1</b>	<b>Joint 'C' Spherical Male Leg (Side View)</b> .....	<b>106</b>
<b>E-1</b>	<b>Accelerometer position, lead orientation and channel numbering</b> ....	<b>116</b>



## List of Tables

2.1	Joint masses .....	19
6.1	Average transmission efficiency for Leg 2 given longitudinal excitation on Leg 1 .....	46
6.2	Average transmission efficiency for Leg 3 given longitudinal excitation on Leg 1 .....	47
6.3	Average longitudinal transmission efficiency for Leg 2 given excitation on Leg 1 .....	47
6.4	Average longitudinal transmission efficiency for Leg 3 given excitation on Leg 1 .....	47
6.5	Comparative values for Leg 2 flexural transmission (y-direction) given longitudinal excitation on Leg 1 .....	53
6.6	Comparative values for Leg 2 flexural transmission (x-direction) given longitudinal excitation on Leg 1 .....	53
6.7	Comparative values for Leg 2 torsional transmission given longitudinal excitation on Leg 1 .....	53
6.8	Comparative values for Leg 2 longitudinal transmission given longitudinal excitation on Leg 1 .....	54
6.9	Comparative values for Leg 3 flexural transmission (y-direction) given longitudinal excitation on Leg 1 .....	54
6.10	Comparative values for Leg 3 flexural transmission (x-direction) given longitudinal excitation on Leg 1 .....	54
6.11	Comparative values for Leg 3 torsional transmission given longitudinal excitation on Leg 1 .....	55
6.12	Comparative values for Leg 3 longitudinal transmission given longitudinal excitation on Leg 1 .....	55
6.13	Comparative values for Leg 2 longitudinal transmission given flexural (y-direction) excitation on Leg 1 .....	55

6.14	Comparative values for Leg 2 longitudinal transmission given flexural (x-direction) excitation on Leg 1 .....	56
6.15	Comparative values for Leg 2 longitudinal transmission given torsional excitation on Leg 1 .....	56
6.16	Comparative values for Leg 3 longitudinal transmission given flexural (y-direction) excitation on Leg 1 .....	56
6.17	Comparative values for Leg 3 longitudinal transmission given flexural (x-direction) excitation on Leg 1 .....	57
6.18	Comparative values for Leg 3 longitudinal transmission given torsional excitation on Leg 1 .....	57
E.1	Leg 1 Wave Formulae .....	117
E.2	Leg 2 Wave Formulae .....	117
E.3	Leg 3 Wave Formulae .....	117

# List of Symbols

## *English Capitals*

$F_{f_{in}}$	input flexural force
$F_{f_{out}}$	output flexural force
$F_{l_{in}}$	input longitudinal force
$F_{l_{out}}$	longitudinal output force
$F_{xr}(f)$	output flexural waveform (x-direction) from input waveform (example)
$F_{yr}(f)$	output flexural waveform (y-direction) from input waveform (example)
$F_{ys}(f)$	input flexural waveform (y-direction) (example)
$L_r(f)$	output longitudinal waveform from input waveform (example)
$L_s(f)$	input longitudinal waveform (example)
$M_1$	moment acting on joint (leg 1)
$M_2$	moment acting on joint (leg 2)
$P_{f_{in}}$	input flexural wave power
$P_{f_{out}}$	output flexural wave power
$P_{l_{in}}$	input longitudinal wave power
$P_{l_{out}}$	output longitudinal wave power
$T_F$	flexural transmission function
$T_L$	longitudinal transmission function
$T_r(f)$	output torsional waveform from input waveform (example)
$T_s(f)$	input torsional waveform (example)
$X$	joint displacement in the x-direction
$Y$	joint displacement in the y-direction
$Z_{f_{out}}$	output flexural impedance
$Z_{l_{in}}$	input longitudinal impedance

## *English Lower-Case Letters*

$a_{f_{in}}$	input flexural acceleration
--------------	-----------------------------

$a_{i_{in}}$	input longitudinal acceleration
$a_{i_{out}}$	output longitudinal acceleration
$a_{ij}(f)$	elemental reflection function for Joint 'A' Leg 1 scattering matrix
$b_{ij}(f)$	elemental transmission function for Joint 'A' Leg 2 scattering matrix
$c_f$	flexural phase speed
$c_{ij}(f)$	elemental transmission function for Joint 'A' Leg 3 scattering matrix
$c_l$	longitudinal phase speed (5140 m/s)
$c_T$	torsional phase speed (3250 m/s)
$d_{ij}(f)$	elemental reflection function for Joint 'B' Leg 1 scattering matrix
$e_{ij}(f)$	elemental transmission function for Joint 'B' Leg 2 scattering matrix
$f$	frequency (Hz)
$f_{F1}$	flexural force (leg 1)
$f_{F2}$	flexural force (leg 2)
$f_{L1}$	longitudinal force (leg 1)
$f_{L2}$	longitudinal force (leg 2)
$f_{ij}(f)$	elemental transmission function for Joint 'B' Leg 3 scattering matrix
$g_{ij}(f)$	elemental reflection function for Joint 'C' Leg 1 scattering matrix
$h_{ij}(f)$	elemental transmission function for Joint 'C' Leg 2 scattering matrix
$k_{B_2}$	bending wave number on leg 2
$k_f$	flexural wave number
$k_{ij}(f)$	elemental transmission function for Joint 'C' Leg 3 scattering matrix
$k_{L_1}$	longitudinal wave number on leg 1
$k_{L_2}$	longitudinal wave number on leg 2
$m$	joint mass
$r_{LL}$	longitudinal-to-longitudinal reflection coefficient
$s_i(f)$	elemental input function for a scattering matrix (example)
$t_{LB}$	longitudinal-to-bending transmission coefficient
$t_{LL}$	longitudinal-to-longitudinal transmission coefficient

$u_1$	longitudinal displacement (leg 1)
$u_2$	longitudinal displacement (leg 2)
$v_{f_{out}}$	output flexural velocity
$v_{i_{in}}$	input longitudinal velocity
$v_{x1}$	velocity in the x-direction on leg 1
$v_{x2}$	velocity in the x-direction on leg 2
$v_{y2}$	velocity in the y-direction on leg 2
$w_1$	transverse displacement (leg 1)
$w_2$	transverse displacement (leg 2)
$w_1'$	first spatial derivative (angle of rotation of leg 1)
$w_2'$	first spatial derivative (angle of rotation of leg 2)
$y_i(f)$	elemental output function for a scattering matrix (example)
$z_F$	complex flexural spring constant
$z_{ij}(f)$	elemental transmission/reflection function of a scattering matrix (example)
$z_L$	complex longitudinal spring constant
$z_M$	complex rotational spring constant

### *Greek Capitals*

$\Phi$  joint angle of rotation

### *Lower-Case Greek Letters*

$\theta$  angle formed by the intersection of the two legs of the joint

$\kappa$  radius of gyration

$\rho$  density ( $kg / m^3$ )

$\tau_F$  flexural transmission function

$\tau_L$  longitudinal transmission function

$\tau_1$  incident transmission function

$\tau_2$  reciprocal transmission function

$\mu$  non-dimensional frequency parameter

$\omega$  angular frequency (rad/s)

# Chapter 1

## Introduction

Since the conception of the first nuclear-powered submarine in 1954 [1], the USS Nautilus, the internal structure of a submarine has taken many different forms. The intent of these structural modifications has been to continually reduce the submarine's radiated sound pressure level thereby maximizing the tactical advantage that a U.S. submarine has against its adversaries.

Initial internal structural designs consisted of equipment mounted on resiliently mounted decks. These decks were connected directly to the pressure vessel and created significant sound shorts; the vibrational energy passed, relatively unimpeded, from the equipment, to the deck, to the pressure vessel, and into the surrounding medium. Improved designs concentrated on installing equipment which was mounted to the decks with vibration isolation mechanisms. This attempt increased the impedance mismatch at the interface to the deck and significantly reduced the acoustic signature of the submarine.

The concept of mounting equipment on a three-dimensional truss-like structure was initially developed by the French in the early 1980's [2]. This concept relies on the ability of the truss to mitigate the propagation of vibrational energy to the pressure vessel. This is achieved in two ways:

(a) The vibrational energy may be dissipated within the truss through either active or passive vibration damping mechanisms.

(b) The vibrational energy can effectively be isolated from the pressure vessel by judiciously selecting the proper truss/vessel attachments and minimizing the number of those attachments. By using a minimal number of attachment points and maximizing the impedance mismatch of each attachment point the dynamic behavior of the truss can be, effectively, decoupled from the dynamic behavior of the pressure vessel.

Structural joints play a critical role in the dynamic behavior of structures [3]. The vibrational energy present in a structure propagates along the individual members and interacts at the joints where the energy is scattered and/or dissipated. Scattering produces transmission and reflection as well as conversion to flexural, longitudinal and torsional waves. Transmission and reflection are a measure of the extent to which vibrational energy is isolated while the scattering behavior of a specific joint can be advantageous for converting a certain wave type into a different wave type which may be more sensitive to dissipation.

Vibration isolation can be achieved by trapping a wave within a member of the structure, however, damping mechanisms must be incorporated in the joint or in the member to achieve adequate dissipation. Of particular interest is the ability of a structure to minimize transmission of longitudinal waves. Longitudinal waves possess high phase speed and practical means to dissipate longitudinal waves are not easily achieved. By maximizing the extent to which longitudinal waves are reflected from a joint is it then possible to trap the longitudinal energy and prevent the energy from propagating through the structure and, ultimately, into an undesirable medium, for example, the volume external to the hull of a submarine.

Dissipation mechanisms are easily achieved for flexural waves. This is important since flexural waves are often most easily excited in structures and much of the energy content of all wave types is present in the form of flexural waves. A structure whose joints maximize reflection is most desirable since the vibrational energy will be trapped within the structure. When this cannot be achieved it is desirable that longitudinal-to-flexural conversion occur at the joint. This may produce reflection and transmission in the form of flexural energy where the performance of dissipative mechanisms can be maximized. This is especially important when those members, intended to dissipate vibrational energy, provide support for very noisy equipment.

## **1.1 Previous Research**

The research conducted in support of this thesis involved three joints: two different spherical pinned-joints and one rigid joint. Considerable research has been conducted in regard to rigid joints. Most of the work has been conducted on two-dimensional, compliant and non-compliant, right-angled joints [4-9]. More generalized work on compliant and non-compliant two-dimensional joints which are not restricted to right-angles has recently been conducted by Guo [10].

Limited work has been conducted with regard to spherical joints. Space joint systems often use special connectors formed by spherical balls for attachment of the truss members. One type of spherical joint that has been developed by Wayne State University [11, 12] is a hollow sphere containing a number of hollow spheres with the intent that the spherical configuration forms a structurally rigid node. All spheres are in contact with one another and the spaces between the spheres may be filled with material to take advantage of its damping behavior.

Mathematical modeling and stochastic simulation of a three-dimensional spherical joint similar in design to that at Wayne State University has been investigated [13, 14]. Most published information on spherical joint behavior is, however, experimental and is devoted to a specific joint configuration without generalization of the results. It has been observed [15] that much of the design knowledge for spherical joints is proprietary and is not published.

## **1.2 Objective**

In order to facilitate proper design of the truss it is essential to understand the dynamic behavior of its structural joints since joint behavior plays a critical role in determining overall structural response to excitation. The objective of this thesis is to study the behavior of three simple, yet very different, laboratory-scale three-dimensional



joints through experimentation and application of analytical theory. Of primary interest is understanding the scattering of an incident longitudinal wave in each of the joints.

It is expected that the joints will behave significantly differently from one another and once this difference is recognized and understood it will be possible to utilize these characteristics to the greatest advantage. The pragmatic objective in understanding joint behavior is to be able to utilize favorable characteristics of specific joints to resolve specific vibration problems.

### **1.3 Approach**

The three joints are designed such that the angular positions of the legs are identical to the simplest joint in the three-dimensional truss used in previous research in the MIT Acoustics and Vibration Laboratory [16]. In each experiment, each leg of each joint is connected to a 14' stainless steel leg extension to facilitate data collection. Impulse excitation is used to generate longitudinal incident waves. Accelerometers are placed on each leg to measure the acceleration from each wave type. Measurement of each wave type permits the determination of the transmission efficiency of each joint.

The intent is to gain an understanding of the scattering processes that occur when an incident longitudinal wave interacts with each joint. To this end, a scattering matrix is introduced which relates the input wave types to the output wave types. The elements of the scattering matrix are transfer functions which, in essence, are reflection and transmission functions of frequency. By experimentally determining the transfer functions it is possible to predict the output wave types for any given input; inherent in the use of the scattering matrix in the assumption of linearity. Comparison is then made to analytical two-dimensional work [4, 8, 10].

# Chapter 2

## Apparatus

The apparatus discussed in this chapter includes the descriptions of the joints, experimental configuration, and the data acquisition equipment.

### 2.1 Joint Descriptions

Three joints were used in the laboratory experiments. Joint 'A' is a rigid joint similar in construction to the joints used in the three-dimensional truss [16]. Joint 'B' is a spherical pinned-joint with contact surfaces coated with Teflon. Behavior is intended to be similar to a frictionless pinned-joint. Joint 'C' is very similar in design to Joint 'B' but with the contact surface comprising visco-elastic material. The visco-elastic material is discussed in Appendix C. Each joint has three legs, the simplest configuration used in the three-dimensional truss. Design details of each joint are included in Appendices A, B, and C for Joints 'A', 'B' and 'C', respectively. Figs. 2-1, 2-2, and 2-3 depict each joint as used in the laboratory.

The joints are similar in size to those in the three-dimensional truss. Joint 'A' most closely resembles the joint in the truss. The intent of the design of each joint was to maximize simplicity without compromising practical application. Table 2.1 depicts the mass of each joint. It should be noted that the mass of Joint 'A' has been corrected to take into account the fact that its legs are longer than those of Joints 'B' and 'C'; the mass of Joint 'A', presented in Table 2.1, is its effective mass.

Joints 'A', 'B', and 'C' are geometrically identical. Legs 1 and 3 intersect at 90 degrees. Leg 2 lies at 63.4 degrees to the plane formed by Legs 1 and 3; its normal projection onto the plane formed by Legs 1 and 3 bisects the angle formed by Leg 1 and Leg 3.

Joint	Mass (g)
'A' (Rigid)	588
'B' (Teflon)	997
'C' (Visco-Elastic)	979

Table 2.1: Joint masses.

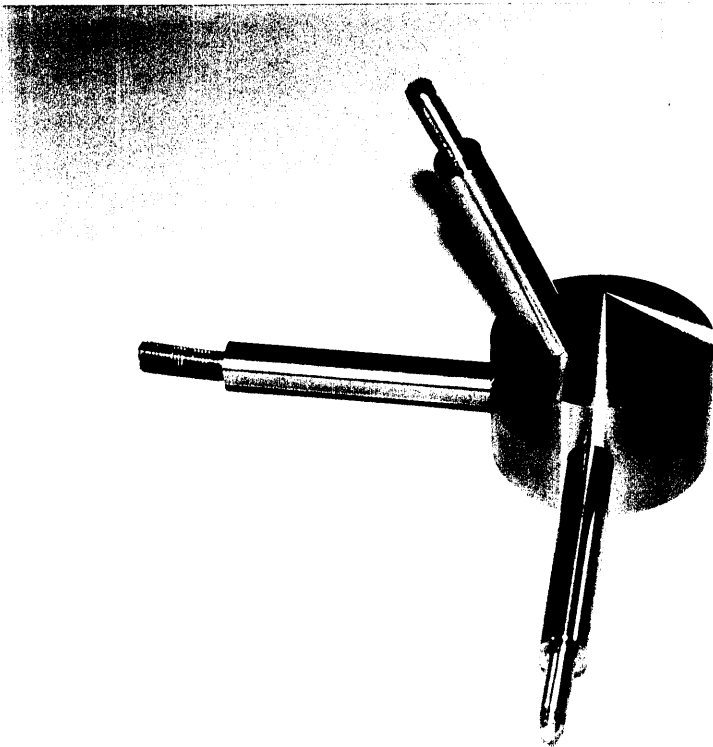


Figure 2-1: Joint 'A' (Rigid Joint).

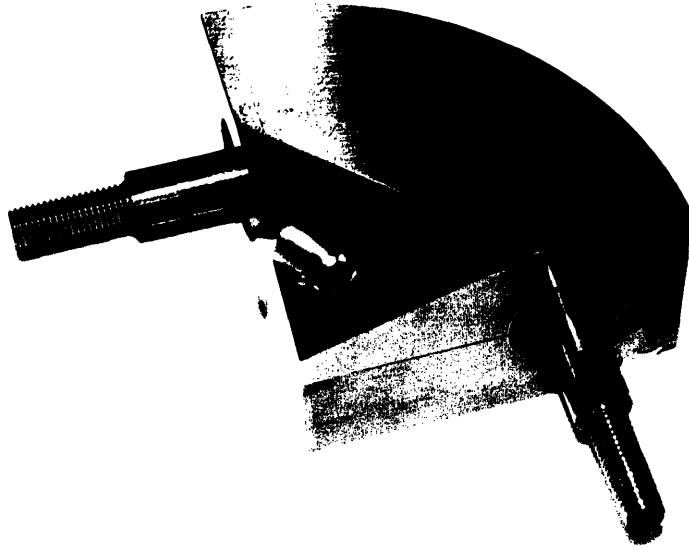


Figure 2-2: Joint 'B' (Spherical Pinned-Joint, Teflon coated contact surfaces. Joint 'C' is identical at this scale.).

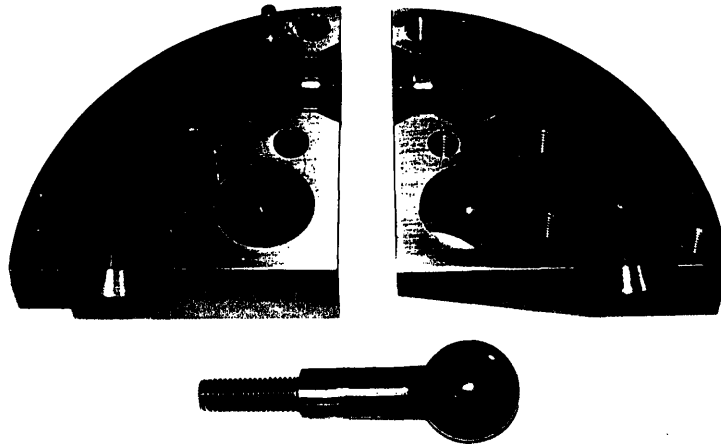


Figure 2-3: Joint 'B' (top section, bottom section, and spherical male leg).

## 2.2 Experimental Configuration

Figure 2-4 shows the laboratory experimental configuration. Each leg depicted in Fig. 2-4 is 14 ft. long. Legs 2 and 3 are bare with no damping treatment while Leg 1 has damping treatment. The intent of the damping treatment is to dissipate flexural energy created by the longitudinal impulse such that a pure longitudinal wave is incident at the joint.

Each joint is connected to the 14' legs by threaded connections. The tripod configuration provides the support for each joint. Leg 1 is also supported by bungee cord at the mid-section since the weight of the leg and the damping treatment is enough to cause it to collapse.

Not depicted in Fig. 2-4 is a loading configuration which was applied during all phases of experimentation. A force of 89 N was applied as shown in Figure 2-5. This loading configuration ensured that each leg remained under an equal static compressive load of 60 N. It also ensured that the spherical male legs of Joints 'B' and 'C' remained in contact (under static conditions) with the joint body, thereby preventing an artificially high impedance mismatch at the leg/joint body connection.

There is no theoretical basis for the selection of the value of the applied force. The objective in selecting the magnitude of the force was: (1) the force would be great enough to ensure that the spherical male legs remained in contact with the spherical recesses of the joint body under static conditions and (2) the load would not cause the leg extensions to buckle. The magnitude of the load does not ensure that the spherical male legs will remain in contact with the surfaces of the recesses of the joint body during high levels of excitation.

### *Coordinate System*

A coordinate system is established for each leg. It is this coordinate system, shown in Fig. 2-6, to which reference is made in regard to flexural wave measurement. The y-axis is perpendicular to a given leg and has a component directed vertically downward. The x-axis is horizontally directed.

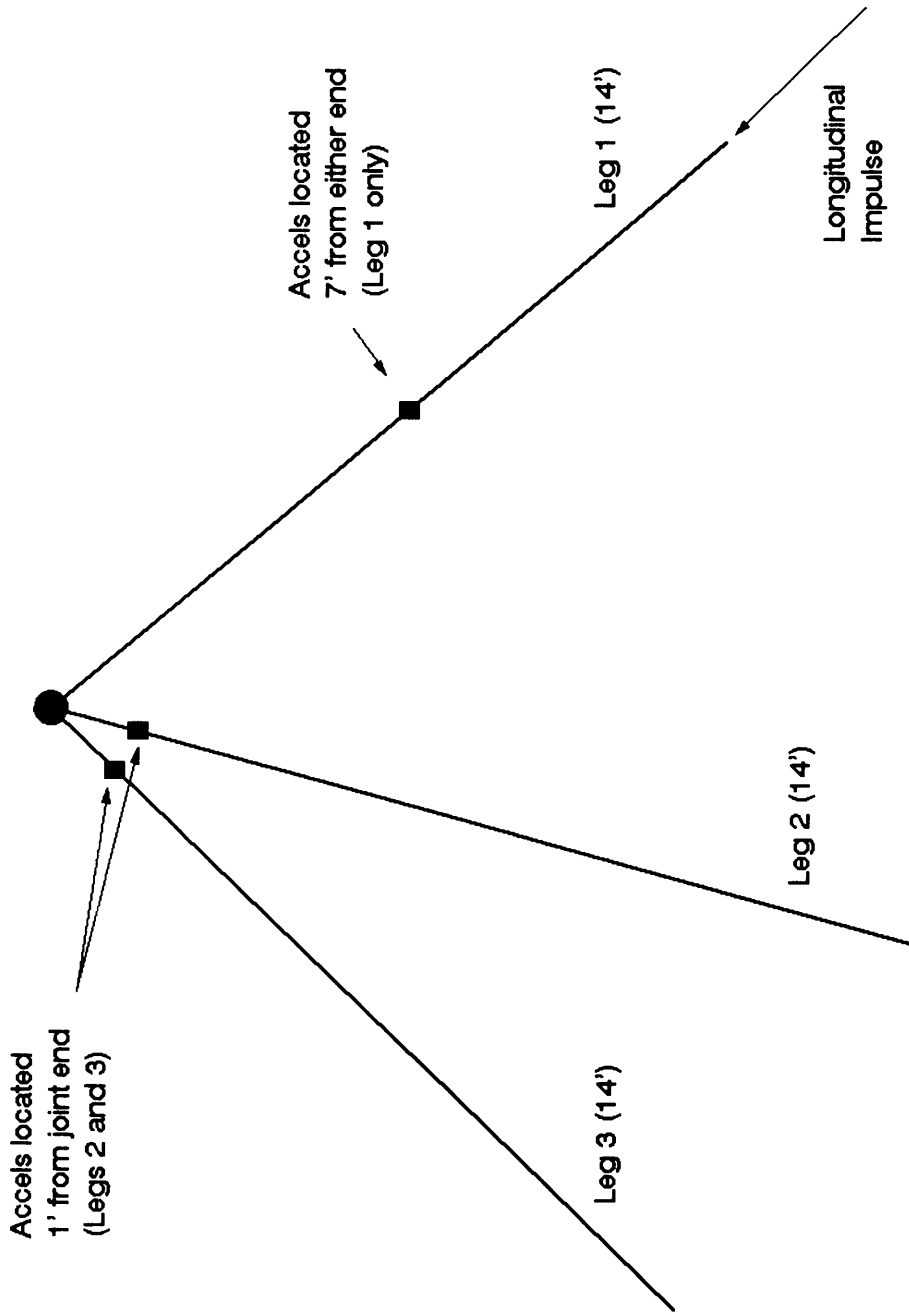


Figure 2-4: Laboratory experimental configuration.

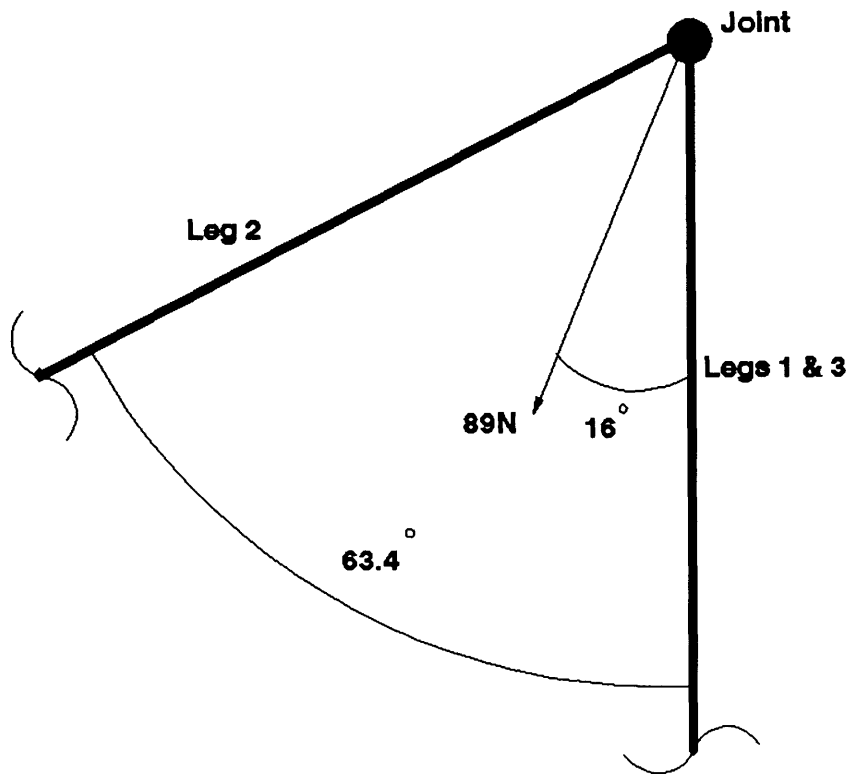


Figure 2-5: Static compressive loading configuration (cut-away side view of experimental model).

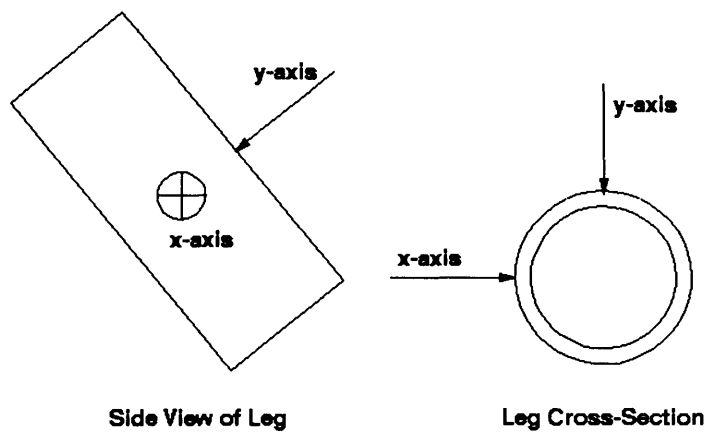


Figure 2-6: Coordinate system.

## **2.3 Data Acquisition Equipment**

Vibrational excitation was achieved by using an instrumented impulse hammer. The impulse hammer was a PCB Impulse Hammer with a plastic/vinyl tuning mass and an aluminum extender. 8 Kistler 0.5 gm Type 8616A500 accelerometers were attached to each leg to be able to differentiate between four different waves present in each leg, e.g., longitudinal, torsional, and two orthogonal flexural waves. The accelerometers have a measuring range of  $\pm 500$  g and a transverse sensitivity of 5.0%. The low mass of the accelerometers minimizes the added mass effect when mounted on a leg while providing sufficient frequency range and sensitivity. Each accelerometer is attached with bee's wax which provides a rigid connection to the leg over the frequency range of interest. Fig. 2-7 depicts the attachment of the accelerometers to a leg. Fig. 2-8 illustrates how each pair of accelerometers are arranged to permit wave type determination. Appendix E provides greater detail of exact accelerometer position and orientation.

Fig. 2-9 shows the equipment used for data acquisition. This consisted of the following:

- (a) one HP 9000 Model 735/125 workstation
- (b) one HP E1401A High-Power Mainframe
- (c) six HP E1431A 25.6 kHz Eight Channel VXI Input Modules

The HP 9000 Model 735/125 is a high-performance PA-RISC-based workstation that is designed to run the HP-UX operating system.

The six HP E1431A 25.6 kHz Eight Channel VXI Input Modules are installed in the HP E1401A High-Power Mainframe forming a 48-channel data acquisition platform. Each module is capable of sensing input frequencies ranging from 0.39 Hz to 25,600 Hz. The sampling rate can be adjusted from 1 to 65536 samples per second providing a minimum sampling interval of  $1.52588 \times 10^{-5}$  sec. The sampling interval throughout the experimentation was  $1.52588 \times 10^{-5}$  sec.



The accelerometers are mounted onto the experimental model and are then connected by a thin coaxial cable to the HP E1431A Input Modules of the HP E1401A High-Power Mainframe.

The software used for data acquisition and post-processing was SDRC I-DEAS Master Series 2.0.

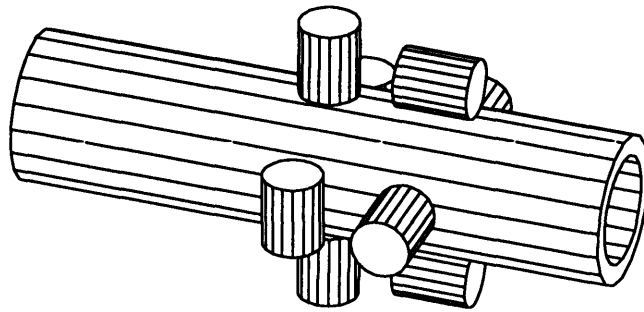


Figure 2-7: Accelerometer configuration.

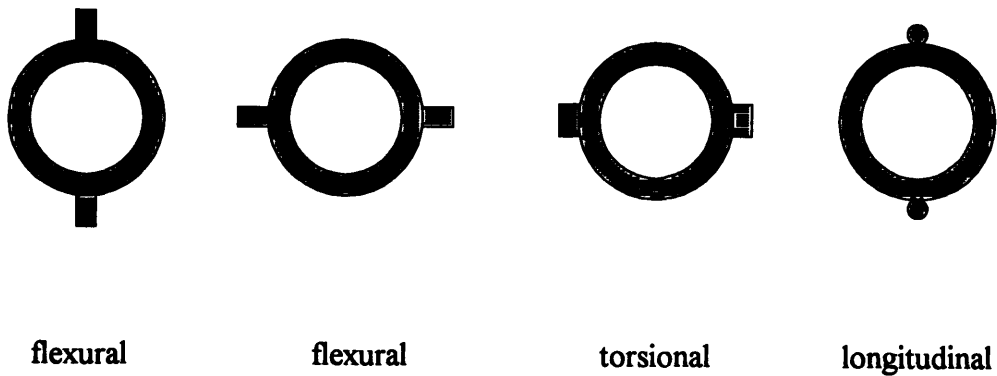


Figure 2-8: Orientation of an accelerometer pair in a typical cross-section to measure wave types. Specific polarity for each leg is depicted in Appendix E.

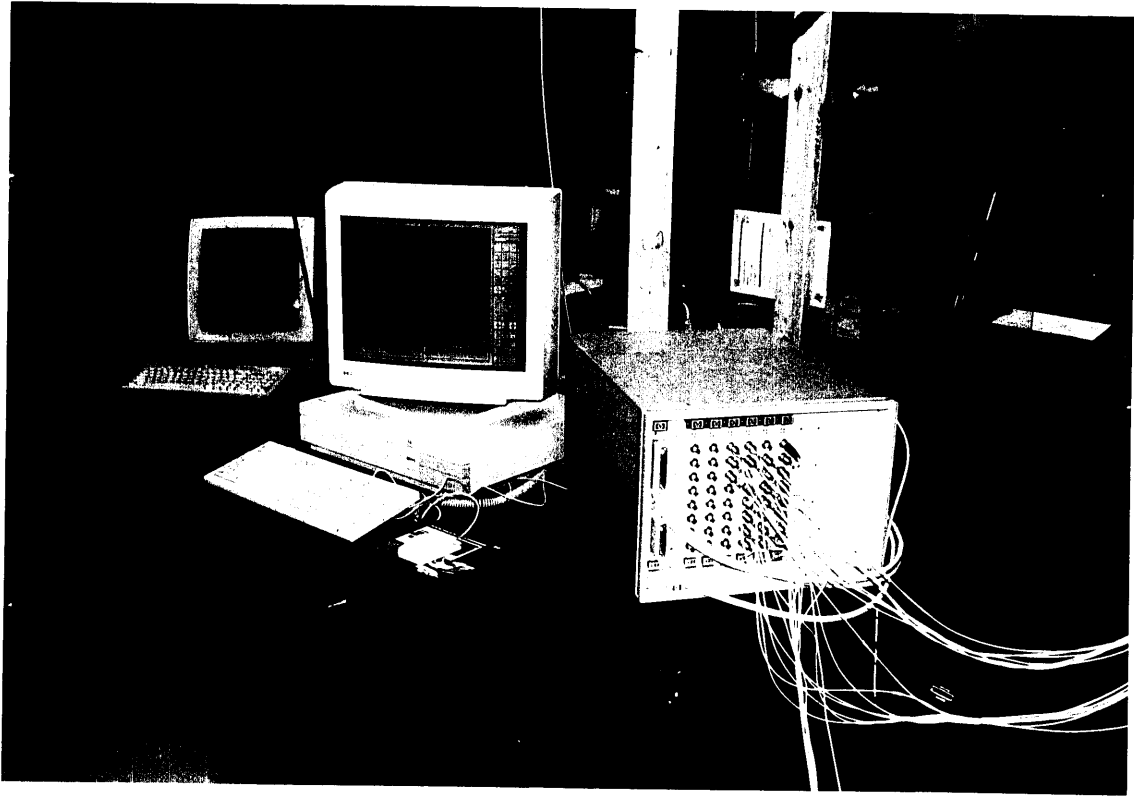


Figure 2-9: Data acquisition equipment.

# Chapter 3

## Experimental Execution

### 3.1 Impulse Excitation

Excitation for all phases of experimentation was conducted with an impulse generated by an instrumented impulse hammer discussed in Chapter 2. The duration of each impulse was typically 0.1 - 0.2 msec. Impulse excitation is the only viable means to ascertain joint dynamic behavior due to the limitations of the experimental model and the high phase speed of the longitudinal wave (approx. 5140 m/s). All joints were tested under two conditions: 1) an impulse to create a pure longitudinal wave, and 2) an impulse to create a pure flexural wave. Generation of a pure longitudinal incident wave was successful. Generation of a pure flexural incident wave was not successful; this is discussed fully in Appendix E. Each joint was tested with ten impulses for each of the two different types of impulses. The remainder of this thesis will focus on the incident longitudinal wave experiments.

### 3.2 Windowing

Time-gating the experimental data was necessary to prevent contamination. Contamination would come from reflection at the joint or reflection from the ends of the legs. As such, each leg was time-gated prior to the arrival of any reflected waves. The length of the window is solely dependent upon the speed of the longitudinal wave. The window established for Leg 1 was different than the window for Legs 2 and 3 as shown in Figs. 3-1 and 3-2.

The temporal windowing function applied in the windowing process is a flat filter of value 1.0 with ends tapered according to the function  $\cos^2 t$ . The tapering is necessary to mitigate Gibbs phenomenon [17].

### *Leg 1 Windowing*

Given that the length of each leg is 14', the propagation time for a longitudinal wave from the end of Leg 1 to the joint is 0.83 msec. This is the same time for the longitudinal wave to travel from the set of accelerometers to the joint and, after reflection, back to the accelerometers. To avoid contamination from reflection, the window for Leg 1 was selected to be 0.83 msec (54 data points) starting at 0.42 msec and ending at 1.25 msec after the pulse was initiated. Fig. 3-1 illustrates the temporal windowing function and a typical waveform before and after the use of the window for an incident longitudinal wave on Leg 1.

### *Leg 2 Windowing*

The propagation time for a longitudinal wave to travel from the end of Leg 1 to the group of accelerometers on Legs 2 or 3 is approximately 0.89 msec. Given that the distance from the group of accelerometers to the end of Legs 2 and 3 is 13', the propagation time for a longitudinal wave to travel from the group of accelerometers and back to the group, after reflection, is approximately 1.54 msec (99 data points). Hence, the window for Legs 2 and 3 was selected to be 1.54 msec wide starting at 0.89 msec and ending at 2.43 msec after the pulse was initiated. Fig. 3-2 illustrates the temporal windowing function and a typical waveform before and after the use of the window for a transmitted longitudinal wave on Leg 3.

It should be noted that the selection of the window also precludes contamination from the second scattering event from Leg 1 since this would occur at 2.55 msec after the initial impulse.

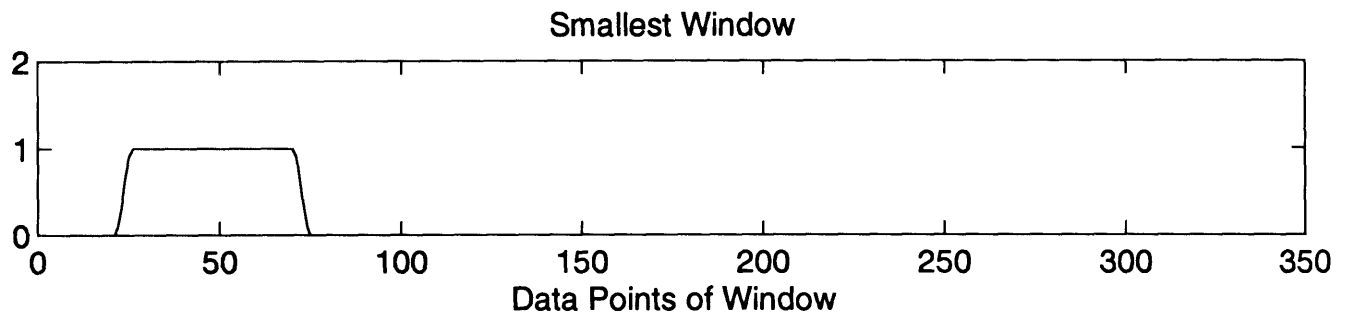
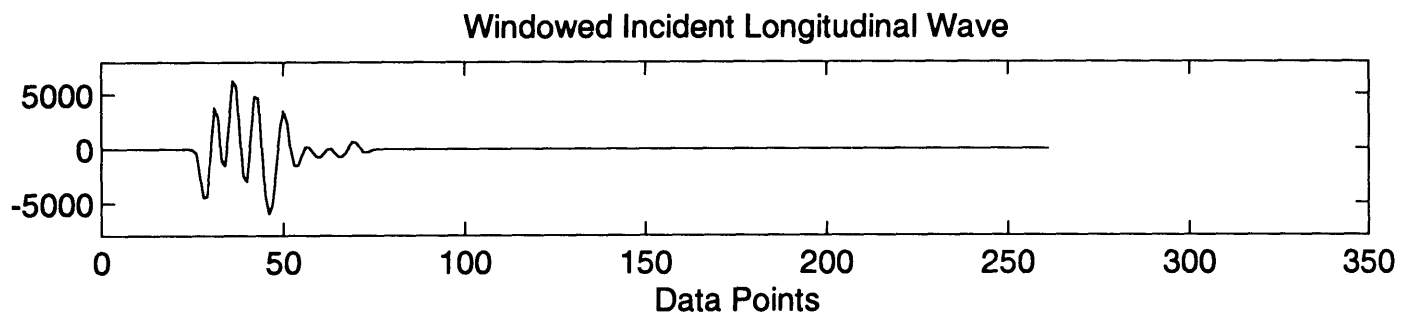
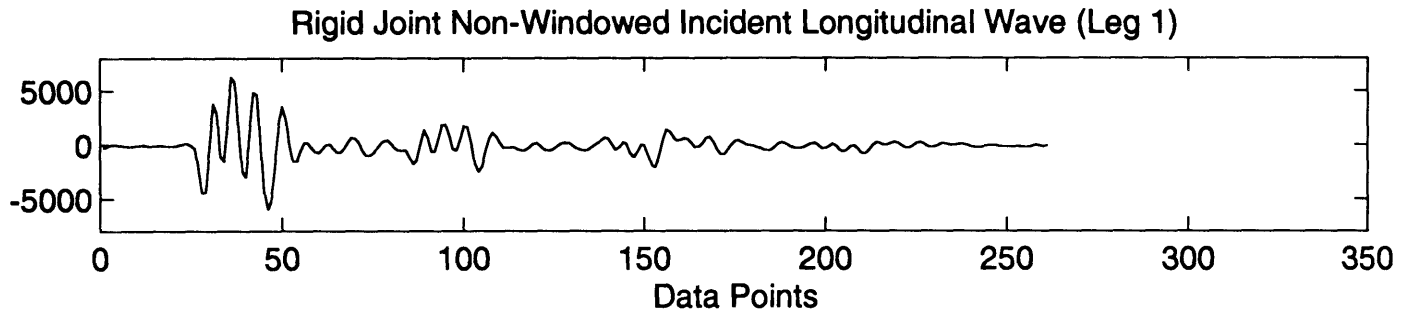


Figure 3-1: Example of the windowing process for a typical incident longitudinal waveform (Leg 1).

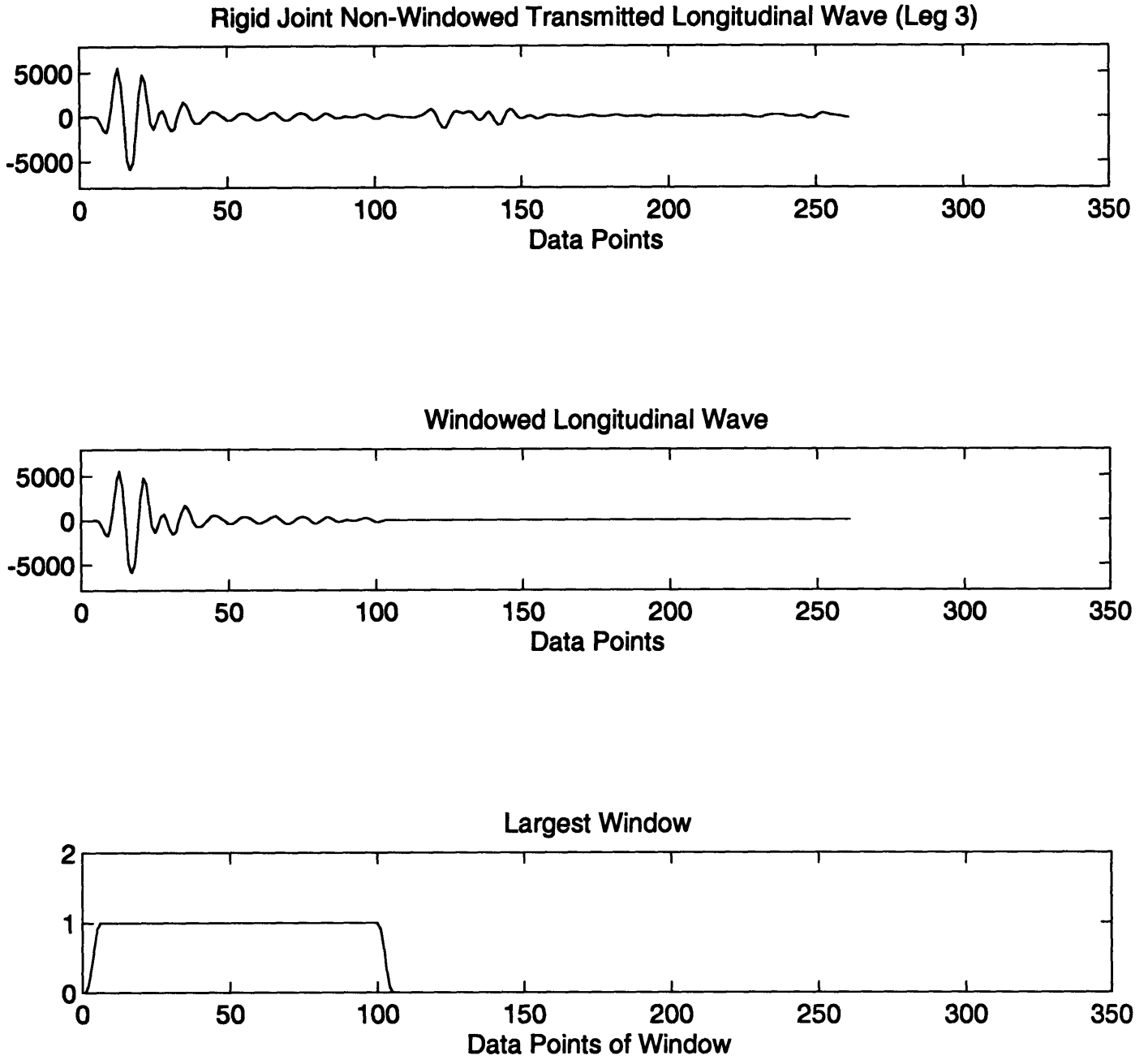


Figure 3-2: Example of the windowing process for a typical transmitted longitudinal waveform. (Leg 3).

# Chapter 4

## Scattering Matrix

### 4.1 Principle

Conceptually, the dynamic behavior of each joint can be described by a matrix whose elements are transfer functions. If a specific known wave type propagates along one leg of the joint, it will be scattered at the joint and typically form, through transmission and reflection, four different waves in each leg. These will comprise a longitudinal wave, a torsional wave, and two orthogonal flexural waves. If, for example, Leg 1 is excited by a pure longitudinal wave, that wave will propagate along the leg and undergo scattering at the joint. Legs 2 and 3 will possess all waveforms that were transmitted from the joint upon scattering. Leg 1 will not only be excited by the initial wave type, it will also be excited by the reflection from the joint.

This matrix will be termed a 'scattering matrix'. The scattering matrix has the form,

$$\begin{bmatrix} z_{11}(f) & z_{12}(f) & z_{13}(f) & z_{14}(f) \\ z_{21}(f) & z_{22}(f) & z_{23}(f) & z_{24}(f) \\ z_{31}(f) & z_{32}(f) & z_{33}(f) & z_{34}(f) \\ z_{41}(f) & z_{42}(f) & z_{43}(f) & z_{44}(f) \end{bmatrix}$$

where each element is an explicit function of frequency (Hz).

The scattering matrix may be used to determine the resulting output waveforms of each leg by post-multiplying by the input function. The input function takes the form of a 4x1 matrix where  $s_1(f)$  may, for example, be the input longitudinal wave:

$$\begin{bmatrix} s_1(f) & s_2(f) & s_3(f) & s_4(f) \end{bmatrix}^T$$

The resulting output from the scattering process has the form:

$$\begin{bmatrix} y_1(f) \\ y_2(f) \\ y_3(f) \\ y_4(f) \end{bmatrix} = \begin{bmatrix} z_{11}(f) & z_{12}(f) & z_{13}(f) & z_{14}(f) \\ z_{21}(f) & z_{22}(f) & z_{23}(f) & z_{24}(f) \\ z_{31}(f) & z_{32}(f) & z_{33}(f) & z_{34}(f) \\ z_{41}(f) & z_{42}(f) & z_{43}(f) & z_{44}(f) \end{bmatrix} \begin{bmatrix} s_1(f) \\ s_2(f) \\ s_3(f) \\ s_4(f) \end{bmatrix}$$

## 4.2 Joint Scattering Matrices

Associated with each joint are three scattering matrices, one scattering matrix for each leg. The scattering matrices determine the wave types that will be present in a specific leg for a given input. Joints 'A', 'B', and 'C' thus require the determination of 9 unique matrices to describe their dynamic behavior. All Leg 1 matrices contain elements which are reflection functions. All Leg 2 and Leg 3 matrices contain elements which are transmission functions.

The first column of each matrix contains the functions which are the response due to flexural excitation in the y-direction. The second column contains the functions which are the response due to flexural excitation in the x-direction. The third column contains the functions which are the response due to torsional excitation. Lastly, the fourth column contains the functions which are the response due to longitudinal excitation.



### 4.2.1 Joint 'A' Scattering Matrices

The three scattering matrices associated with Joint 'A' are formally defined below for further reference.

Joint 'A' Leg 1 Scattering Matrix:

$$\begin{bmatrix} a_{11}(f) & a_{12}(f) & a_{13}(f) & a_{14}(f) \\ a_{21}(f) & a_{22}(f) & a_{23}(f) & a_{24}(f) \\ a_{31}(f) & a_{32}(f) & a_{33}(f) & a_{34}(f) \\ a_{41}(f) & a_{42}(f) & a_{43}(f) & a_{44}(f) \end{bmatrix}$$

Joint 'A' Leg 2 Scattering Matrix:

$$\begin{bmatrix} b_{11}(f) & b_{12}(f) & b_{13}(f) & b_{14}(f) \\ b_{21}(f) & b_{22}(f) & b_{23}(f) & b_{24}(f) \\ b_{31}(f) & b_{32}(f) & b_{33}(f) & b_{34}(f) \\ b_{41}(f) & b_{42}(f) & b_{43}(f) & b_{44}(f) \end{bmatrix}$$

Joint 'A' Leg 3 Scattering Matrix:

$$\begin{bmatrix} c_{11}(f) & c_{12}(f) & c_{13}(f) & c_{14}(f) \\ c_{21}(f) & c_{22}(f) & c_{23}(f) & c_{24}(f) \\ c_{31}(f) & c_{32}(f) & c_{33}(f) & c_{34}(f) \\ c_{41}(f) & c_{42}(f) & c_{43}(f) & c_{44}(f) \end{bmatrix}$$

### 4.2.2 Joint 'B' Scattering Matrices

The three scattering matrices associated with Joint 'B' are formally defined below for further reference.

Joint 'B' Leg 1 Scattering Matrix:

$$\begin{bmatrix} d_{11}(f) & d_{12}(f) & d_{13}(f) & d_{14}(f) \\ d_{21}(f) & d_{22}(f) & d_{23}(f) & d_{24}(f) \\ d_{31}(f) & d_{32}(f) & d_{33}(f) & d_{34}(f) \\ d_{41}(f) & d_{42}(f) & d_{43}(f) & d_{44}(f) \end{bmatrix}$$

Joint 'B' Leg 2 Scattering Matrix:

$$\begin{bmatrix} e_{11}(f) & e_{12}(f) & e_{13}(f) & e_{14}(f) \\ e_{21}(f) & e_{22}(f) & e_{23}(f) & e_{24}(f) \\ e_{31}(f) & e_{32}(f) & e_{33}(f) & e_{34}(f) \\ e_{41}(f) & e_{42}(f) & e_{43}(f) & e_{44}(f) \end{bmatrix}$$

Joint 'B' Leg 3 Scattering Matrix:

$$\begin{bmatrix} f_{11}(f) & f_{12}(f) & f_{13}(f) & f_{14}(f) \\ f_{21}(f) & f_{22}(f) & f_{23}(f) & f_{24}(f) \\ f_{31}(f) & f_{32}(f) & f_{33}(f) & f_{34}(f) \\ f_{41}(f) & f_{42}(f) & f_{43}(f) & f_{44}(f) \end{bmatrix}$$

### 4.2.3 Joint 'C' Scattering Matrices

The three scattering matrices associated with Joint 'C' are formally defined below for further reference.

Joint 'C' Leg 1 Scattering Matrix:

$$\begin{bmatrix} g_{11}(f) & g_{12}(f) & g_{13}(f) & g_{14}(f) \\ g_{21}(f) & g_{22}(f) & g_{23}(f) & g_{24}(f) \\ g_{31}(f) & g_{32}(f) & g_{33}(f) & g_{34}(f) \\ g_{41}(f) & g_{42}(f) & g_{43}(f) & g_{44}(f) \end{bmatrix}$$

Joint 'C' Leg 2 Scattering Matrix:

$$\begin{bmatrix} h_{11}(f) & h_{12}(f) & h_{13}(f) & h_{14}(f) \\ h_{21}(f) & h_{22}(f) & h_{23}(f) & h_{24}(f) \\ h_{31}(f) & h_{32}(f) & h_{33}(f) & h_{34}(f) \\ h_{41}(f) & h_{42}(f) & h_{43}(f) & h_{44}(f) \end{bmatrix}$$

Joint 'C' Leg 3 Scattering Matrix:

$$\begin{bmatrix} k_{11}(f) & k_{12}(f) & k_{13}(f) & k_{14}(f) \\ k_{21}(f) & k_{22}(f) & k_{23}(f) & k_{24}(f) \\ k_{31}(f) & k_{32}(f) & k_{33}(f) & k_{34}(f) \\ k_{41}(f) & k_{42}(f) & k_{43}(f) & k_{44}(f) \end{bmatrix}$$

### 4.3 Determination of Joint Scattering Matrices

As discussed previously, output wave types can be determined by post-multiplying a specific scattering matrix by the input function. Experimentally, however, the objective is to determine the scattering matrix from the given input and resulting output. The elements of the scattering matrix are most easily determined by injecting pure waves of one type into the joint. This permits determination of the elemental transfer function directly from known input and known output.

If, for example, a pure torsional wave is injected into Leg 1 of a joint, Leg 1 will experience reflection and all four waves (longitudinal, torsional, and two orthogonal flexural waves) will, typically, be present. Similarly, each of Legs 2 and 3 will, typically, be excited by four transmitted waves.

The problem of determining the elemental transfer functions is much more difficult if more than one wave type is simultaneously injected into the leg. By injecting pure waves into a leg the scattering matrix can be simplified and the elemental transfer functions can be readily determined. Let the input matrix be specified as

$$\left[ F_{ys}(f) \quad F_{xs}(f) \quad T_s(f) \quad L_s(f) \right]^T,$$

where  $F_{ys}(f)$  is the flexural wave in the y-direction,  $F_{xs}(f)$  is the flexural wave in the x-direction,  $T_s(f)$  is the torsional wave, and  $L_s(f)$  is the longitudinal wave. If a pure flexural wave in the y-direction is injected into Joint 'A', the input matrix simplifies to:

$$\left[ F_{ys}(f) \quad 0 \quad 0 \quad 0 \right]^T.$$

The resulting scattering equation for Leg 1 of Joint 'A' becomes:

$$\begin{bmatrix} F_{yr}(f) \\ F_{xr}(f) \\ T_r(f) \\ L_r(f) \end{bmatrix} = \begin{bmatrix} a_{11}(f) \\ a_{12}(f) \\ a_{13}(f) \\ a_{14}(f) \end{bmatrix} \begin{bmatrix} F_{ys}(f) \end{bmatrix}.$$

The elemental transfer functions for the pure input flexural wave (in the y-direction) are thus readily determined to be:

$$\begin{aligned} a_{11}(f) &= \frac{F_{yr}(f)}{F_{ys}(f)}, & a_{12}(f) &= \frac{F_{xr}(f)}{F_{ys}(f)}, \\ a_{13}(f) &= \frac{T_r(f)}{F_{ys}(f)}, & a_{14}(f) &= \frac{L_r(f)}{F_{ys}(f)}. \end{aligned}$$

By injecting a pure wave of each type into Leg 1 it is possible to determine the elemental transfer functions for each of the three matrices of Joints 'A', 'B', and 'C'; this method computes the columns of each scattering matrix. In principle, the determination of the elemental transfer functions for each matrix is straight forward. In practice, it is not easily achieved.

#### 4.3.1 Transmission Function Derivation Using the Concept of Reciprocity

Describing the dynamic response of a structure to a given excitation is a very difficult problem. Consideration is made of the simple case where a structure is excited by a single force component at one location and the response velocity is measured at another location. By using transfer mobility it is possible to relate the force at one location to the response velocity at another location. It is also possible to demonstrate that the transfer

mobility is reciprocal [5]. Namely, the ratio of the excitation force at some location ‘a’ to the response velocity at location ‘b’ is equal to the ratio of the force measured at location ‘b’ and the velocity at location ‘a’.

Reciprocity is only valid if three basic requirements are satisfied:

1. The system should be passive; no sources other than those used for excitation should exist.
2. The system should be linear; the response should be at the same frequency as the excitation and proportional to it.
3. The system should be bilateral. When the phase or direction of the excitation is altered the response should change in a likewise manner.

Reciprocity can also be viewed as: the ratio of the power in a transmitted flexural wave to that in an incident longitudinal wave equaling the ratio of the power in a transmitted longitudinal wave to that in an incident flexural wave [4]. Namely,

$$\frac{P_{f_{out}}}{P_{l_{in}}} = \frac{P_{l_{out}}}{P_{f_{in}}}. \quad (4.1)$$

As an example, acceleration for an input longitudinal wave takes the following form

$$a_{l_{in}} = \omega v_{l_{in}} = \frac{\omega F_{l_{in}}}{Z_{l_{in}}} = \frac{\omega F_{l_{in}}}{\rho c_l}. \quad (4.2)$$

Likewise, acceleration for an output flexural wave takes the following form

$$a_{f_{out}} = \omega v_{f_{out}} = \frac{\omega F_{f_{out}}}{Z_{f_{out}}} = \frac{\omega F_{f_{out}}}{\rho c_f}. \quad (4.3)$$

The transmission function for each joint is defined as the ratio of the output acceleration of a specific wave type to the input acceleration of a specific wave type. For the case where the excitation wave type is longitudinal and the output wave type is flexural the

transmission function,  $\tau_1$ , is defined as

$$\tau_1 \equiv \frac{a_{f_{out}}}{a_{l_{in}}} \equiv \frac{F_{f_{out}} c_l}{F_{l_{in}} c_f}. \quad (4.4)$$

Using reciprocity it is then possible to determine the transmission function,  $\tau_2$ , for a given input flexural wave and a resulting longitudinal wave

$$\tau_2 \equiv \frac{a_{l_{out}}}{a_{f_{in}}} \equiv \frac{F_{l_{out}} c_f}{F_{f_{in}} c_l}. \quad (4.5)$$

It is this tool, reciprocity, which permits additional elemental transmission functions of the scattering matrices to be determined.

Expanding (4.1) results in

$$\frac{F_{f_{out}} a_{f_{out}}}{F_{l_{in}} a_{l_{in}}} = \frac{F_{l_{out}} a_{l_{out}}}{F_{f_{in}} a_{f_{in}}} \quad (4.6)$$

for a harmonic response.

Substitution of  $\tau_1$  and  $\tau_2$  into (4.6) yields

$$\frac{F_{f_{out}}^2}{F_{l_{in}}^2} = \frac{F_{l_{out}}^2 c_f^2}{F_{f_{in}}^2 c_l^2}, \quad (4.7)$$

and simplification results in

$$\frac{c_l}{c_f} \frac{F_{f_{out}}}{F_{l_{in}}} = \frac{F_{l_{out}}}{F_{f_{in}}}. \quad (4.8)$$

The left-hand side of (4.8) is, by definition,  $\tau_1$  and multiplying both sides of (4.8) by the ratio of flexural phase speed to longitudinal phase speed results in

$$\tau_1 \frac{c_f}{c_l} = \frac{F_{l_{out}}}{F_{f_{in}}} \frac{c_f}{c_l}. \quad (4.9)$$

The right-hand side of (4.9) is, by definition,  $\tau_2$  and further manipulation of (4.9) results in the reciprocal relation between  $\tau_1$  and  $\tau_2$ ,

$$\tau_2 = \tau_1 \frac{c_f}{c_l}. \quad (4.10)$$

Alternatively, (4.10) may be written as

$$\tau_2 = \tau_1 \sqrt{\frac{\omega \kappa}{c_l}}, \quad (4.11)$$

where  $c_f = \sqrt{\omega \kappa c_l}$ .

Similarly, for the case in which the reciprocal transmission function is desired for the case in which a torsional waveform is present, the relation becomes

$$\tau_2 = \tau_1 \frac{c_T}{c_l}. \quad (4.12)$$



# Chapter 5

## Analytical Models and Predictions

### 5.1 Transmission from Flexural Wave Excitation

Wave transmission through right-angled structural joints has been studied previously [3 - 9]. Guo developed a generalized analytical formulation [10] focusing on flexural wave transmission through structural joints without the restriction to a right-angle. This analysis is two-dimensional and is based on a joint with two elastic beams joined at an angle  $\theta$  depicted in Fig. 5-1. The joint is illustrated in Fig. 5-2 and is modeled with stiffness, dissipation, and mass, in three degrees of freedom.

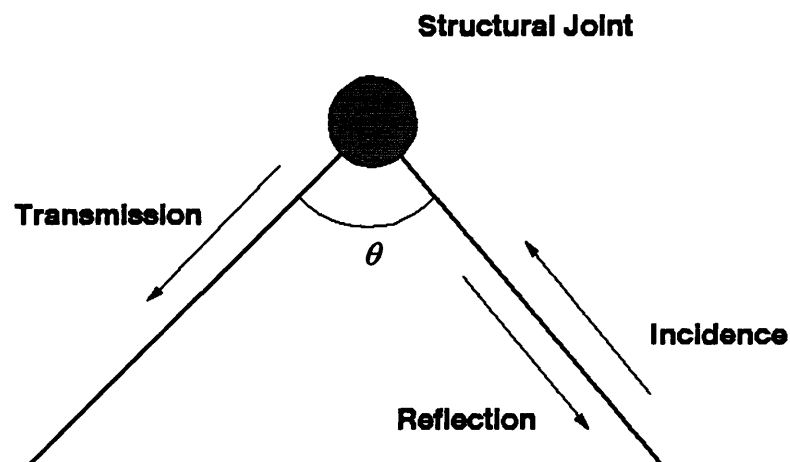


Figure 5-1: Two-dimensional structural joint.

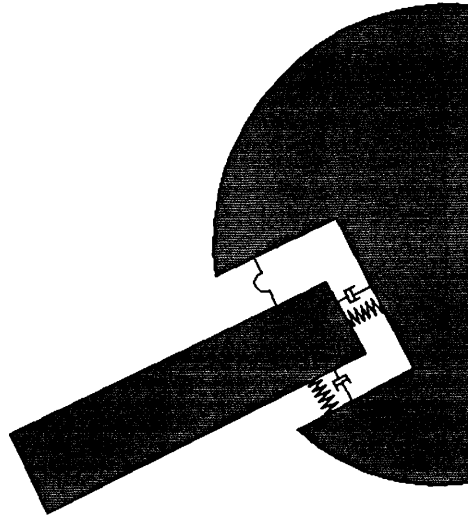


Figure 5-2: Model of two-dimensional joint with stiffness, dissipation and mass.

This model assumes incident flexural waves are produced at a distance far away from the joint so that the evanescent field from incident bending motion can be neglected. In studying wave-joint interactions the energy carried by the different wave types is used to measure reflection, transmission, dissipation, and conversion. For this case of harmonic waves, the energy is measured by the power flow of flexural and longitudinal displacements.

In this model, incident waves may cause motion at the joint in three degrees of freedom: longitudinal displacement, transverse displacement, and rotation. Spring-dashpots are used in all degrees of freedom so that the effects of joint constraints on motion can be studied independently. The springs are assumed to have complex spring constants such that the real part specifies the spring stiffness and the imaginary part specifies the loss factor. Through the use of complex spring impedances, the forces acting on the joint include both spring forces and dissipative forces. Similarly, the moments are given by the rotation of the joint through the use of a complex spring constant in rotation. The equations of motion of the joint are determined to be

$$\omega^2 mX = \sin(\theta / 2)(f_{L1} - f_{L2}) + \cos(\theta / 2)(f_{F1} + f_{F2}), \quad (5.1)$$

$$\omega^2 mY = \cos(\theta / 2)(f_{L2} - f_{L1}) + \sin(\theta / 2)(f_{F1} + f_{F2}), \quad (5.2)$$

$$\omega^2 m\Phi = (M_2 - M_1) / \kappa^2. \quad (5.3)$$

The motion of the joint can then be specified by balancing all forces and moments acting on the joint, these forces and moments being identical to those acting on the two connecting beams at the point where the two meet. The forces acting on the joint are

$$f_{L1} = z_L [Y \cos(\theta / 2) + X \sin(\theta / 2) - u_1], \quad (5.4)$$

$$f_{L2} = z_L [Y \cos(\theta / 2) - X \sin(\theta / 2) + u_2], \quad (5.5)$$

$$f_{F1} = z_F [Y \sin(\theta / 2) - X \cos(\theta / 2) - w_1], \quad (5.6)$$

$$f_{F2} = z_F [Y \sin(\theta / 2) + X \cos(\theta / 2) - w_2]. \quad (5.7)$$

Similarly, the moments are given by the rotation of the joint,  $\Phi$ , and rotation present at the ends of the two beams,  $w_1'$  and  $w_2'$ ,

$$M_1 = z_M (w_1' - \Phi) \text{ and } M_2 = z_M (\Phi - w_2'). \quad (5.8)$$

By substituting (5.4) through (5.8) into (5.1) through (5.3) the displacements and rotation may be determined as

$$X = \frac{z_L \sin(\theta / 2)(u_1 + u_2) - z_F \cos(\theta / 2)(w_1 - w_2)}{2z_L \sin^2(\theta / 2) + 2z_F \cos^2(\theta / 2) - \omega^2 m}, \quad (5.9)$$

$$Y = \frac{z_L \cos(\theta / 2)(u_1 - u_2) + z_F \sin(\theta / 2)(w_1 + w_2)}{2z_L \cos^2(\theta / 2) + 2z_F \sin^2(\theta / 2) - \omega^2 m}, \quad (5.10)$$

$$\Phi = \frac{z_M (w_1' + w_2')}{2z_M - \omega^2 m \kappa^2}. \quad (5.11)$$

By setting  $M$  to zero and setting all joint stiffnesses to infinity it is possible to derive the efficiency of transmission for the rigid joint.

For rigid joints without mass [10], the flexural-to-longitudinal transmission function (ratio of output acceleration to input acceleration) is

$$T_L = -2\mu \sin \theta \frac{[2(i + \mu) + (i\mu + 1)(1 - \cos \theta)]}{\mu(1+i)(2 \cos \theta - 3 - 3 \cos^2 \theta) - 2(\mu^2 + i) \sin^2 \theta}, \quad (5.12)$$

where  $\mu = \frac{c_f}{c_l}$ .

Since no analytical solutions exist for the three-dimensional joint, comparison will be made between the two-dimensional analytical model and the three-dimensional physical model. For an incident flexural wave on Leg 1 and a transmitted longitudinal wave on Leg 3 ( $\theta = 90^\circ$ ), (5.12) reduces to

$$T_L = 2\mu \frac{(2i + 2\mu + i\mu + 1)}{(3\mu + 3i\mu + 2\mu^2 + 2i)}. \quad (5.13)$$

Similarly, for an incident flexural wave on Leg 1 and a transmitted longitudinal wave on Leg 2 ( $\theta = 71.5^\circ$ ), (5.12) reduces to

$$T_L = \frac{3.8\mu i + 3.8\mu^2 + 1.298\mu^2 i + 1.298\mu}{2.667\mu + 2.667\mu i + 1.8\mu^2 + 1.8i}. \quad (5.14)$$

## 5.2 Transmission from Longitudinal Wave Excitation

Longitudinal wave propagation through right-angled joints has been analyzed by Leung and Pinnington [8]. The analytical solutions for the rigid joint approach that presented by Cremer [4]. This model assumes an incident longitudinal wave of the form

$$v_{x1} = v_{x1+} (e^{-jk_{L1}x} + r_{LL} e^{+jk_{L1}x}). \quad (5.15)$$

The transmitted waves take the form of

$$v_{x2} = v_{x1+} (t_{LB} e^{-jk_{B2}y} + t_{jLB} e^{-k_{B2}y}), \quad (5.16)$$

$$v_{y2} = v_{x1+} t_{LL} e^{-jk_{L2}y}. \quad (5.17)$$

These equations are then substituted into the boundary conditions. The boundary conditions consist of matching moments and rotational velocity on both sides of the joint. The final boundary condition which must be applied consists of matching shear forces. The incident longitudinal shear force will create a bending wave in the second leg and this force is equal to the bending shear force in the second leg. The incident longitudinal force has no effect on the longitudinal wave in the second leg.

It is from these boundary conditions that the transmission efficiencies are derived. In the case of a rigid joint for which the x-direction, y-direction, and rotational impedances are infinite, the flexural transmission function (ratio of output acceleration to input acceleration) for an incident longitudinal wave [4] is expressed as

$$\tau_F = \frac{5\mu + 8\mu^2}{2 + 6\mu + 9\mu^2}. \quad (5.18)$$

Similarly, the longitudinal transmission function (ratio of output acceleration to input acceleration) for an incident longitudinal wave can be expressed as

$$\tau_L = \frac{\mu^2}{2 + 6\mu + 9\mu^2}. \quad (5.19)$$

# Chapter 6

## Experimental Results

This chapter presents all of the experimentally determined data. Section 6.1 presents averaged wave type transmission efficiencies for data determined experimentally. Section 6.2 presents averaged wave type transmission efficiencies for data determined through reciprocity. Section 6.3 provides relative joint transmission efficiencies. Scattering matrix elements determined through experimentation and through reciprocity are presented in Sections 6.4 and 6.5, respectively. Some of the figures in Sections 6.4 and 6.5 exhibit nodal behavior. Nodal behavior is that behavior where the response is very small because the accelerometers are positioned at or close to a node for a specific frequency.

### 6.1 Experimentally Determined Data

Tables 6.1 through 6.4 depict the average transmission efficiency (dB) for each wave type for each joint. The data has been averaged, in dB-space, over the frequency range 0 - 15 kHz. Tables 6.1 and 6.2 depict the transmission efficiencies of each wave type for longitudinal excitation. Tables 6.3 and 6.4, in contrast to Tables 6.1 and 6.2, depict the longitudinal transmission efficiencies for the incident wave types presented; this data has been determined through reciprocity.

	Joint 'A'	Joint 'B'	Joint 'C'
Flexural (y-direction)	-16	-23	-41
Flexural (x-direction)	-15	-41	-53
Torsional	-23	-29	-44
Longitudinal	-14	-22	-40

Table 6.1: Average transmission efficiency for Leg 2 given longitudinal excitation on Leg 1.

	Joint 'A'	Joint 'B'	Joint 'C'
Flexural (y-direction)	-11	-22	-45
Flexural (x-direction)	-18	-30	-48
Torsional	-17	-30	-53
Longitudinal	-7	-10	-31

Table 6.2: Average transmission efficiency for Leg 3 given longitudinal excitation on Leg 1.

	Joint 'A'	Joint 'B'	Joint 'C'
Flexural (y-direction)	-32	-38	-57
Flexural (x-direction)	-31	-57	-68
Torsional	-27	-33	-48

Table 6.3: Average longitudinal transmission efficiency for Leg 2 given excitation on Leg 1.

	Joint 'A'	Joint 'B'	Joint 'C'
Flexural (y-direction)	-27	-38	-60
Flexural (x-direction)	-34	-46	-64
Torsional	-21	-34	-57

Table 6.4: Average longitudinal transmission efficiency for Leg 3 given excitation on Leg 1.

It should be noted that for all wave types Joint 'C' exhibits, overall, the least transmission. Joint 'B' exhibits greater transmission, overall, for all wave types with Joint 'A' clearly demonstrating maximum, overall, transmission of all wave types.

### *Joint 'A' (Rigid Joint)*

Predicted transmission functions do not exist for elements b14, b24, b34, and b44 since an analytical solution is only available for a right-angled joint. Elements b14 through b44 are wave type transmission functions on Leg 2 for longitudinal excitation on Leg 1.

The flexural transmission functions for Leg 3, c14 and c24 (Fig. 6-5), roughly obey the predicted functions. The predicted values approximately equal the experimental values between 4 and 9 kHz. At frequencies above 10 kHz there is a significant reduction in transmission when compared to the prediction. The flexural transmission (y-direction) exhibits significant reduction at 6.2 kHz since this is likely to be a result of nodal behavior (flexural wavelength at 6.2 kHz is 0.056 m).

Longitudinal transmission, c44 (Fig. 6-6), deviates significantly from the predicted function. It is believed that this response is specific to the design of this joint and that it cannot be explained by the simplified two-dimensional analytical model on which the solution is based. This behavior may be explained by three separate mechanisms.

First, as the wave interacts with the joint the radial oscillatory expansion and contraction of the leg forces that portion of the joint body which is in direct contact (a physical boundary condition) with the leg to undergo identical oscillatory radial expansion and contraction as illustrated in Fig. 6-1. This creates a radially outward propagating longitudinal wave in the joint body. This wave propagates around the circumference of the joint body until it interacts with Leg 3 and causes Leg 3 to undergo oscillatory expansion and contraction in a similar, but reverse, manner that the incident wave on Leg 1 had on the joint body. This results in longitudinal wave generation in Leg 3.

Secondly, as the longitudinal wave propagates along the leg it exhibits translational oscillatory behavior. This oscillatory translation forces that portion of the joint body which is in direct contact (a physical boundary condition) with the leg to undergo identical oscillatory translational movement as illustrated in Fig. 6-2. This movement creates a radial flexural wave which propagates around the body until it interacts with the opposite leg (Leg 3) in a similar, but reverse, manner that the incident wave on Leg 1 had on the joint body. This flexural wave causes translational oscillation in Leg 3 thereby creating a longitudinal wave in Leg 3.



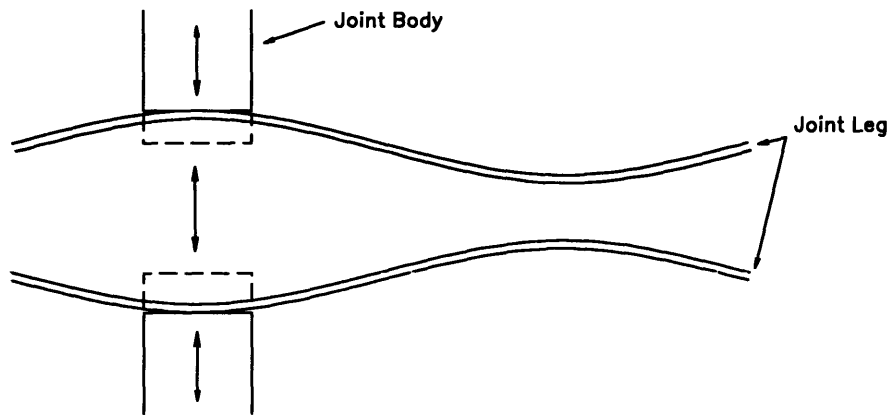


Figure 6-1: Cross-section of the leg/joint interaction demonstrating radial oscillatory expansion and contraction (deflection is greatly exaggerated).

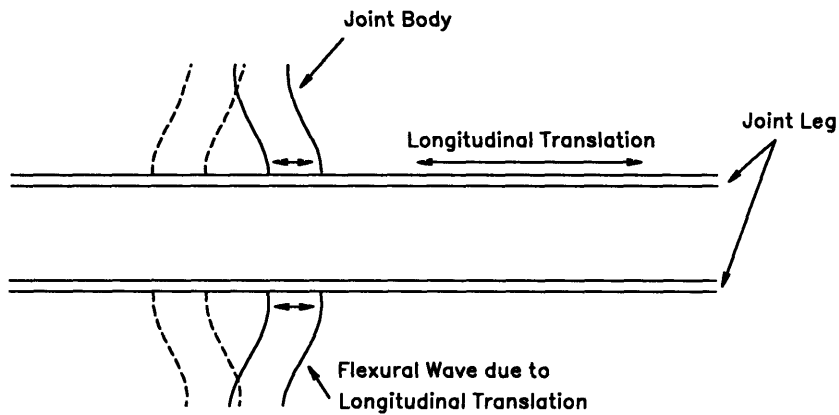


Figure 6-2: Cross-section of the leg/joint interaction demonstrating translational oscillatory behavior (deflection is greatly exaggerated).

Lastly, it should be noted that all the legs of the rigid joint are spot-welded not only where the legs penetrate the joint body, but at their ends to one another in the interior of the hollow joint body. This forces a portion of the translational oscillatory behavior that Leg 1 possessed to be transmitted into Leg 3, thereby creating a longitudinal wave in Leg 3.

It is important to note that the longitudinal transmission function of Leg 3 (c44) indicates values above 0 dB from 4.5 kHz to 6.5 kHz. Values as high as +3 dB are noted. This is believed to be due to the contamination from the transverse sensitivity of the accelerometer or from slight misalignment of the accelerometers. An estimation of the level of contamination due to transverse sensitivity alone results in no more than 5 dB. Although not confirmed through experimentation, the rigid joint is not expected to exhibit non-linear response to excitation. Therefore, non-linearity of the rigid joint is not believed to be a contributing factor.

#### *Joint 'B' (Teflon-Coated Joint)*

Predicted transmission functions do not exist for any of the scattering matrix elements for Joint 'B'. Torsional transmission for Leg 2, e34 (Fig. 6-8), is on the average -30 dB with slightly higher values below 3 kHz and above 11 kHz. It is expected that torsional transmission will be very low because of the relaxed rotational stiffness associated with the Teflon coated spheres.

Longitudinal transmission function, f44 (Fig. 6-10), exhibits positive values of transmission efficiency. It is believed that these values are evidence of contamination from accelerometer transverse sensitivity, slight accelerometer misalignment, and non-linear behavior of Joint 'B'. In the case of Joint 'B', it is probable that the joint exhibits non-linear behavior due to the presence of 'stiction' which is a phenomenon generally known to be present when surfaces must move relative to one another.

#### *Joint 'C' (Visco-Elastic Joint)*

Predicted transmission functions do not exist for any scattering matrix elements for Joint 'C'. Flexural transmission in Leg 2, h14 and h24 (Fig. 6-11), is very low at frequencies above 7.5 kHz. Average transmission efficiency for the flexural wave in the y-direction above 7.5 kHz is approximately -60 dB. Average transmission efficiency for the flexural wave the x-direction

above 7.5 kHz is approximately -70 dB. Torsional transmission efficiency in Leg 2, h34 (Fig. 6-12), exhibits a relatively uniform decrease with nodal response at approximately 5.5 kHz.

Flexural transmission efficiency in Leg 3, k14 and k24 (Fig. 6-13), exhibits relatively low levels above 7.5 kHz. Average flexural transmission efficiency in the y-direction above 7.5 kHz is approximately -60 dB. Average flexural transmission efficiency in the x-direction above 7.5 kHz is approximately -70 dB. Torsional transmission efficiency in Leg 3, k34 (Fig. 6-14) exhibits nodal behavior at approximately 1.5 kHz.

## **6.2 Data Determined by Reciprocity**

### *Joint 'A' (Rigid joint)*

Predicted transmission functions exist for scattering matrix elements b41, b42, c41, and c42; a physical interpretation of the use of reciprocity may be found in Chapter 4. Predicted transmission functions do not exist for elements b43 and c43 since analytical solutions do not exist in the case of an incident torsional wave and an output longitudinal wave.

The most significant feature about flexural excitation on Leg 2 and Leg 3 (elements b41, b42, c41, and c42 (Fig. 6-15 through Fig. 6-17)) is the disparity between the experimental functions and the predicted functions. The predicted function is, on average, 20 dB greater than the experimental result. It is believed that this discrepancy can be attributed to the effect of blocking mass. The predicted function is modeled after a joint with zero mass. As the mass increases, the impedance mismatch between longitudinal waves and flexural waves increases. The energy converted from flexural to longitudinal waves decreases rapidly as this impedance mismatch increases.

It is also believed that this disparity is not attributable to the structural discontinuity where the leg extensions are screwed into the joint legs. A simple model involving a junction between a hollow leg (0.5 inch diameter and 0.068 inch wall thickness) and a solid leg (0.5 inch diameter) indicates that the flexural energy transmitted, past this discontinuity, to the joint is reduced by less than 1 dB.

In addition to the disparity between the predicted function and the experimentally determined function, scattering element, c41 (Fig. 6-16), exhibits nodal behavior at approximately 6.5 kHz.

#### *Joint 'B' (Teflon-Coated Joint)*

Predicted transmission functions, derived by reciprocity, do not exist for any scattering matrix elements for the Joint 'B'.

#### *Joint 'C' (Visco-Elastic Joint)*

Predicted transmission functions, derived by reciprocity, do not exist for any scattering matrix elements for Joint 'C'. Longitudinal transmission in Leg 2 due to flexural excitation, h41 and h42 (Fig. 6-21), is very low at frequencies above 7.5 kHz. Average longitudinal transmission efficiency for the flexural wave excitation in the y-direction above 7.5 kHz is approximately -70 dB. Average longitudinal transmission efficiency for the flexural wave in the x-direction above 7.5 kHz is approximately -80 dB. Longitudinal transmission efficiency in Leg 2 from torsional excitation on Leg 1, h43 (Fig. 6-22), exhibits a relatively uniform decrease with nodal response at approximately 5.5 kHz.

Longitudinal transmission efficiency in Leg 3 for flexural excitation on Leg 1, k41 and k42 (Fig. 6-22 and Fig. 6-23), is relatively low above 7.5 kHz. Average longitudinal transmission efficiency in the y-direction above 7.5 kHz is approximately -75 dB. Average longitudinal transmission efficiency in the x-direction above 7.5 kHz is approximately -80 dB. Longitudinal transmission efficiency in Leg 3 for torsional excitation, k43 (Fig. 6-23), exhibits nodal behavior at approximately 1.5 kHz.

### **6.3 Relative Joint Response**

Tables 6.5 through 6.18 illustrate Joint 'B' and 'C' performance relative to Joint 'A'. Positive values indicate higher transmission for the respective joint while negative numbers

indicate transmission levels that are less than Joint 'A'. Bandwidth averaging was conducted in dB-space.

Frequency Band (kHz)	Joint 'B'	Joint 'C'
0 - 3	4	+1
3 - 6	-13	-14
6 - 9	-15	-39
9 - 12	-7	-38
12 - 15	-3	-41

Table 6.5: Comparative values for Leg 2 flexural transmission (y-direction) given longitudinal excitation on Leg 1.

Frequency Band (kHz)	Joint 'B'	Joint 'C'
0 - 3	-11	-9
3 - 6	-38	-34
6 - 9	-36	-44
9 - 12	-38	-50
12 - 15	-16	-49

Table 6.6: Comparative values for Leg 2 flexural transmission (x-direction) given longitudinal excitation on Leg 1.

Frequency Band (kHz)	Joint 'B'	Joint 'C'
0 - 3	+5	0
3 - 6	-16	-18
6 - 9	-18	-31
9 - 12	-4	-25
12 - 15	0	-32

Table 6.7: Comparative values for Leg 2 torsional transmission given Longitudinal excitation on Leg 1.

Frequency Band (kHz)	Joint 'B'	Joint 'C'
0 - 3	-3	-2
3 - 6	-12	-25
6 - 9	-23	-36
9 - 12	-10	-33
12 - 15	+3	-37

Table 6.8: Comparative values for Leg 2 longitudinal transmission given longitudinal excitation on Leg 1.

Frequency Band (kHz)	Joint 'B'	Joint 'C'
0 - 3	-2	-3
3 - 6	-15	-31
6 - 9	-18	-47
9 - 12	-10	-43
12 - 15	-11	-47

Table 6.9: Comparative values for Leg 3 flexural transmission (y-direction) given longitudinal excitation on Leg 1.

Frequency Band (kHz)	Joint 'B'	Joint 'C'
0 - 3	-7	+5
3 - 6	-34	-24
6 - 9	-20	-42
9 - 12	-2	-43
12 - 15	+3	-44

Table 6.10: Comparative values for Leg 3 flexural transmission (x-direction) given longitudinal excitation on Leg 1.

Frequency Band (kHz)	Joint 'B'	Joint 'C'
0 - 3	-6	-12
3 - 6	-16	-31
6 - 9	-20	-41
9 - 12	-14	-45
12 - 15	-10	-51

Table 6.11: Comparative values for Leg 3 torsional transmission given longitudinal excitation on Leg 1.

Frequency Band (kHz)	Joint 'B'	Joint 'C'
0 - 3	+2	-2
3 - 6	-13	-21
6 - 9	-15	-35
9 - 12	+3	-26
12 - 15	+8	-32

Table 6.12: Comparative values for Leg 3 longitudinal transmission given longitudinal excitation on Leg 1.

Frequency Band (kHz)	Joint 'B'	Joint 'C'
0 - 3	+4	+1
3 - 6	-12	-9
6 - 9	-15	-39
9 - 12	-7	-38
12 - 15	-3	-41

Table 6.13: Comparative values for Leg 2 longitudinal transmission given flexural (y-direction) excitation on Leg 1.

Frequency Band (kHz)	Joint 'B'	Joint 'C'
0 - 3	-11	-9
3 - 6	-38	-34
6 - 9	-36	-44
9 - 12	-28	-49
12 - 15	-16	-50

**Table 6.14: Comparative values for Leg 2 longitudinal transmission given flexural (x-direction) excitation on Leg 1.**

Frequency Band (kHz)	Joint 'B'	Joint 'C'
0 - 3	+5	0
3 - 6	-16	-19
6 - 9	-18	-31
9 - 12	-5	-25
12 - 15	0	-32

**Table 6.15: Comparative values for Leg 2 longitudinal transmission given torsional excitation on Leg 1.**

Frequency Band (kHz)	Joint 'B'	Joint 'C'
0 - 3	-2	-3
3 - 6	-15	-31
6 - 9	-18	-47
9 - 12	-10	-38
12 - 15	-11	-47

**Table 6.16: Comparative values for Leg 3 longitudinal transmission given flexural (y-direction) excitation on Leg 1.**



Frequency Band (kHz)	Joint 'B'	Joint 'C'
0 - 3	-9	+5
3 - 6	-34	-23
6 - 9	-20	-42
9 - 12	-2	-43
12 - 15	+3	-43

Table 6.17: Comparative values for Leg 3 longitudinal transmission given flexural (x-direction) excitation on Leg 1.

Frequency Band (kHz)	Joint 'B'	Joint 'C'
0 - 3	-6	-12
3 - 6	-16	-31
6 - 9	-20	-41
9 - 12	-14	-45
12 - 15	-10	-51

Table 6.18: Comparative values for Leg 3 longitudinal transmission given torsional excitation on Leg 1.

For the tables shown above the relative differences in the performance of Joints 'B' and 'C' are sometimes quite small (within 3 to 5 dB). For these cases it is not possible to determine, with reasonable confidence, which joint exhibits reduced transmission since these differences are statistically insignificant. It is only for very limited frequency bandwidths that Joint 'B' exhibits lower relative transmission than Joint 'C'. Joint 'B' Leg 3 flexural transmission (x-direction) in the bandwidth 3 - 6 kHz (Table 6.10) exhibits approximately a 10 dB lower transmission level than Joint 'C'. Joint 'B' longitudinal transmission on Leg 3, given flexural excitation (x-direction) on Leg 1, exhibits approximately a 11 dB lower transmission level than Joint 'C'. For all other wave types, Joint 'C' exhibits lower levels of transmission for which there is statistical

significance. It should also be noted that Joint 'C' exhibits especially low levels of transmission at high frequencies (12 - 15 kHz). For only one case, Table 6.16, is the relative transmission level between Joint 'C' and 'B' less than 30 dB. Similar differences are also noted for many of the wave types in the next higher frequency range (9 - 12 kHz), although the differences are not as consistent and substantial.

Two-dimensional analytical theory [10] indicates that changes in rotational stiffness result in no noticeable change in conversion from flexural to longitudinal energy. This is clearly not the case from experimental data (Tables 6.16 and 6.17). Joints 'B' and 'C' demonstrate significant reductions in transmission for frequencies greater than 3 kHz.

Two-dimensional analytical theory also indicates that for the right-angled joint reduction in rotational stiffness results in a reduction in flexural transmission for longitudinal excitation. For a right-angled joint transverse displacement of one leg is coupled to longitudinal displacement in the other. Transmission of flexural waves is largely due to bending moments, regardless of the frequency domain. If the rotational stiffness is decreased, the only mechanism that transmits flexural waves is weakened. Hence, flexural wave transmission is reduced essentially over the entire frequency domain. This is supported by Table 6.2. Joint 'B', relative to Joint 'A', exhibits an 11 dB and 12 dB reduction in flexural (y and x-direction, respectively) transmission on Leg 3 for longitudinal excitation on Leg 1. Joint 'C', relative to Joint 'A', exhibits a 34 dB and 30 dB reduction in flexural (y and x-direction, respectively) transmission on Leg 3 for longitudinal excitation on Leg 1.

The disparity between the levels of transmission of longitudinal waves may also be partially explained on the basis of blocking mass. The mass of the joint causes an impedance mismatch between flexural and longitudinal energy. As the mass increases, the energy converted to longitudinal waves decreases rapidly as the mismatch of impedance increases due to the mass of the joint. Table 2.1 indicates that the mass of Joint 'A' is nearly half the mass of the pinned joints. Joints 'B' and 'C' exhibit much less transmission of longitudinal energy as evident in Tables 6.3 and 6.4. Joint 'B' exhibits an 11 dB and 12 dB reduction in longitudinal transmission on Leg 3 for flexural (y and x-direction, respectively) excitation on Leg 1. Joint 'C' exhibits a 33 dB and 30 dB reduction in longitudinal transmission on Leg 3 for flexural (y and x-direction, respectively) excitation on Leg 1.

The simple two-dimensional model gives good predictions for transmission and conversion provided that the typical wavelength in the legs is much larger than the typical dimension of the joint. Dissipation predictions may, however, under-estimate damping in real joints. This is because the local length scale for damping may be quite small when considering dissipation and the joint may no longer be modeled as a spring-dashpot system of zero size. Thus at high frequencies the damping demonstrated by a real joint may be much greater than that predicted by the two-dimensional model. This deficiency in the model may explain the significant reduction in transmission of flexural energy for longitudinal excitation, h14, h24, k14, and k24 (Fig. 6-11 and Fig. 6-13), above 7.5 kHz. Similarly, the longitudinal transmission for flexural excitation, h41, h42, k41, and k42 (Fig. 6-21 through Fig. 6-23), may be explained by this deficiency in the two-dimensional model.

#### **6.4 Scattering Matrix Elements Determined Experimentally**

Experimentally determined scattering matrix elemental functions are presented in this section. The middle function of each figure represents the average, in linear space, of ten samples. The upper and lower functions represent the upper and lower limits of the ten data samples.

Appendix E provides an example of a typical Matlab file which has been used for data post-processing. The time-series data of each wave type was first windowed as described in Chapter 3. A Fast-Fourier Transform was applied to each wave type. The transmission function was then determined by dividing the output wave type acceleration by the input wave type acceleration. Finally, this transmission function was converted to dB-space.

Graphical comparison is made to the predicted functions for scattering matrix elements c14, c24, and c44. c14 and c24 are transmission functions for output flexural waves in the y and x-directions, respectively, on Leg 3, for longitudinal excitation on Leg 1. c44 is the transmission function for longitudinal output on Leg 3 for longitudinal excitation on Leg 1. The predicted functions are generated from Chapter 5. Specifically, the predicted functions for c14 and c24 are developed from (5.18). The predicted function for c44 is developed from (5.19).

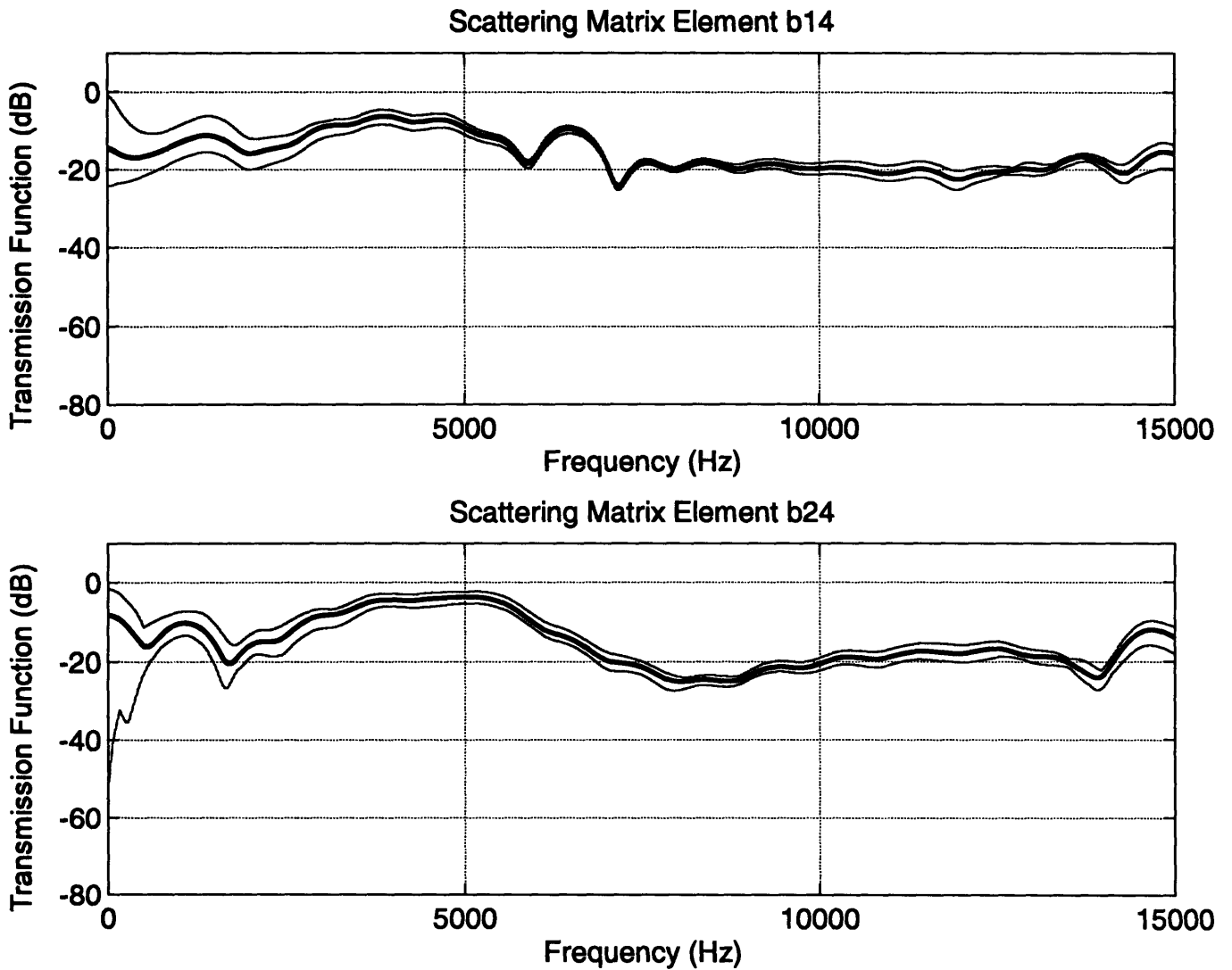


**Figure 6-3: Rigid Joint (Joint 'A') Scattering Matrix Elements b14 and b24 (Transmission Functions for output Flexural Waves measured on Leg 2 in the y-direction and x-direction, respectively, for Longitudinal Wave excitation on Leg 1). Compare to Joint 'B', Fig. 6-7 and Joint 'C', Fig. 6-11.**

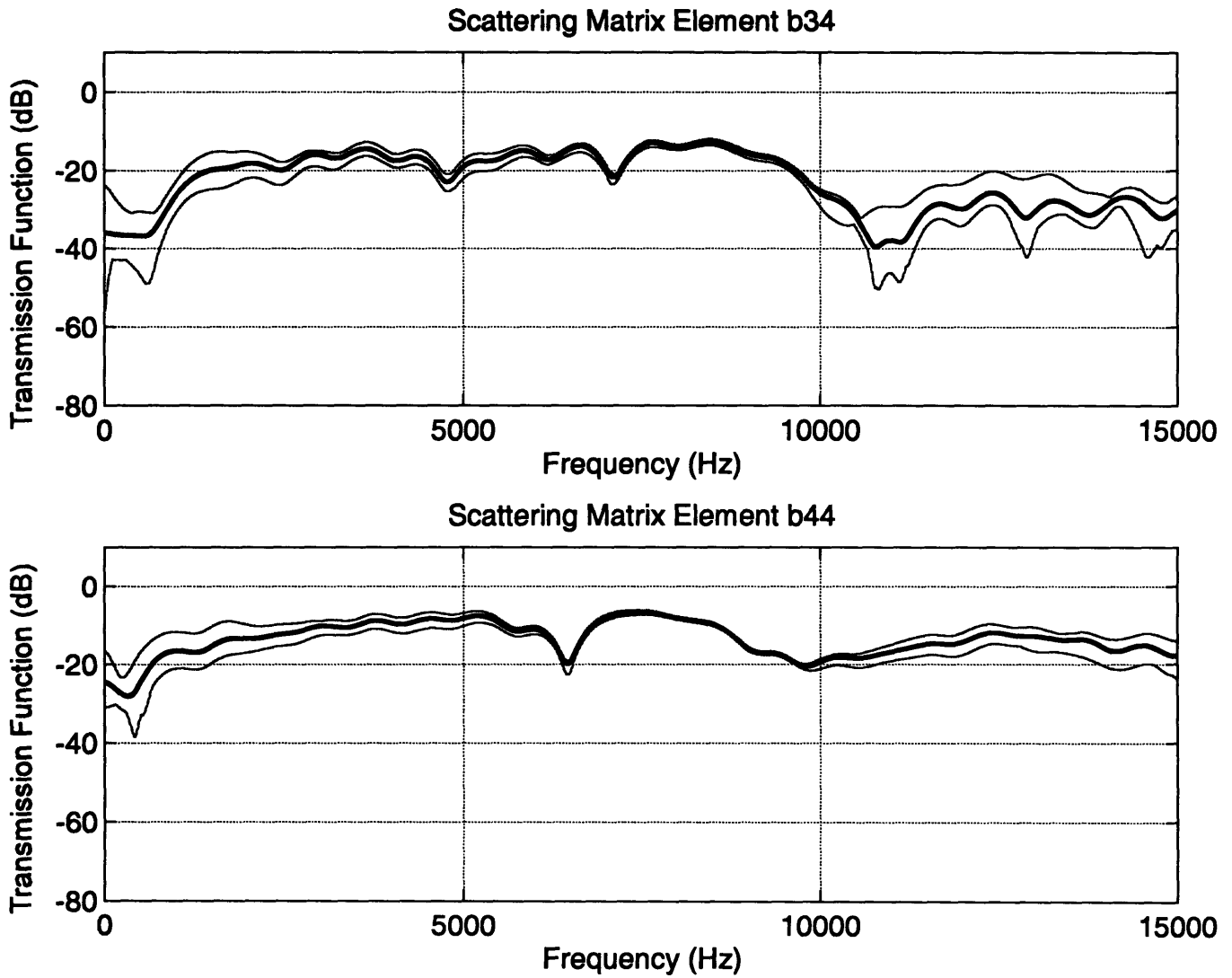


Figure 6-4: Rigid Joint (Joint 'A') Scattering Matrix Elements b34 and b44 (Transmission Functions for output Torsional and Longitudinal Waves measured on Leg 2, respectively, for Longitudinal Wave excitation on Leg 1). Compare to Joint 'B', Fig. 6-8 and Joint 'C', Fig. 6-12.

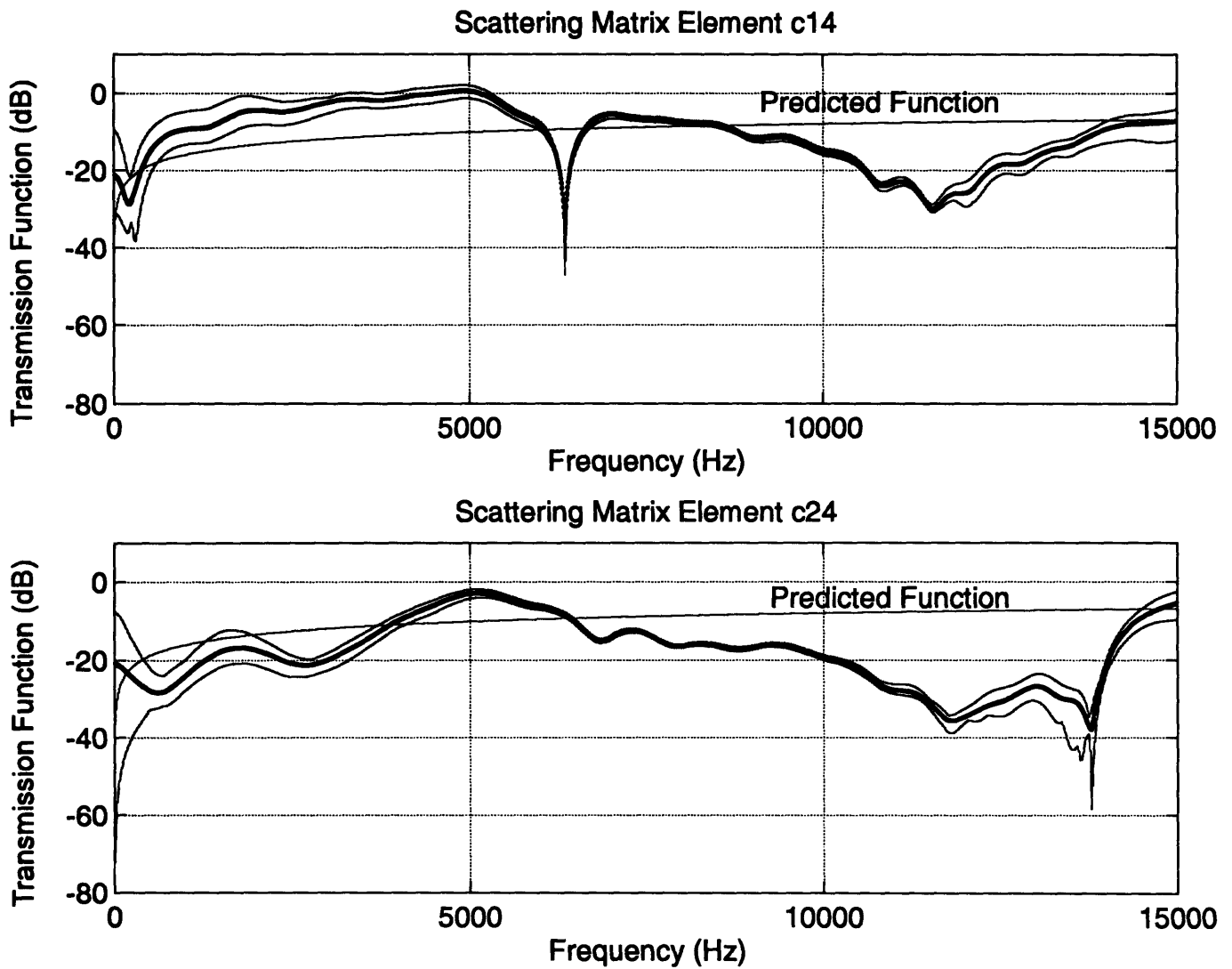


Figure 6-5: Rigid Joint (Joint 'A') Scattering Matrix Elements c14 and c24 (Transmission Functions for output Flexural Waves measured on Leg 3 in the y-direction and x-direction, respectively, for Longitudinal Wave excitation on Leg 1; predicted function provided for c14 and c24). Compare to Joint 'B', Fig. 6-9 and Joint 'C', Fig. 6-13.

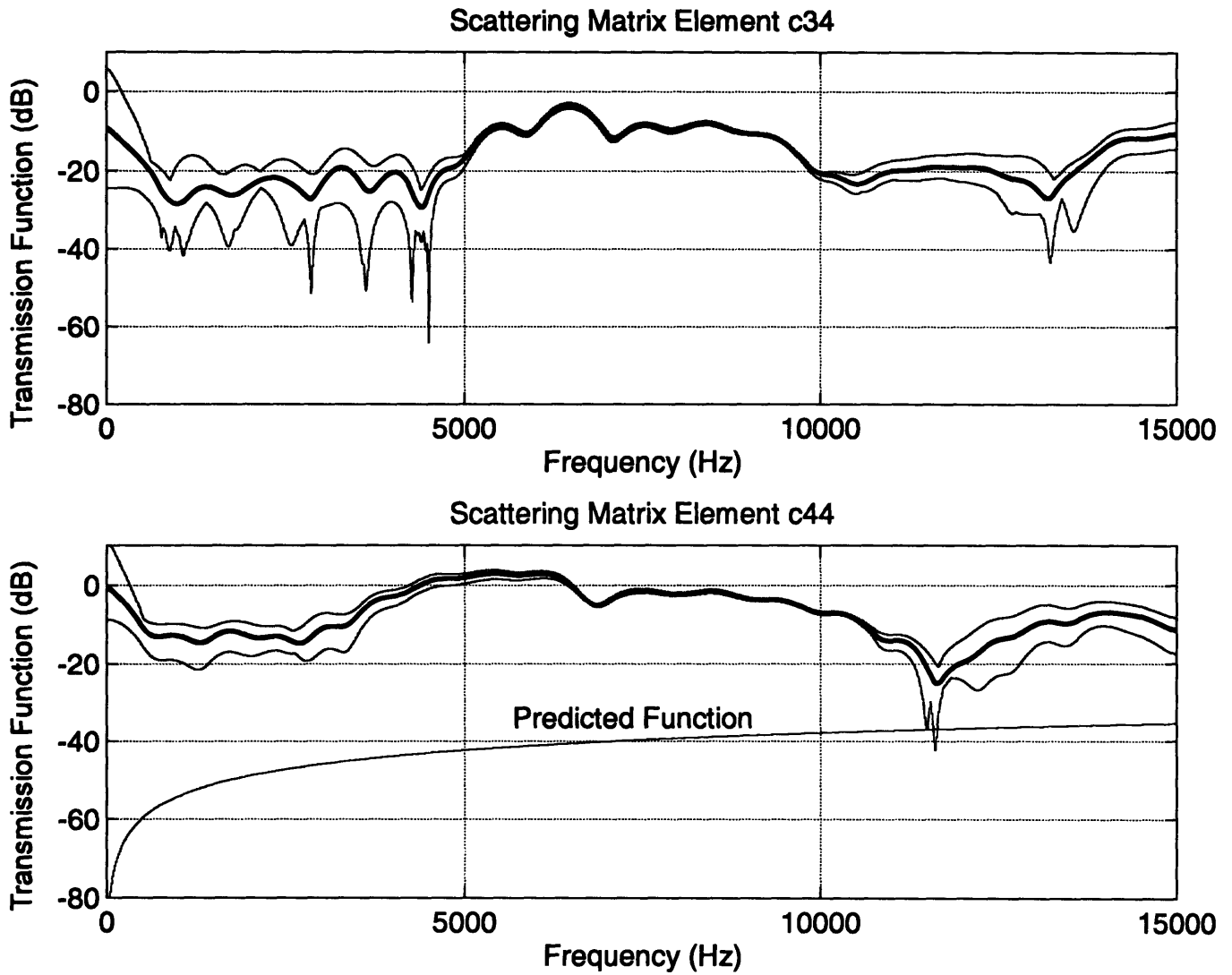
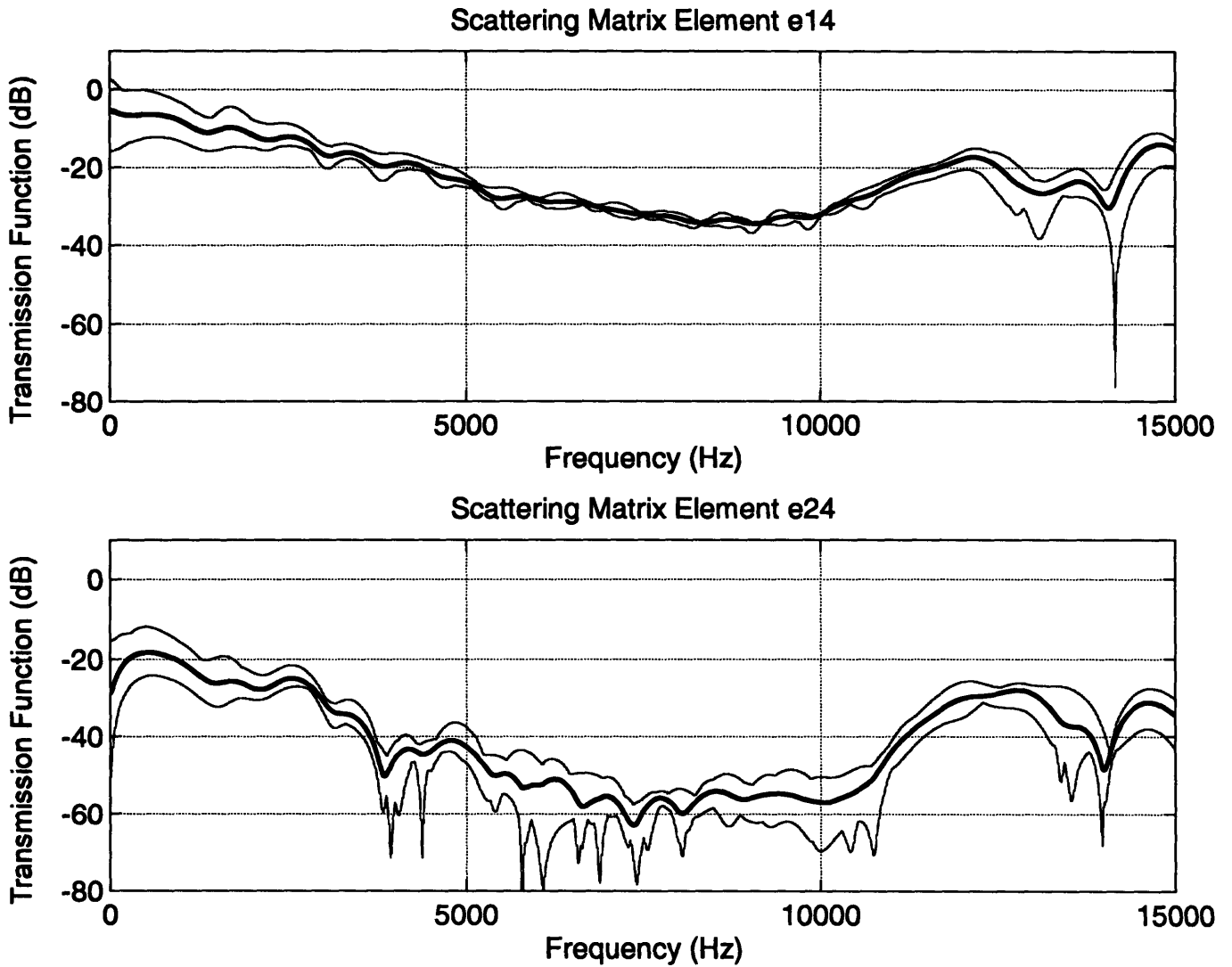


Figure 6-6: Rigid Joint (Joint 'A') Scattering Matrix Elements c34 and c44 (Transmission Functions for output Torsional and Longitudinal Waves measured on Leg 3, respectively, for Longitudinal Wave excitation on Leg 1; predicted function provided for c44). Compare to Joint 'B', Fig. 6-10 and Joint 'C', Fig. 6-14.



**Figure 6-7: Teflon Joint (Joint 'B') Scattering Matrix Elements e14 and e24**  
 (Transmission Functions for output Flexural Waves measured on Leg 2 in the y-direction and x-direction, respectively, for Longitudinal Wave excitation on Leg 1). Compare to Joint 'A', Fig. 6-3 and Joint 'C', Fig. 6-11.



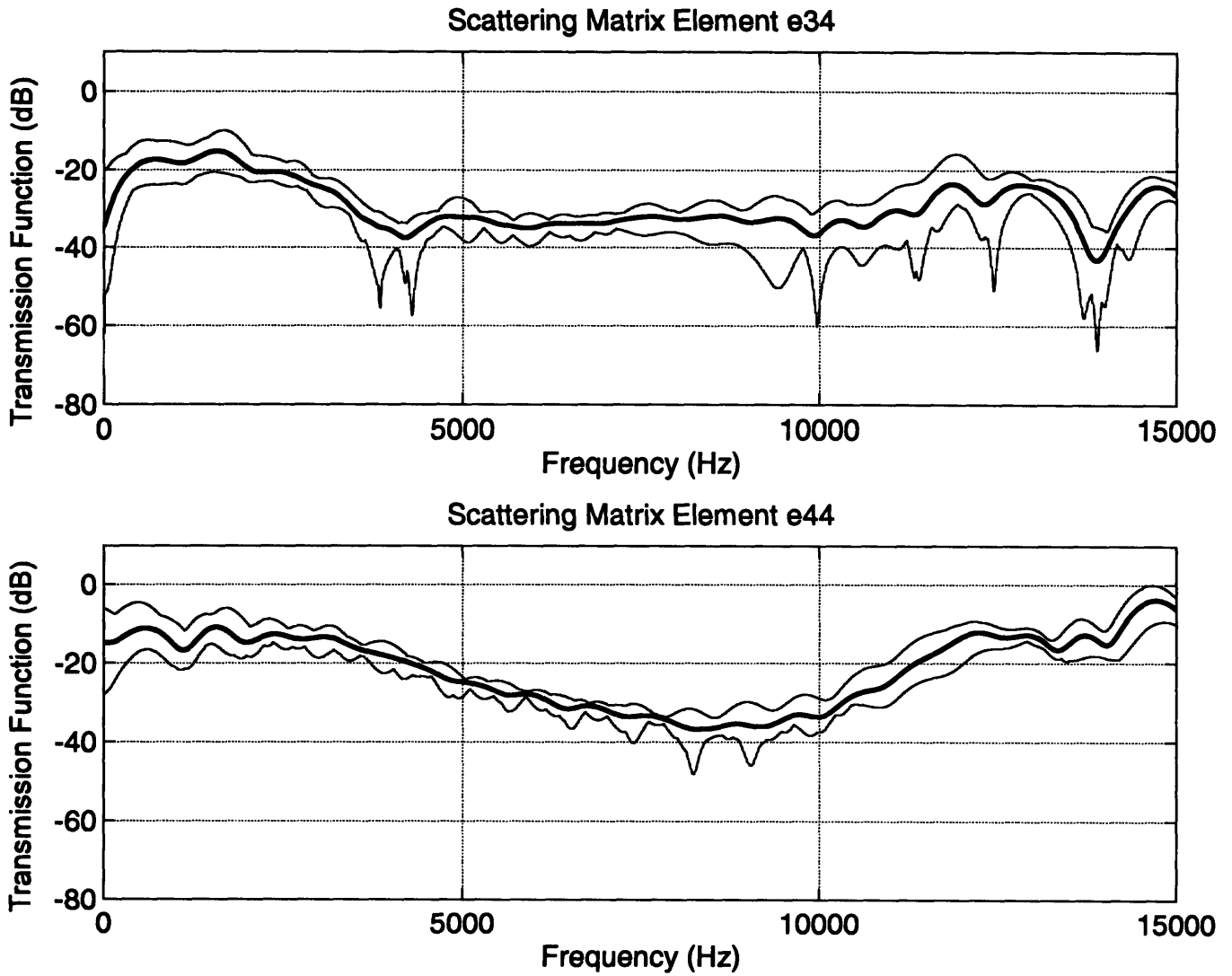


Figure 6-8: Teflon Joint (Joint 'B') Scattering Matrix Elements e34 and e44 (Transmission Functions for output Torsional and Longitudinal Waves measured on Leg 2, respectively, for Longitudinal Wave excitation on Leg 1). Compare to Joint 'A', Fig. 6-4 and Joint 'C', Fig. 6-12.

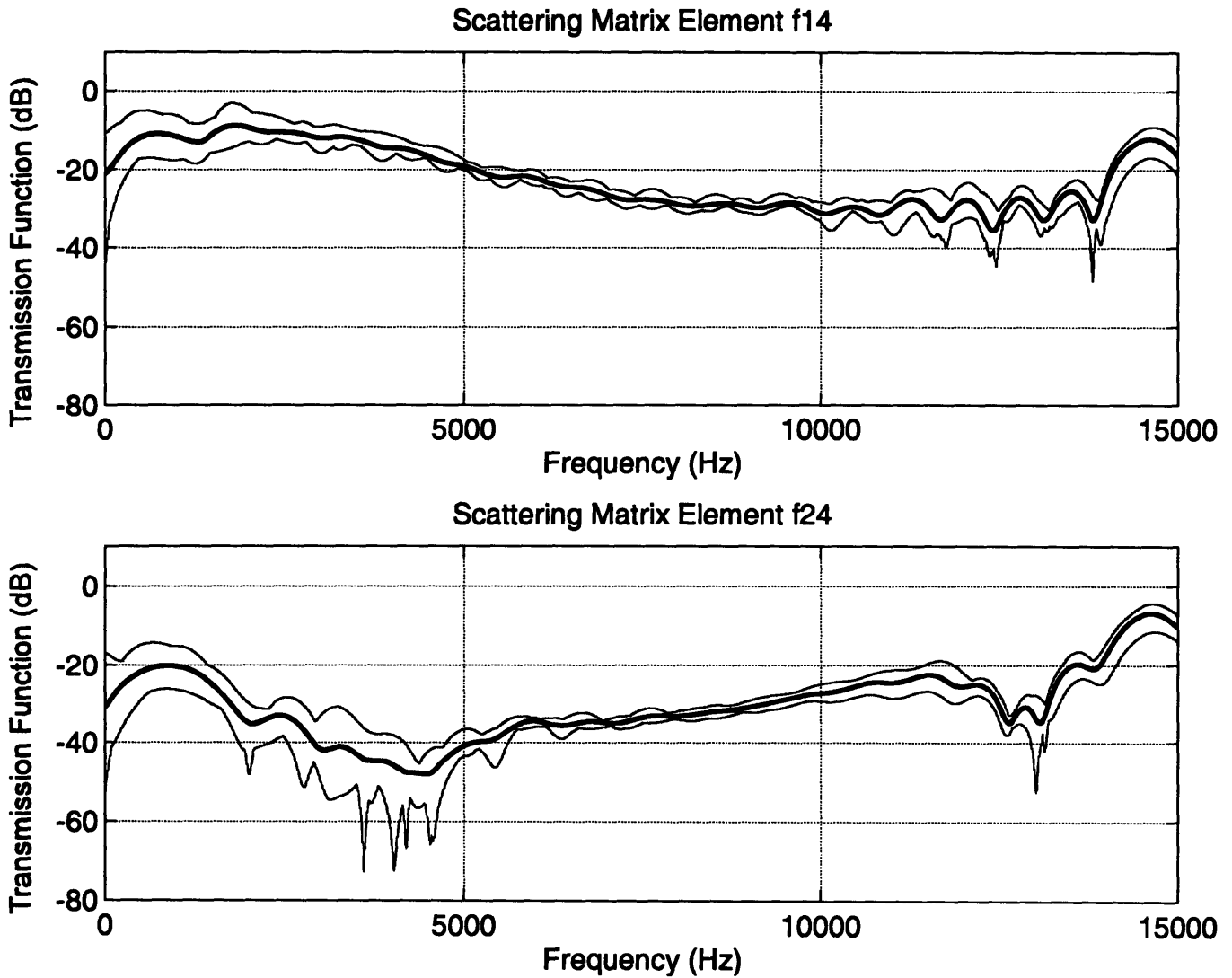


Figure 6-9: Teflon Joint (Joint 'B') Scattering Matrix Elements f14 and f24 (Transmission Functions for output Flexural Waves measured on Leg 3 in the y-direction and x-direction, respectively, for Longitudinal Wave excitation on Leg 1). Compare to Joint 'A', Fig. 6-5 and Joint 'C', Fig. 6-13.

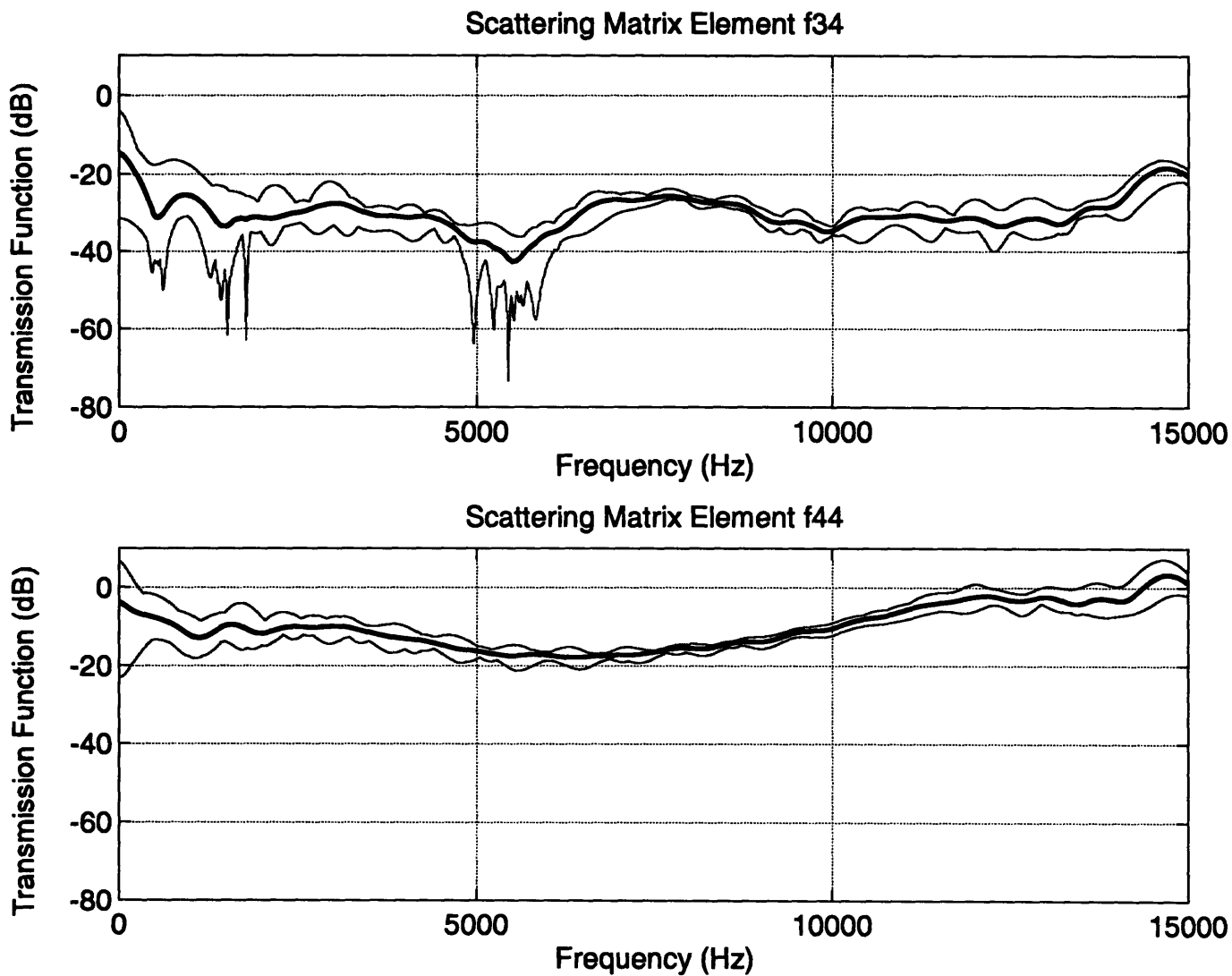


Figure 6-10: Teflon Joint (Joint 'B') Scattering Matrix Elements f34 and f44 (Transmission Functions for output Torsional and Longitudinal Waves measured on Leg 3, respectively, for Longitudinal Wave excitation on Leg 1). Compare to Joint 'A', Fig. 6-6 and Joint 'C', Fig. 6-14.

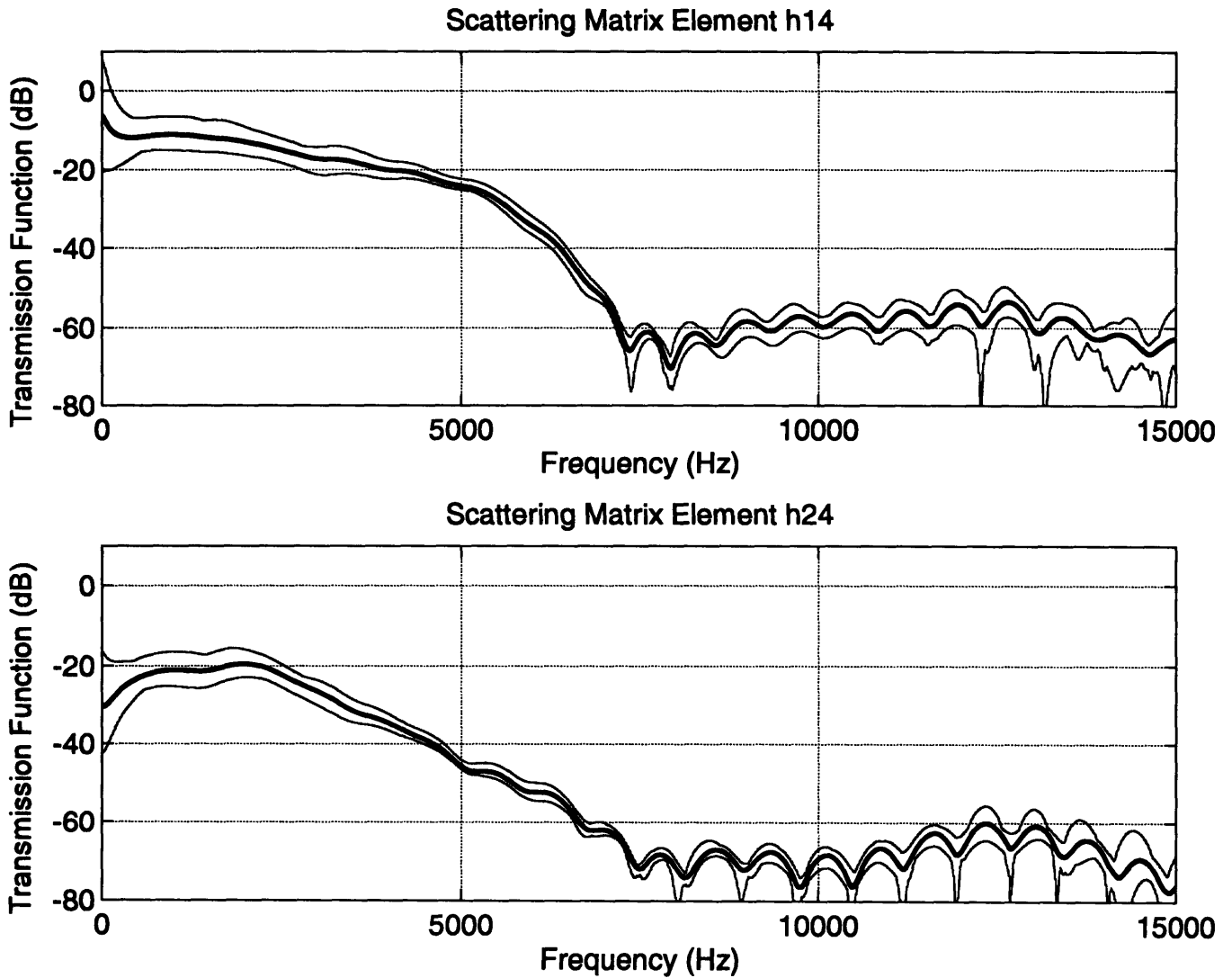


Figure 6-11: Visco-Elastic Joint (Joint 'C') Scattering Matrix Elements h14 and h24 (Transmission Functions for output Flexural Waves measured on Leg 2 in the y-direction and x-direction, respectively, for Longitudinal Wave excitation on Leg 1). Compare to Joint 'A', Fig. 6-3 and Joint 'B', Fig. 6-7.

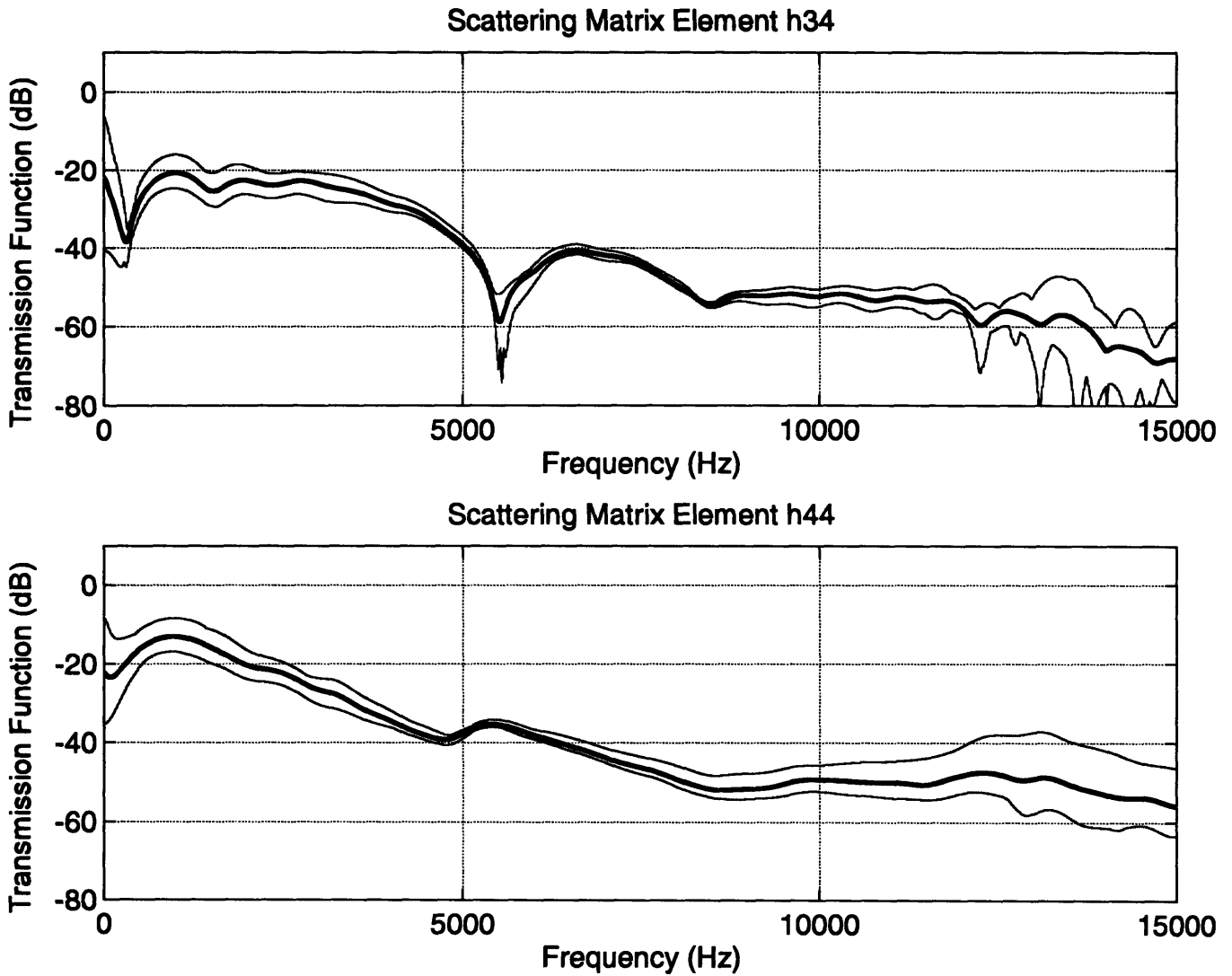


Figure 6-12: Visco-Elastic Joint (Joint 'C') Scattering Matrix Elements h34 and h44 (Transmission Functions for output Torsional and Longitudinal Waves measured on Leg 2, respectively, for Longitudinal Wave excitation on Leg 1). Compare to Joint 'A', Fig. 6-4 and Joint 'B', Fig. 6-8.

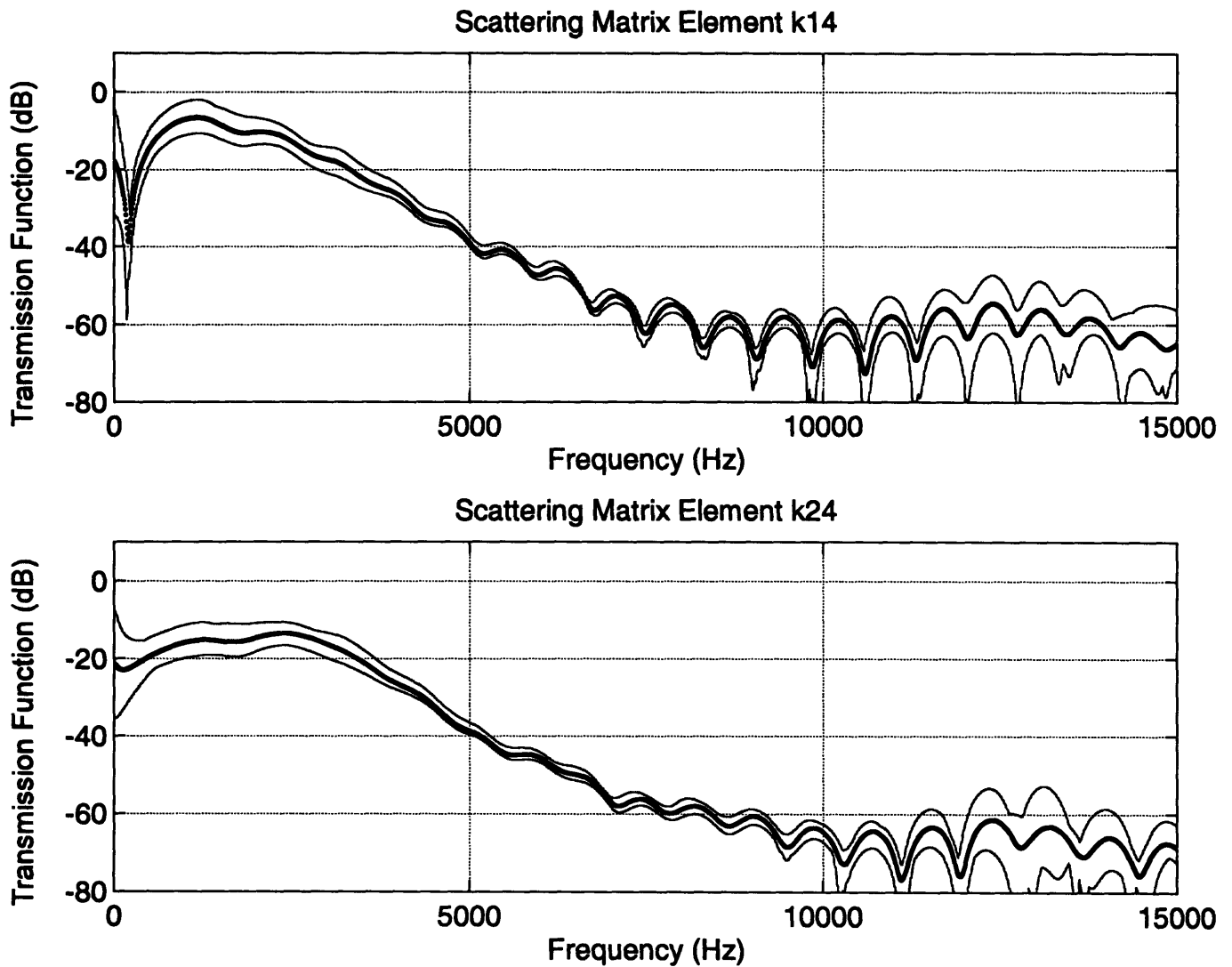


Figure 6-13: Visco-Elastic Joint (Joint 'C') Scattering Matrix Elements k14 and k24 (Transmission Functions for output Flexural Waves measured on Leg 3 in the y-direction and x-direction, respectively, for Longitudinal Wave excitation on Leg 1). Compare to Joint 'A', Fig. 6-5 and Joint 'B', Fig. 6-9.

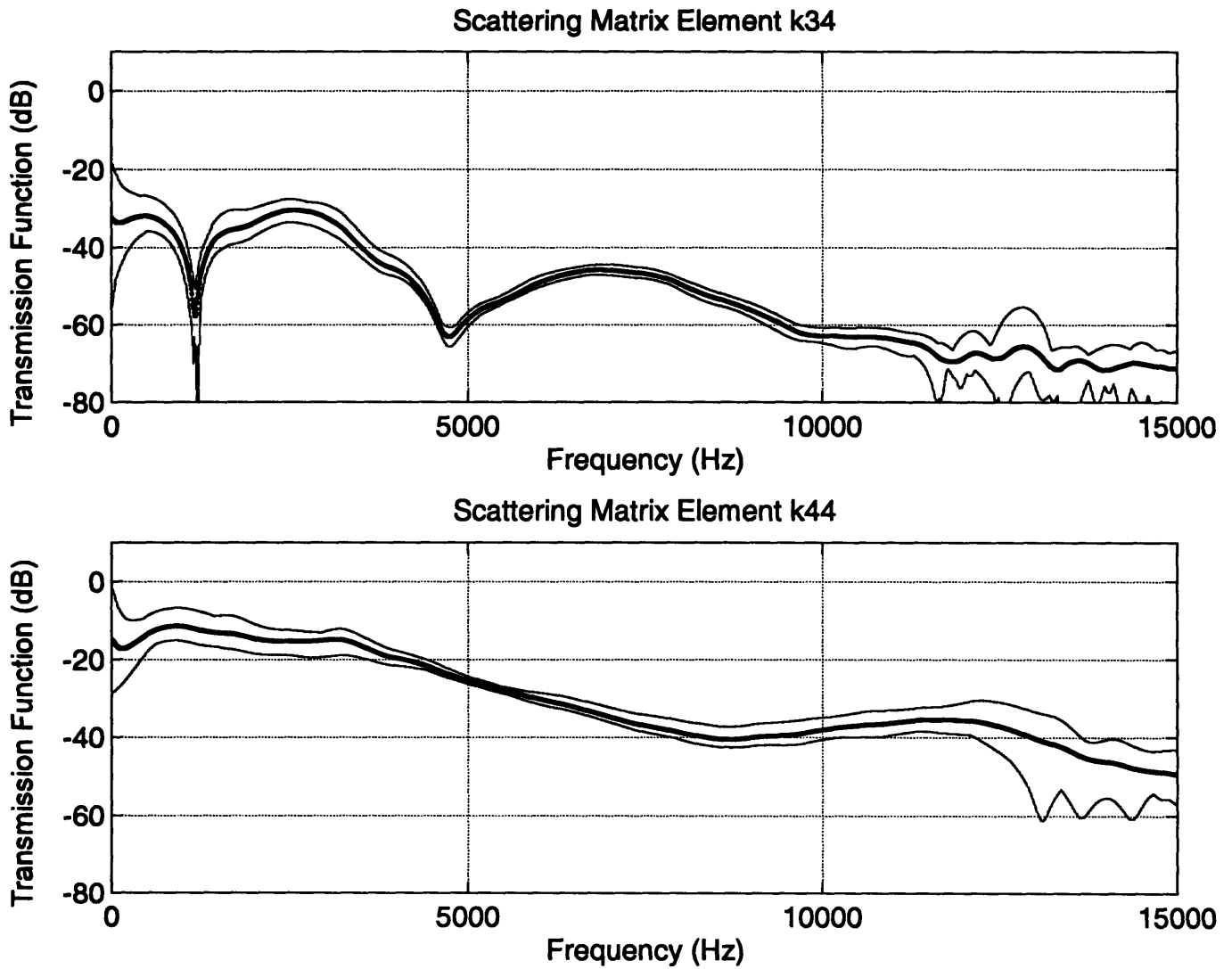


Figure 6-14: Visco-Elastic Joint (Joint 'C') Scattering Matrix Elements k34 and k44 (Transmission Functions for output Torsional and Longitudinal Waves measured on Leg 3, respectively, for Longitudinal Wave excitation on Leg 1). Compare to Joint 'A', Fig. 6-6 and Joint 'B', Fig. 6-10.

## **6.5 Scattering Matrix Elements Determined by Reciprocity**

Scattering matrix elemental functions determined by reciprocity are presented in this section. The middle function of each figure represents the average, in linear space, of ten samples. The upper and lower functions represent the upper and lower limits of the ten data samples.

Appendix E provides an example of a typical Matlab file which has been used for data post-processing. The time-series data of each wave type was first windowed as described in Chapter 3. A Fast-Fourier Transform was applied to each wave type. The transmission function was then determined by dividing the output wave type acceleration by the input wave type acceleration. Finally, this transmission function was converted to dB-space.

Graphical comparison is made to the predicted functions for elements b41, b42, c41, and c42. b41 and b42 are the transmission functions for output longitudinal waves on Leg 2 for flexural excitation in the y and x-directions, respectively, on Leg 1. c41 and c42 are the transmission functions for an output longitudinal wave on Leg 3 for flexural excitation in the y and x directions, respectively, on Leg 1. The predicted functions for b41 and b42 are developed from (5.14). The predicted functions for c41 and c42 are developed from (5.13).



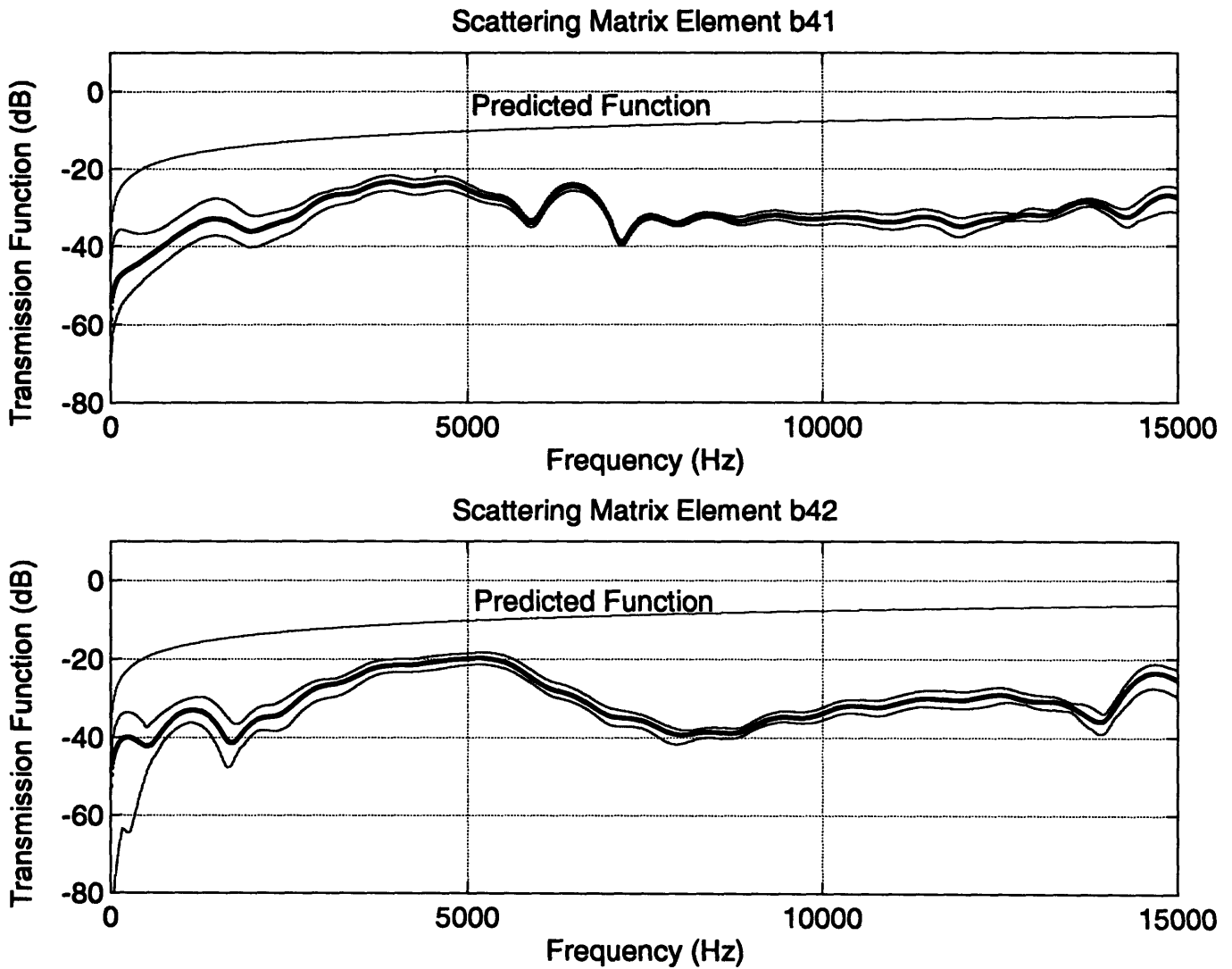


Figure 6-15: Rigid Joint (Joint 'A') Scattering Matrix Elements b41 and b42 determined by Reciprocity (Transmission Functions for output Longitudinal Wave on Leg 2 for Flexural Wave excitation (y-direction and x-direction, respectively) on Leg 1; predicted function provided for b41 and b42). Compare to Joint 'B', Fig. 6-18 and Joint 'C', Fig. 6-21.

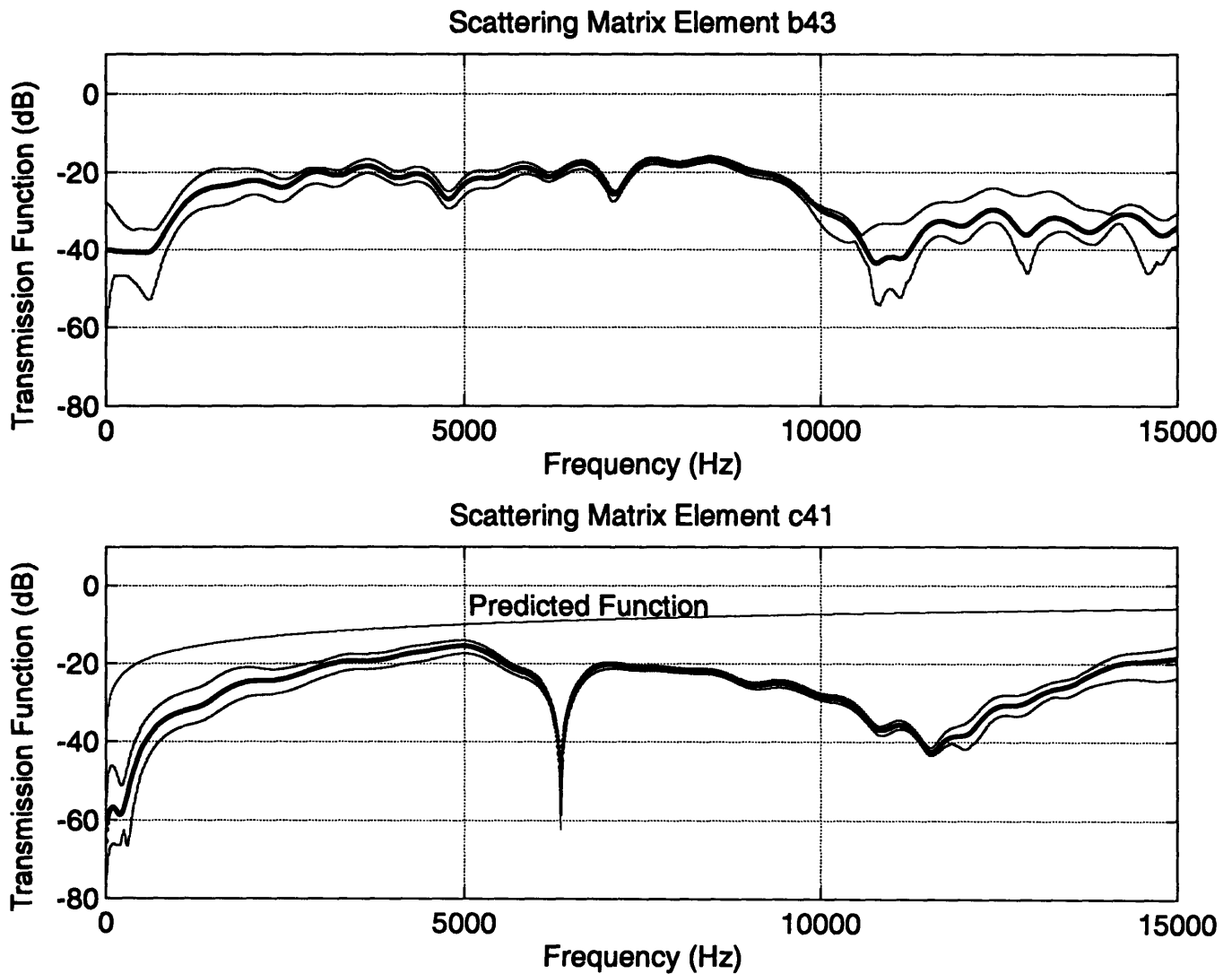


Figure 6-16: Rigid Joint (Joint 'A') Scattering Matrix Elements b43 and c41 determined by Reciprocity (Transmission Functions for output Longitudinal Wave on Leg 2 and Leg 3 with Torsional Wave excitation on Leg 1 and Flexural Wave excitation (y-direction) on Leg 1, respectively; predicted function provided for c41). Compare to Joint 'B', Fig. 6-19 and Joint 'C', Fig. 6-22.

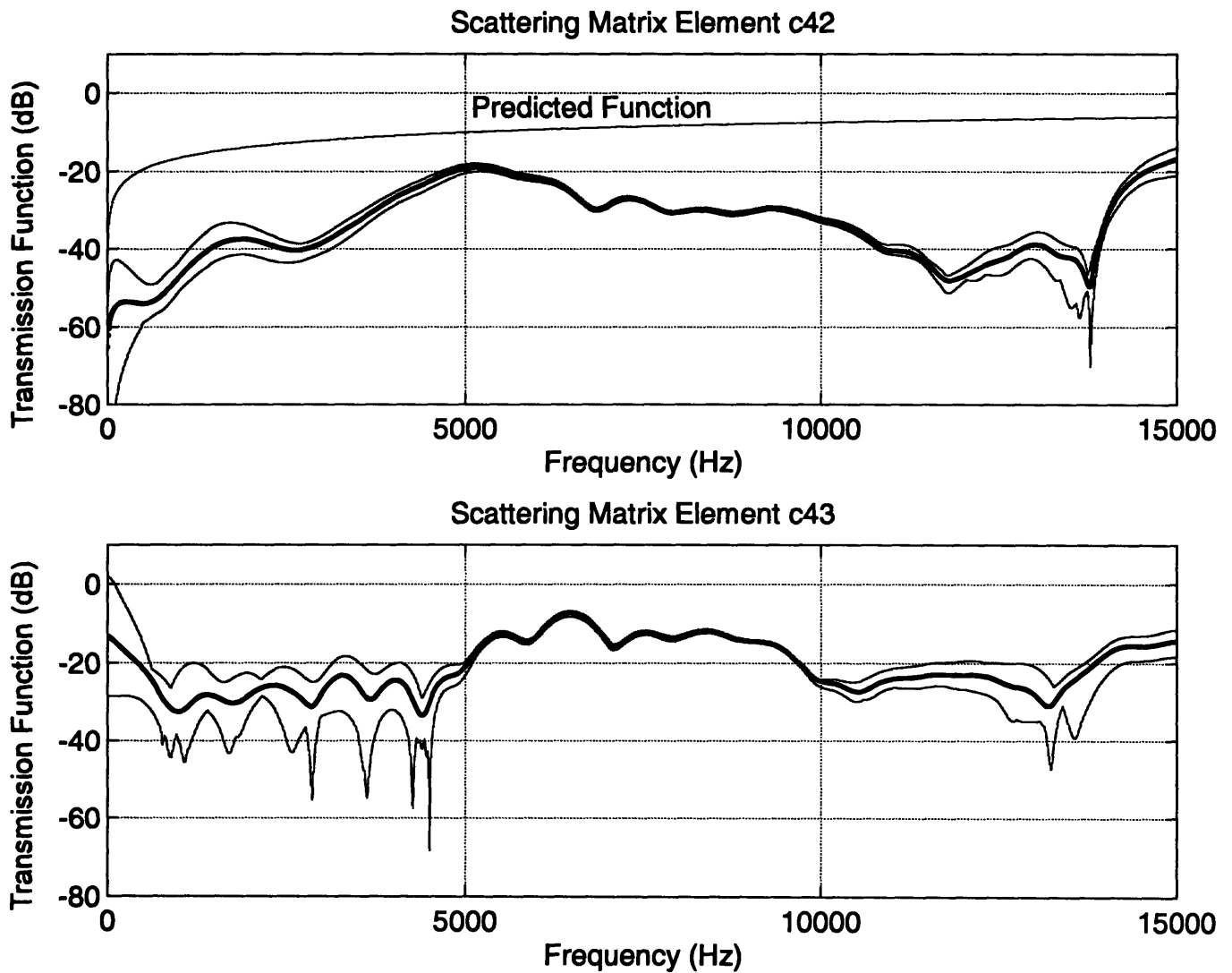


Figure 6-17: Rigid Joint (Joint 'A') Scattering Matrix Elements c42 and c43 determined by Reciprocity (Transmission Functions for output Longitudinal Wave on Leg 3 with Flexural Wave excitation (x-direction) on Leg 1 and Torsional Wave excitation on Leg 1, respectively; predicted function provided for c42). Compare to Joint 'B', Fig. 6-20 and Joint 'C', Fig. 6-23.

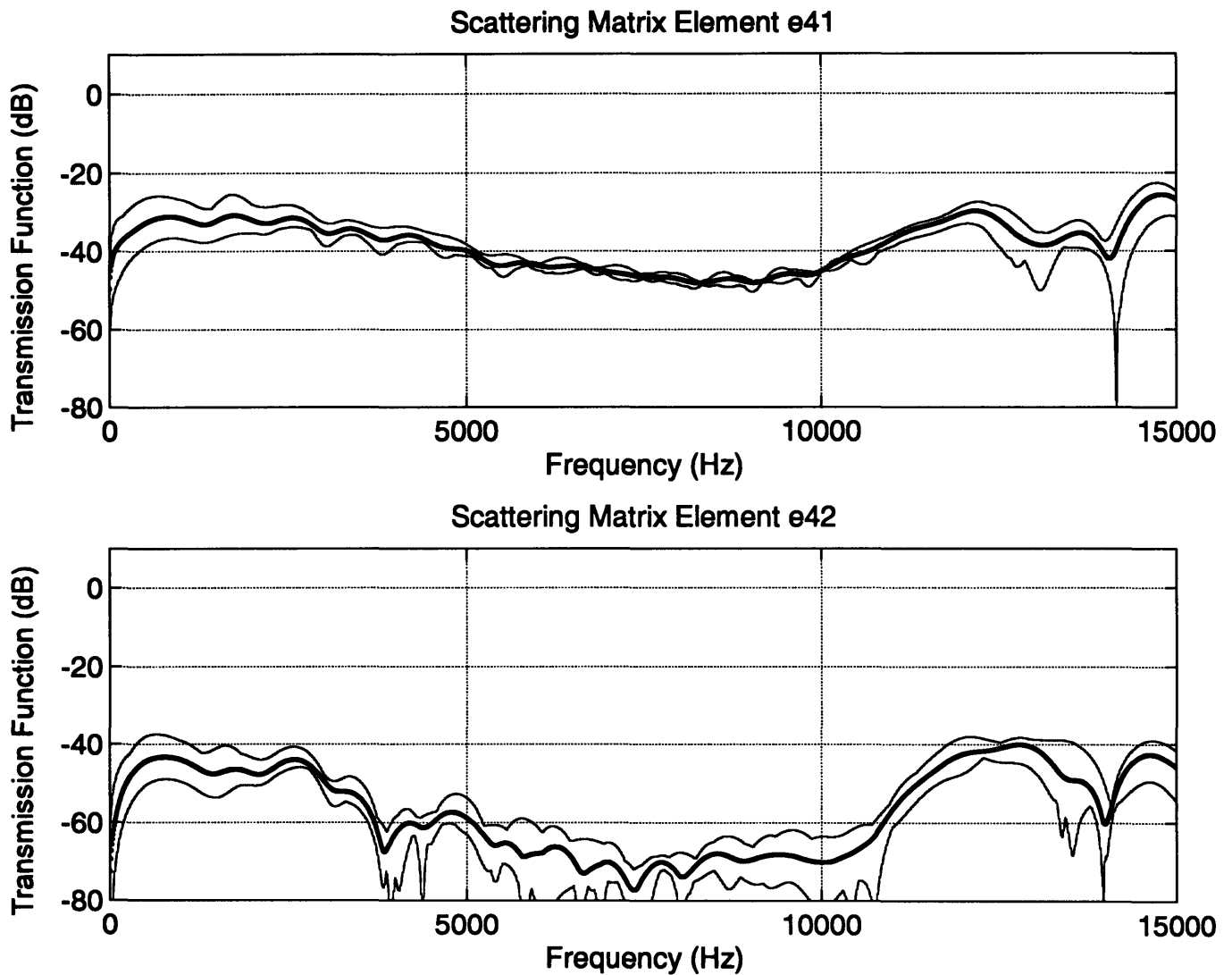


Figure 6-18: Teflon Joint (Joint 'B') Scattering Matrix Elements e41 and e42 determined by Reciprocity (Transmission Functions for output Longitudinal Wave on Leg 2 for Flexural Wave excitation (y-direction and x-direction, respectively) on Leg 1). Compare to Joint 'A', Fig. 6-15 and Joint 'C', Fig. 6-21.

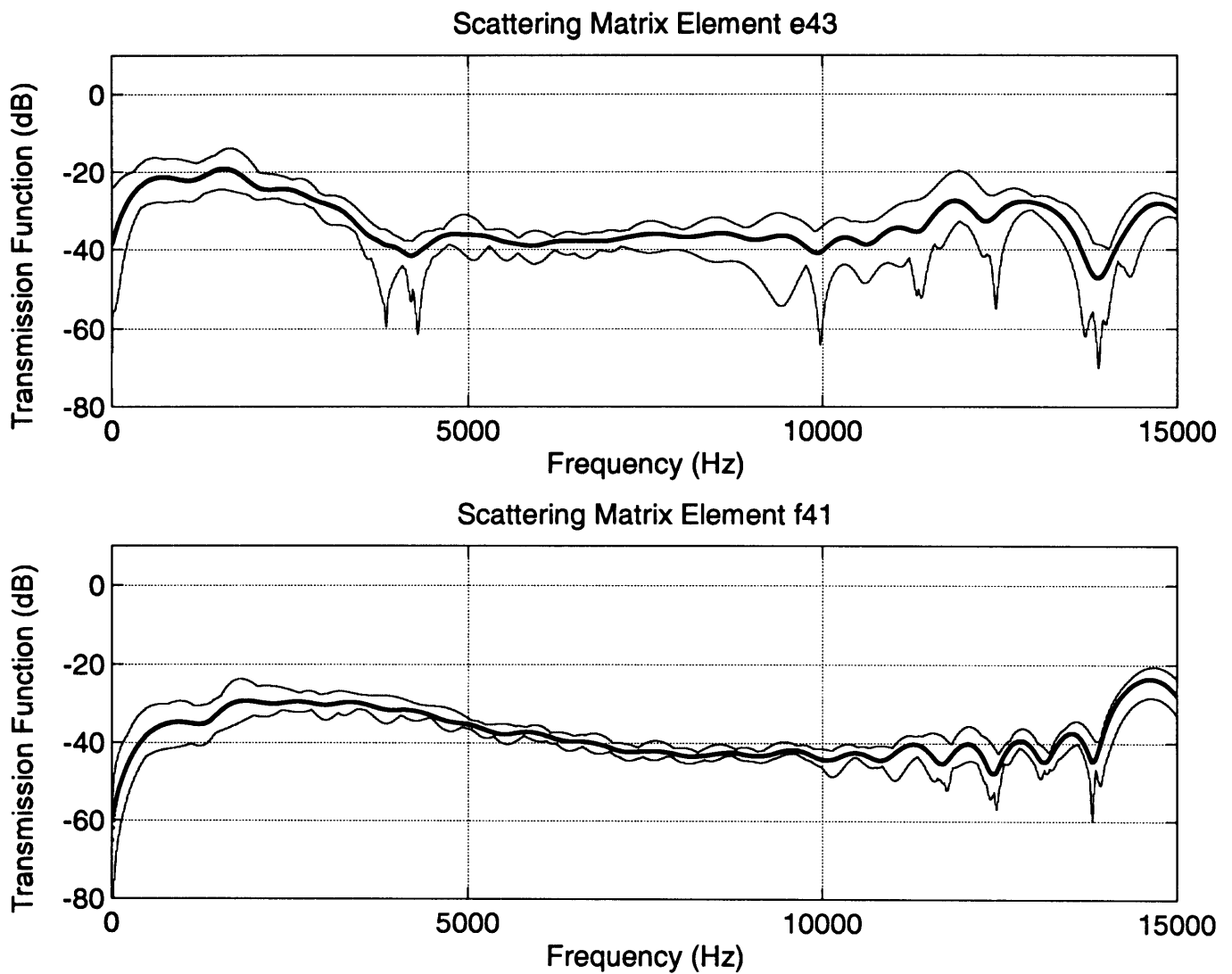
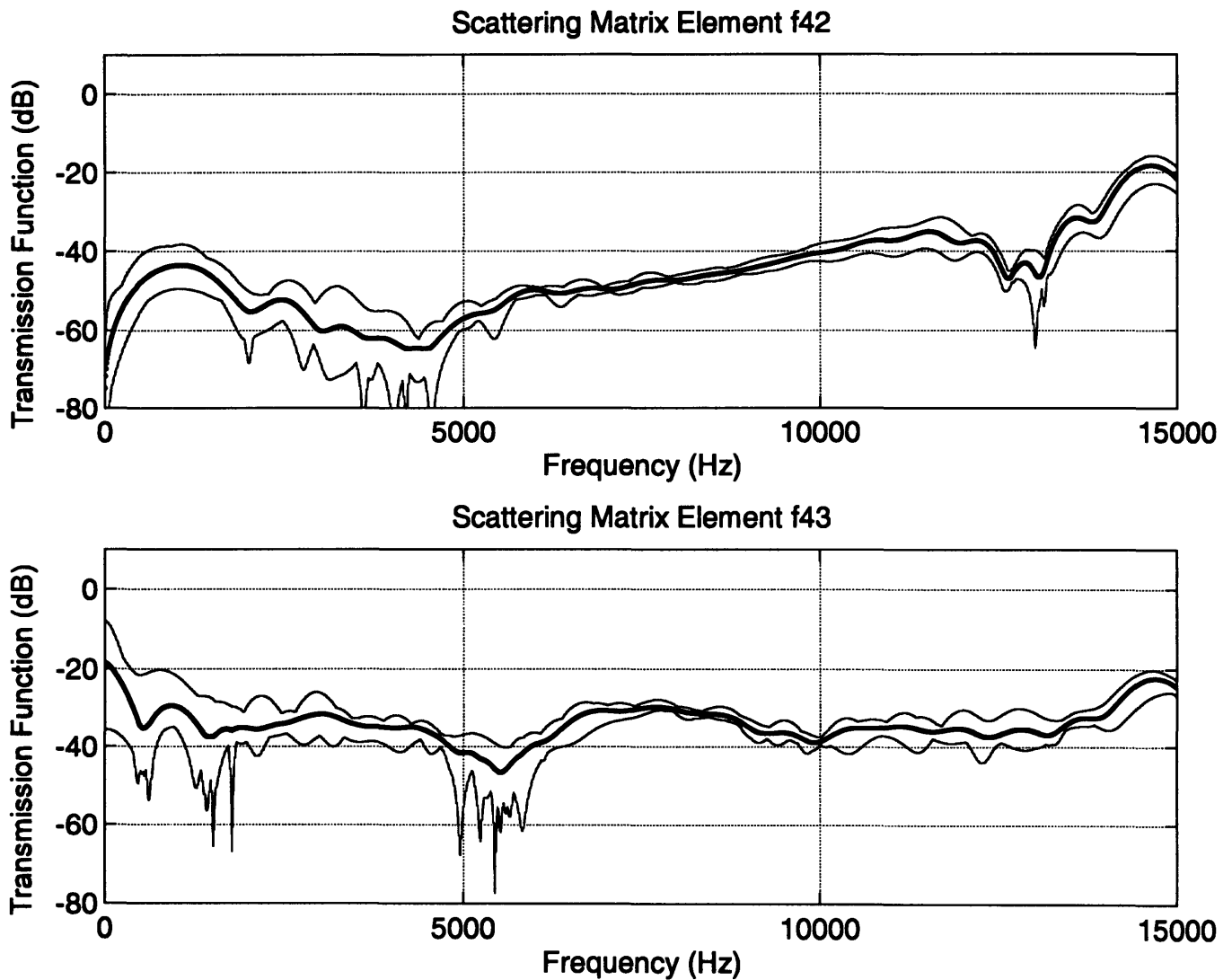


Figure 6-19: Teflon Joint (Joint 'B') Scattering Matrix Elements e43 and f41 determined by Reciprocity (Transmission Functions for output Longitudinal Wave on Leg 2 and Leg 3 with Torsional Wave excitation on Leg 1 and Flexural Wave excitation (y-direction) on Leg 1, respectively). Compare to Joint 'A', Fig. 6-16 and Joint 'C', Fig. 6-22.



**Figure 6-20: Teflon Joint (Joint 'B') Scattering Matrix Elements f42 and f43 determined by Reciprocity (Transmission Functions for output Longitudinal Wave on Leg 3 with Flexural Wave excitation (x-direction) on Leg 1 and Torsional Wave excitation on Leg 1, respectively). Compare to Joint 'A', Fig. 6-17 and Joint 'C', Fig. 6-23.**

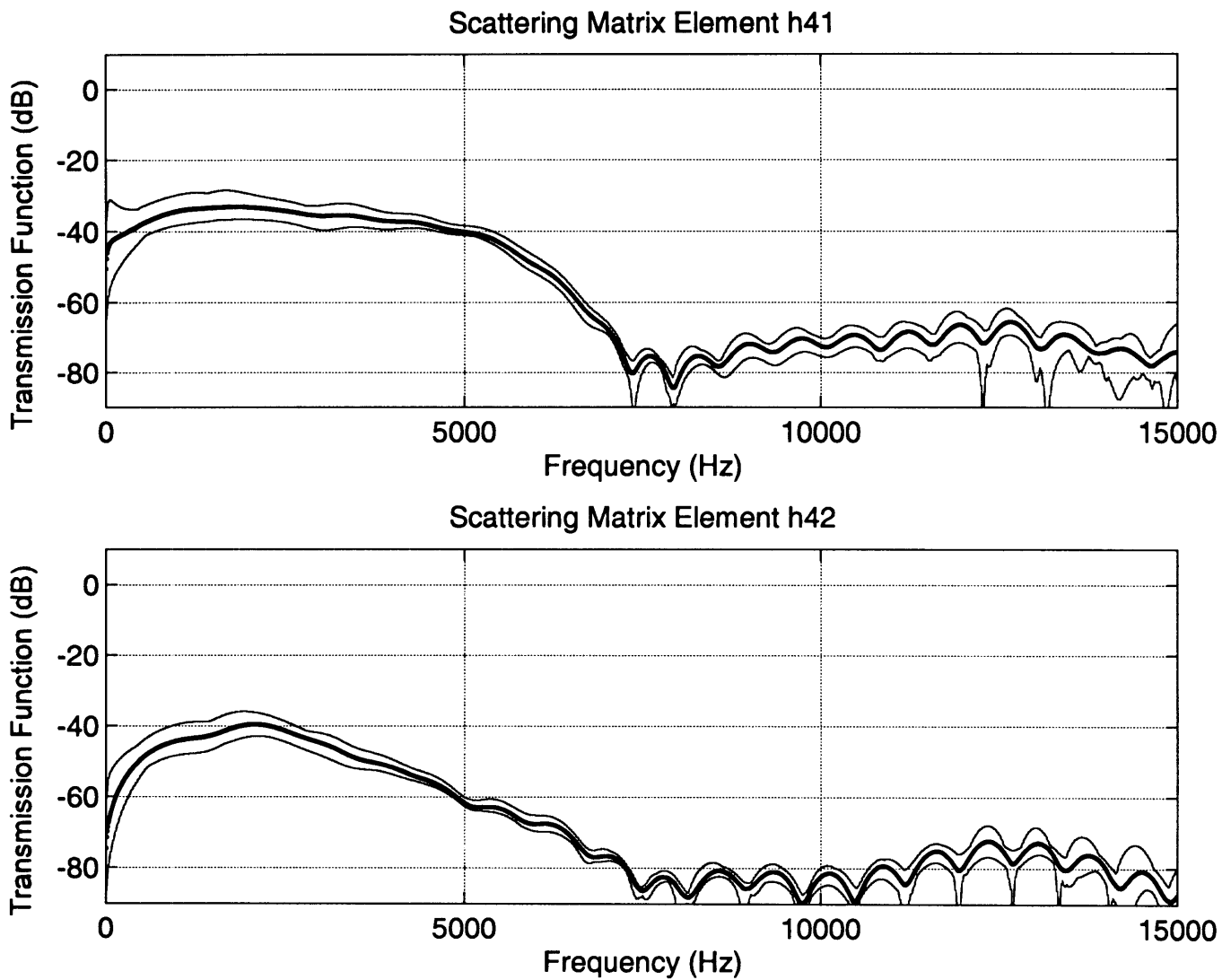


Figure 6-21: Visco-Elastic Joint (Joint 'C') Scattering Matrix Elements h41 and h42 determined by Reciprocity (Transmission Functions for output Longitudinal Wave on Leg 2 for Flexural Wave excitation (y-direction and x-direction, respectively) on Leg 1). Compare to Joint 'A', Fig. 6-15 and Joint 'B', Fig. 6-18.

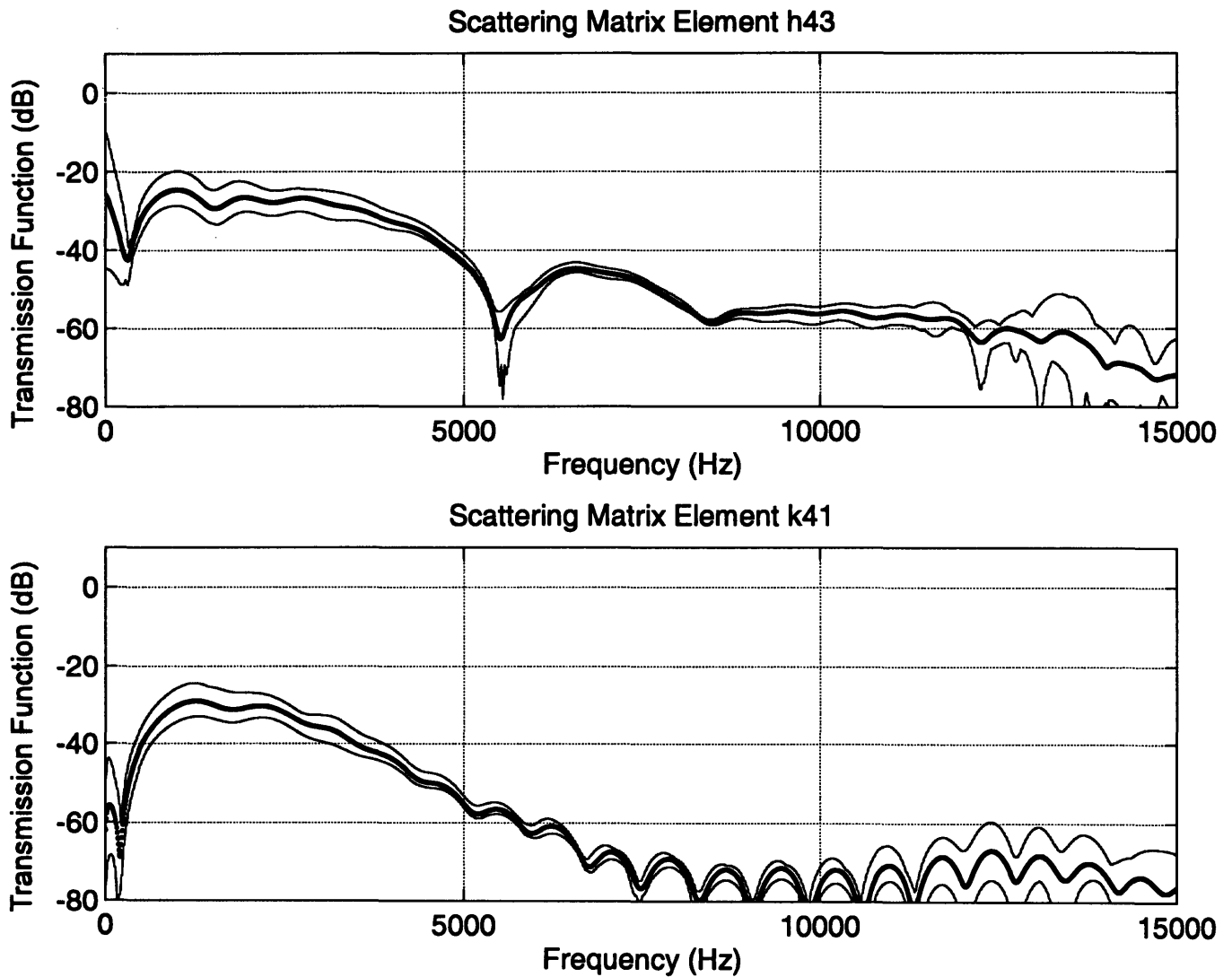


Figure 6-22: Visco-Elastic Joint (Joint 'C') Scattering Matrix Elements h43 and k41 determined by Reciprocity (Transmission Functions for output Longitudinal Wave on Leg 2 and Leg 3 with Torsional Wave excitation on Leg 1 and Flexural Wave excitation (y-direction) on Leg 1, respectively). Compare to Joint 'A', Fig. 6-16 and Joint 'B', Fig. 6-19.



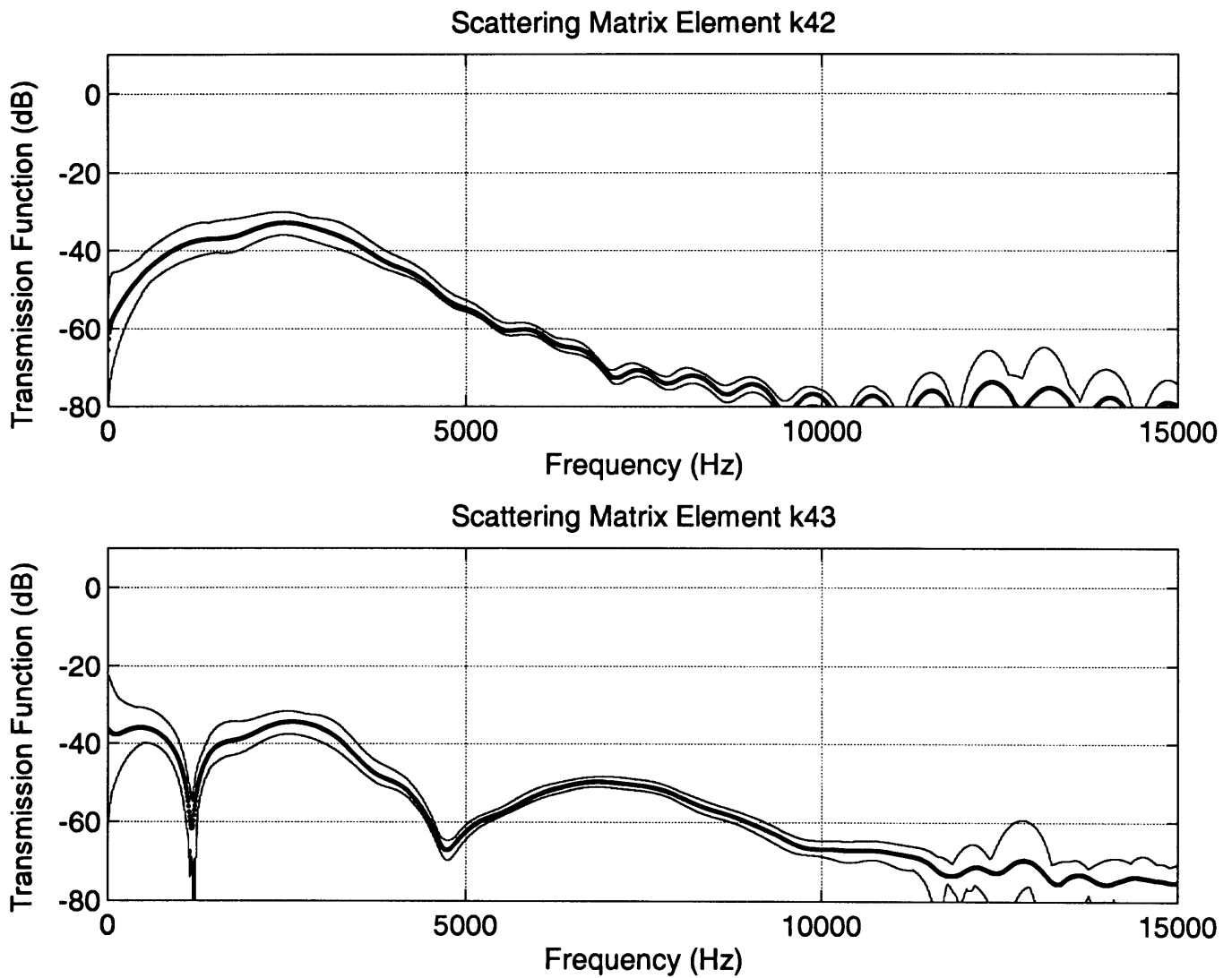


Figure 6-23: Visco-Elastic Joint (Joint 'C') Scattering Matrix Elements k42 and k43 determined by Reciprocity (Transmission Functions for output Longitudinal Wave on Leg 3 with Flexural Wave excitation (x-direction) on Leg 1 and Torsional Wave excitation on Leg 1, respectively). Compare to Joint 'A', Fig. 6-17 and Joint 'B', Fig. 6-20.

# Chapter 7

## Conclusions

### 7.1 Discussion of Results

This thesis has investigated the longitudinal impulse response of three different three-legged joints. Joint 'A' is a rigid joint. Joint 'B' is a spherical pinned-joint with Teflon-coated contact surfaces. Joint 'C' is a spherical pinned-joint with contact surfaces coated with a visco-elastic interface. The dynamic response of each joint is distinctly different from one another with Joint 'C' demonstrating the best overall performance.

With the exception of two cases, Joint 'B' exhibits greater transmission than Joint 'C'. The flexural transmission in the x-direction for Leg 3 given longitudinal excitation on Leg 1 is higher for Joint 'C' than Joint 'B' from 0 kHz to 6 kHz. The longitudinal transmission for Leg 3 given flexural excitation from Leg 1 in the x-direction is higher for Joint 'C' than it is for Joint 'B' from 0 kHz to 6 kHz. For all other conditions, Joint 'C' exhibits transmission at levels that are less than or equal to those of Joint 'B'. Under all conditions, except for certain wave types and low frequencies, Joint 'C' exhibits less transmission than Joint 'A'.

In order to achieve adequate vibration isolation it is desirable that a joint minimize the extent to which longitudinal waves are transmitted. Longitudinal transmission is not desirable because of the high impedance of a longitudinal wave. Joint 'A' transmits relatively high levels of longitudinal energy. For example, Leg 3 of Joint 'A' exhibits only a 7 dB reduction in transmission for longitudinal excitation on Leg 1. Joint 'B' improves this situation by transmitting less longitudinal energy under most situations. As an example, Joint 'B' longitudinal transmission in Legs 2 and 3, given longitudinal excitation on Leg 1, results in a 23 dB and 15 dB reduction over Joint 'A', respectively, for the frequency bandwidth 6 to 9 kHz. Joint 'C' offers the best overall reduction in longitudinal

transmission; this is achieved by incorporating damping into the design. Longitudinal transmission is, on the average, the lowest for Joint 'C' than the other joints. Joint 'C' longitudinal transmission in Legs 2 and 3 (Figs. 6-12 and 6-14), given longitudinal excitation on Leg 1, results in a -55 dB and -50 dB reduction at high frequencies, respectively.

The longitudinal transmission for Joint 'C', averaged (in dB-space) across the entire frequency spectrum, is almost 20 dB lower than for joint 'B'. The average longitudinal transmission for Joint 'C' is -40 dB and -31 dB for Legs 2 and 3, respectively (Tables 6.1 and 6.2).

Flexural waves are much more sensitive to dissipation because of their reduced impedance. Plus, damping mechanisms are much easier to incorporate for a flexural wave than for any other wave type. The most distinctive feature that is evident in flexural transmission is the high frequency response of Joint 'C'; flexural transmission levels are very low for longitudinal excitation (-60 to -70 dB) in the frequency band 7.5 kHz to 15 kHz (Figs. 6-11 and 6-13).

It is evident that incorporating damping characteristics into a pinned joint offers favorable characteristics that promote significant vibration reduction across a broad frequency band.

## **7.2 Recommendations for Future Research**

The designs of the joints investigated in this thesis are simple. The dynamic behavior of the joints, however, is very complicated. The measurements taken in support of this thesis were inadequate to fully understand the behavior of each joint. The following are recommendations for future experimentation.

### *Wave Type Coupling*

Wave type coupling was only partially investigated in this thesis. The coupling which was investigated pertained only to the injection of pure longitudinal waves.

Coupling with respect to injection of pure flexural and pure torsional waves was not investigated. Since part of this thesis was devoted to resolving only a portion of the full scattering matrices it will be worthwhile to develop other means by which the remaining elemental transfer functions may be resolved. It is conceptually trivial to understand that the transfer functions can be determined through the use of pure wave injection. It is an entirely different matter to create pure flexural and torsional waves. This problem may be ameliorated by array processing.

Linearity is a premise in the use of the scattering matrix to understand joint behavior. The extent to which each joint behaves linearly was not fully investigated in this thesis. Only by fully investigating the linearity of each joint will it be possible to assess the legitimacy of the use of scattering matrices as a means of explaining joint dynamic behavior. Joint linearity with respect to amplitude was observed; joint linear/nonlinear frequency dependence was not investigated.

### *Joint and Leg Damping*

It has become evident that energy transmission can be significantly reduced through the use of damping at the joints. It is believed that the joint damping treatment can be significantly improved with the use of commercially available materials whose properties are specifically intended for use in damping. One recommended type of treatment is Norsorex, the suitability of which was not investigated in this thesis.

It also appears that significant flexural wave damping can be achieved through the use of treatment as applied in the experimentation. It is believed that treatment using materials such as Norsorex in the configuration used in the experimental model will significantly improve the extent to which flexural waves are dissipated. It is believed that the leg damping treatment used in the experimentation has wide ranging vibration control applications which lie beyond the scope of this thesis and outside of applications to joints. The leg damping treatment is discussed in Appendix E.

### *Data Acquisition*

The data which has been acquired in support of this thesis was limited by the accelerometer configuration. Each leg was configured with one set of accelerometers at a specific location. As a result, several response transmission functions exhibited nodal behavior at certain frequencies. Because of this nodal behavior, the data does not clearly represent the energy content of a specific wave type.

The robust nature of the data may be enhanced by placing several accelerometer groups along the length of the leg and averaging the response. This has the benefit of measuring the average total energy content of a specific wave type and will provide a more accurate representation of the joint dynamic behavior.

## Appendix A

### Joint 'A' Design

Joint 'A' is a rigid joint similar in construction to the simplest joint used in the three-dimensional truss [16]. The joint is made of Stainless Steel (AISI 430). The body was fabricated out of stock stainless steel then drilled to accommodate the stainless steel legs.

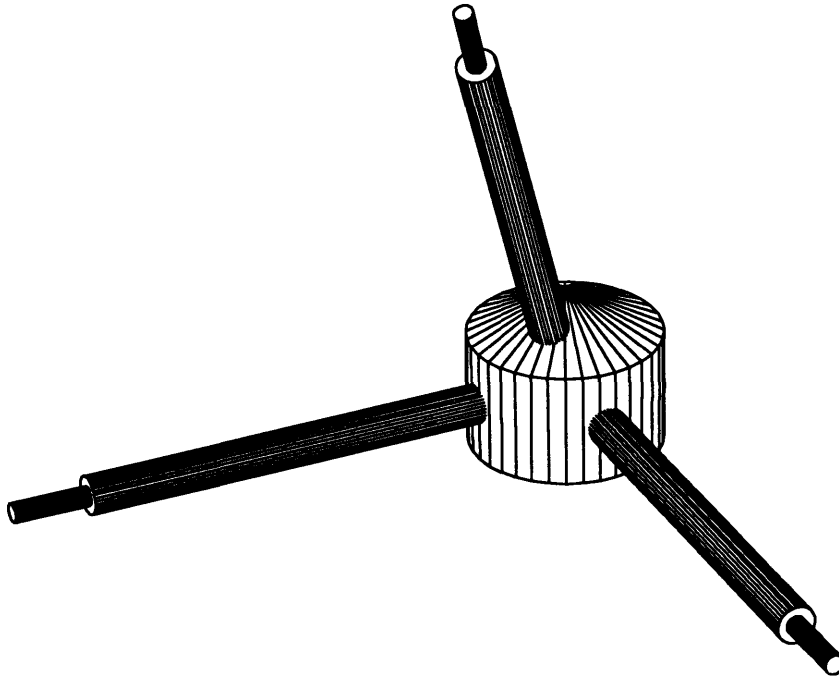


Figure A-1: Joint 'A' (Oblique View).

Each leg is 4.75 inches long, is fitted into the holes, and is welded to the joint body. The legs penetrate 0.50" past the inside surface of the hollow rigid joint body. The ends of the joint legs are tapped to 8 mm threads to permit rigid screwed attachment to the 14' leg extensions. Fig. A-1 shows an oblique view of Joint 'A'. Figs. A-2 through A-4 depict the technical drawings for Joint 'A'. Fig. A-5 demonstrates the means by which the legs are attached to the body of Joint 'A'.

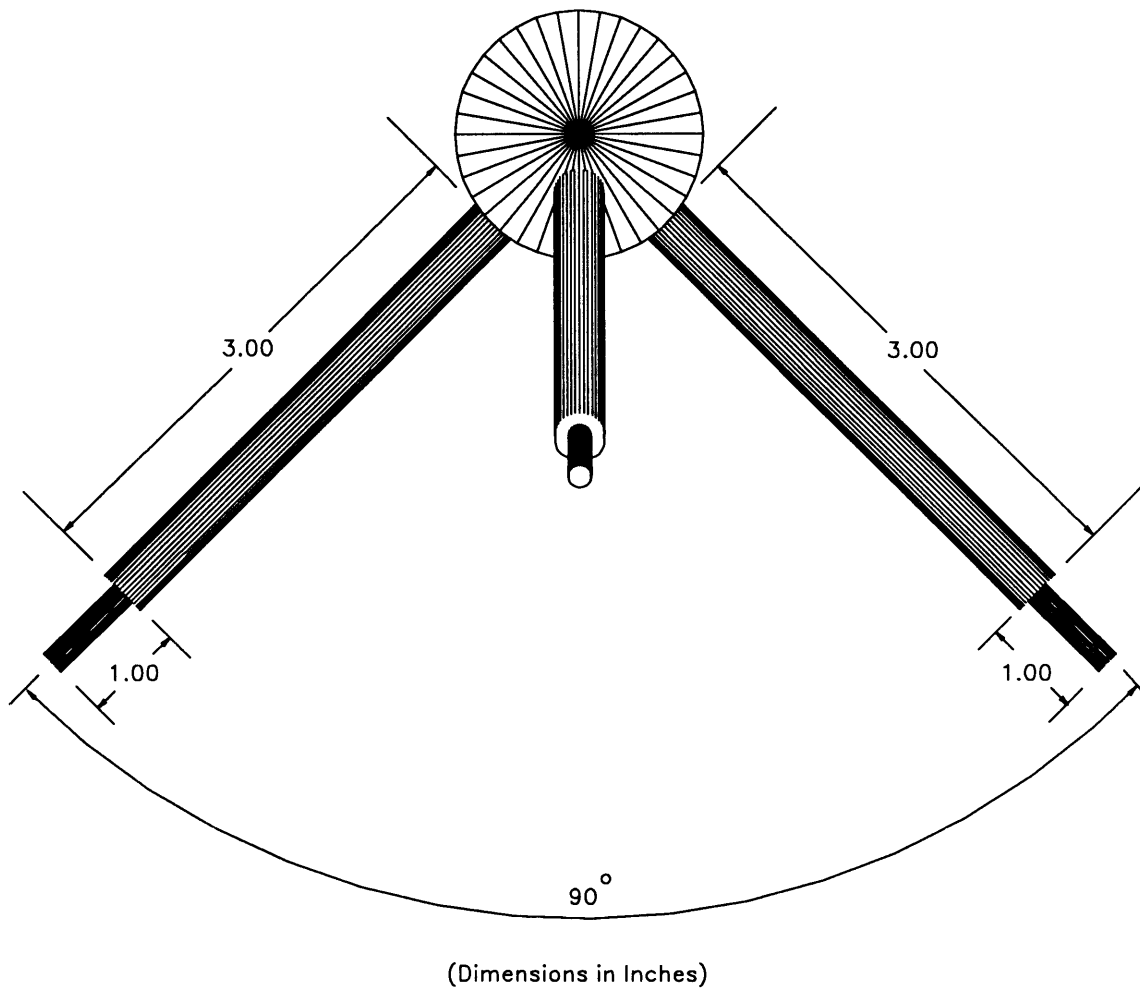
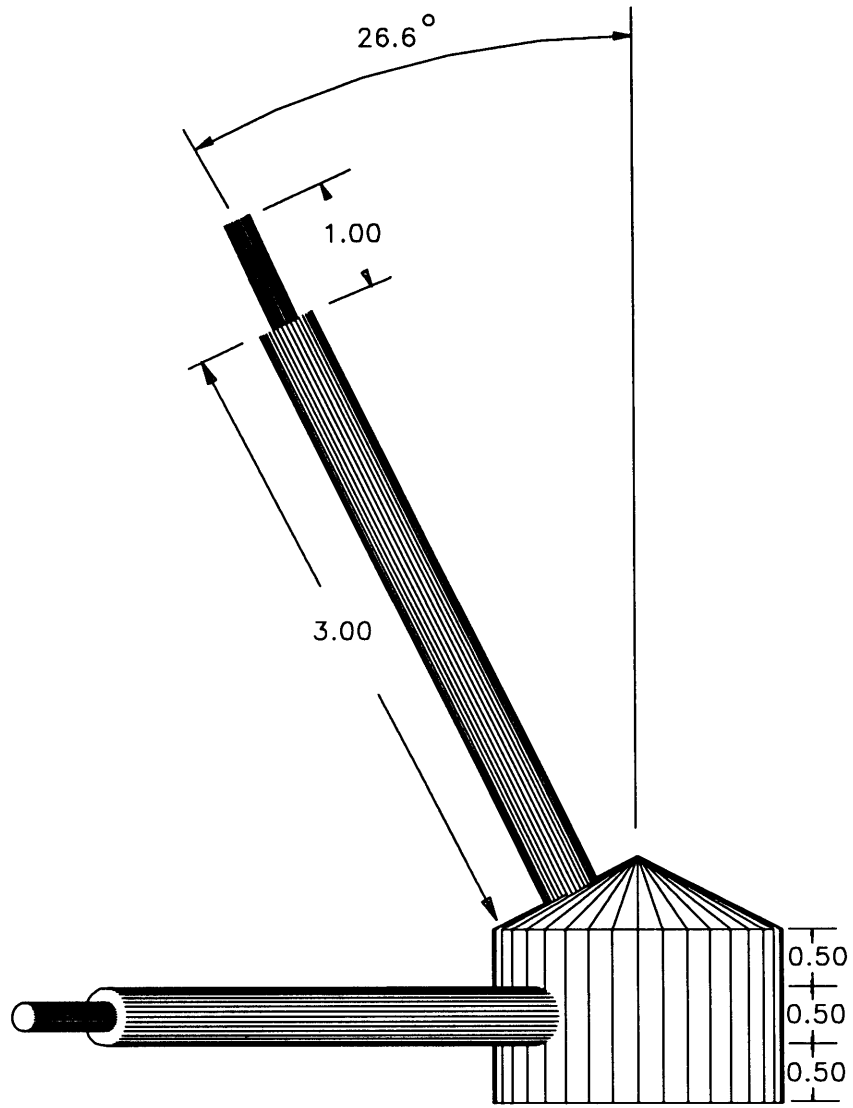


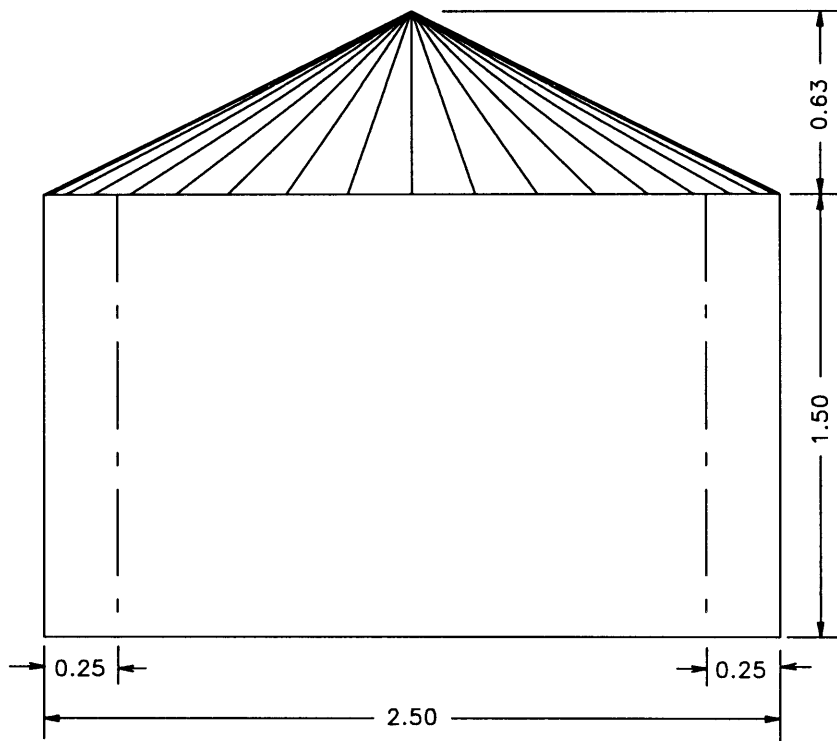
Figure A-2: Joint 'A' (Top View).



(Dimensions in Inches)

Figure A-3: Joint 'A' (Side View).





(Dimensions in Inches)

**Note:** The joint body is hollow with 0.25” walls. The interior of the walls extend from the base of the joint to the plane of the conical top. Leg penetrations are not shown.

**Figure A-4:** Joint ‘A’ Body.

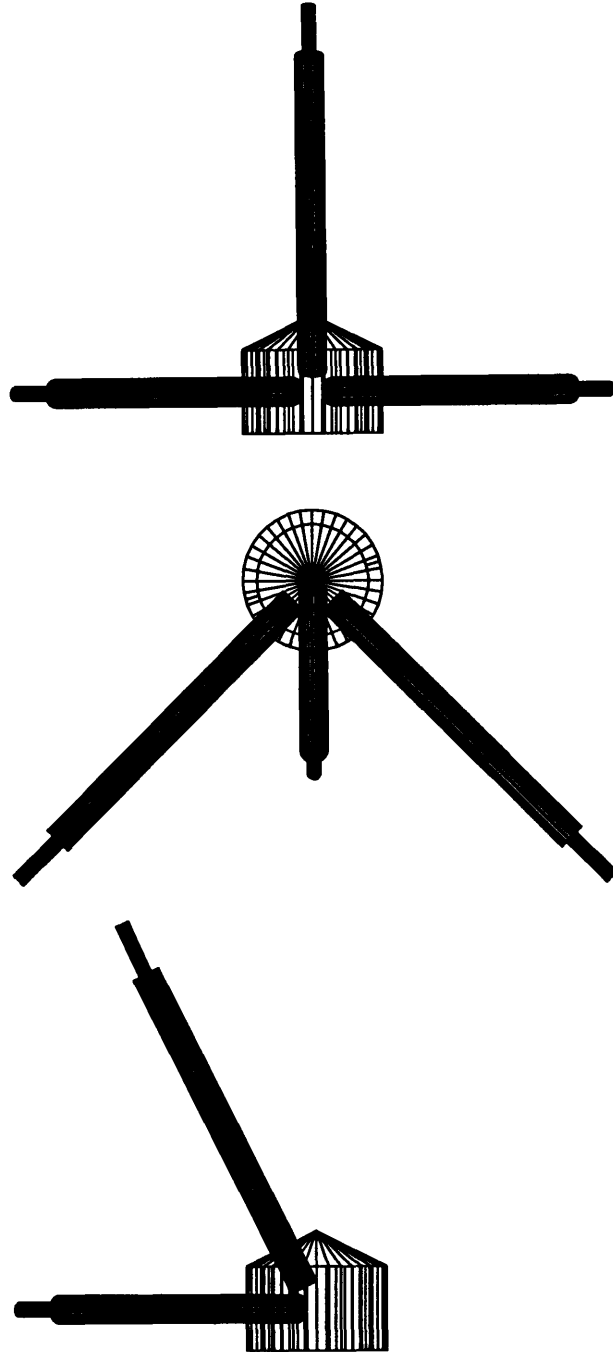


Figure A-5: Joint 'A' Leg Penetrations (see-through view)

## Appendix B

### Joint 'B' Design

Joint 'B' is a pinned spherical joint. The spherical male ends of the legs rest in spherical recesses which are machined into the joint body. The joint is fabricated of Stainless Steel (AISI 430). The joint body is physically separated into two halves which are aligned by alignment pins (not shown on the following drawings). The spherical male ends are placed in the joint body by separating the joint body and inserting the male ends into the recesses. The contact surfaces are coated with 0.001" thick Teflon. The joint is held rigidly together through the use of five stainless steel machined 5 mm threaded screws. Only the top half is threaded to accept the stainless steel screws. The holes in the bottom half are not threaded but are drilled to permit passage of the screw. The screw recesses in the bottom half are designed to permit access to the screw head with a 8 mm socket wrench. The ends of the joint legs are tapped to 8 mm threads to permit rigid screwed attachment to the 14' leg extensions.

Fig. B-1 is an oblique depiction of the joint body with the top and bottom sections together. Figs. B-2 and B-3 show the top section of the joint body in the upright and inverted position, respectively. Figs. B-4 through B-6 provide the dimensions of the upper section. Figs. B-7 and B-8 show the bottom section of the joint body in the upright and inverted position, respectively. Figs. B-9 and B-10 provide the dimensions of the lower section. Fig. B-11 is an oblique view of the spherical male leg. Figs. B-12 and B-13 provide the side view and top view, respectively, of the spherical male leg.

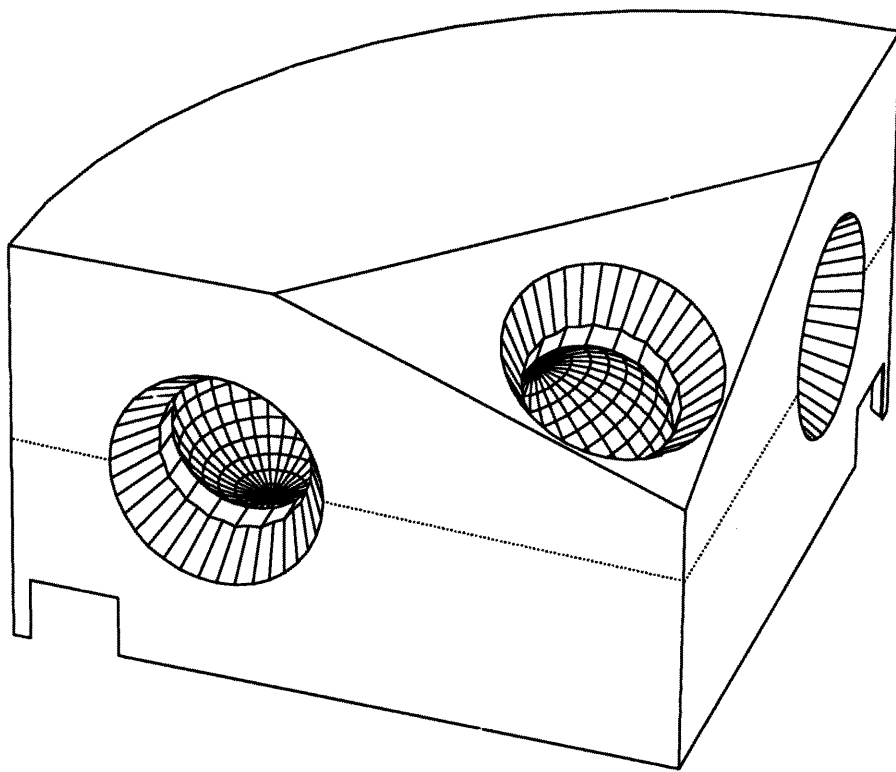


**Figure B-1: Joint 'B' Body (Oblique View).**

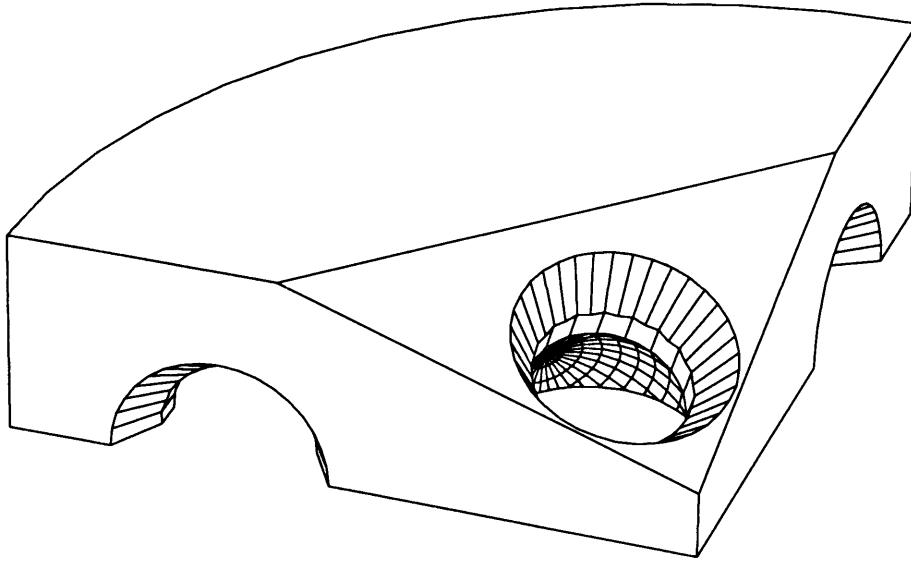


Figure B-2: Joint 'B' Top Section Upright (Oblique View).

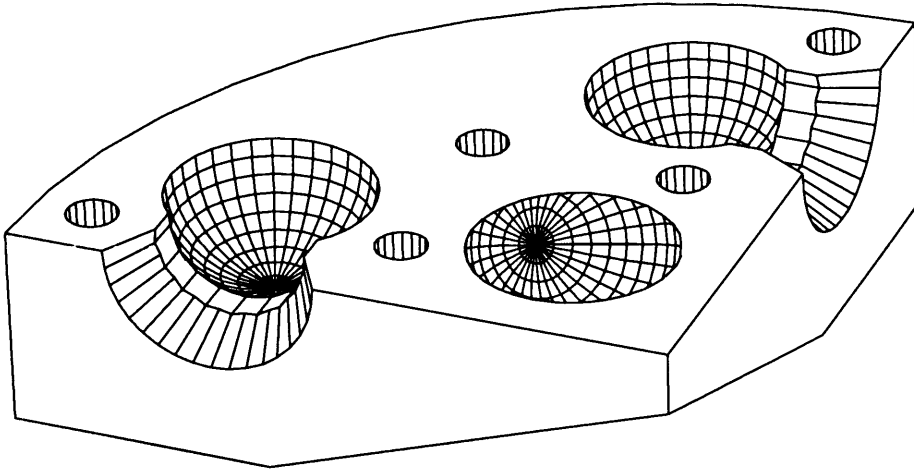
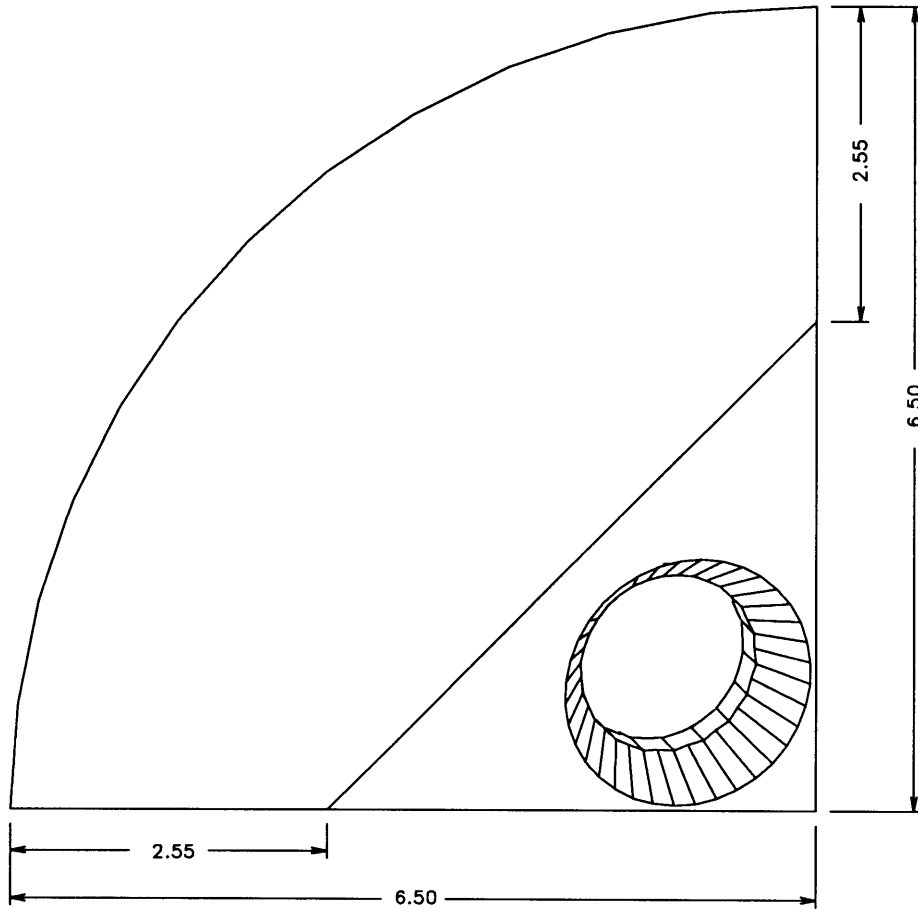
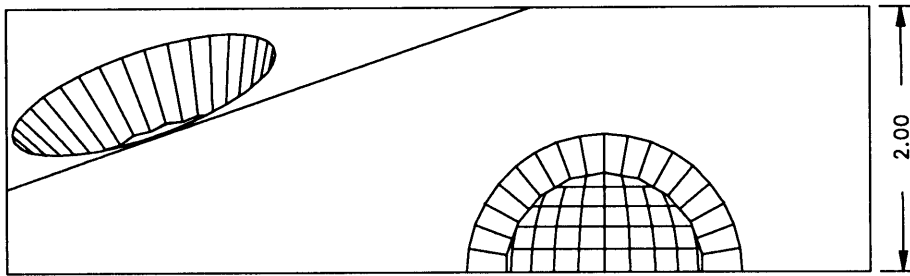


Figure B-3: Joint 'B' Top Section Inverted (Oblique View).



(Dimensions in Centimeters)

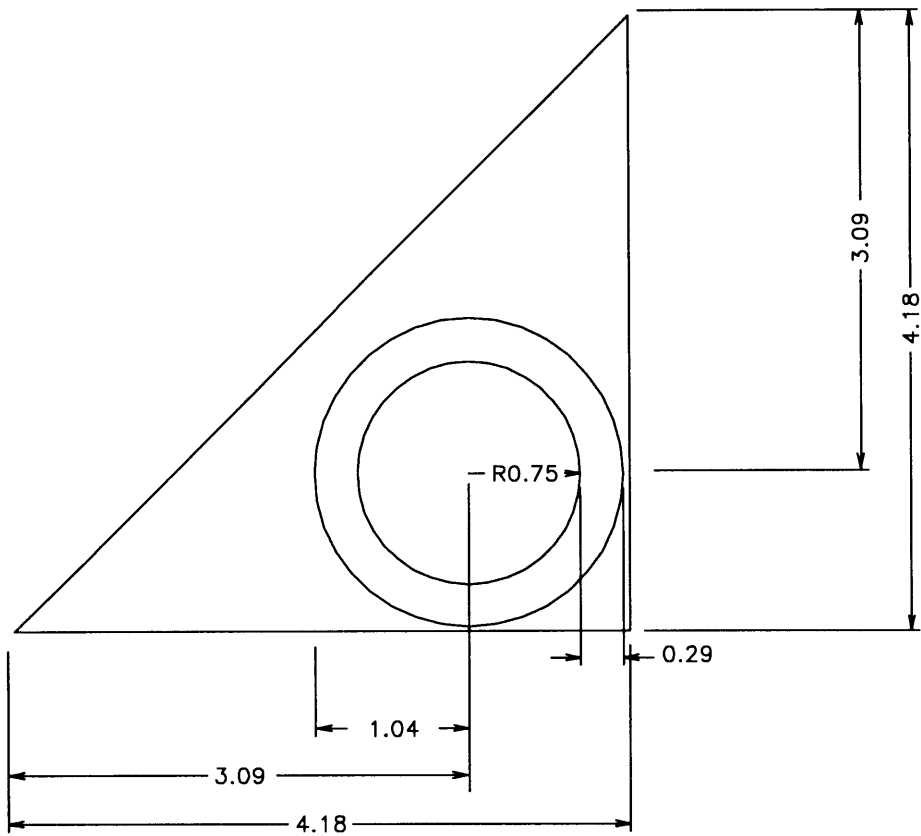
Figure B-4: Joint 'B' Top Section (Top View).



(Dimensions in Centimeters)

Figure B-5: Joint 'B' Top Section (Side View).





(Dimensions in Centimeters)

Figure B-6: Joint 'B' Top Section (Plane Cut View).

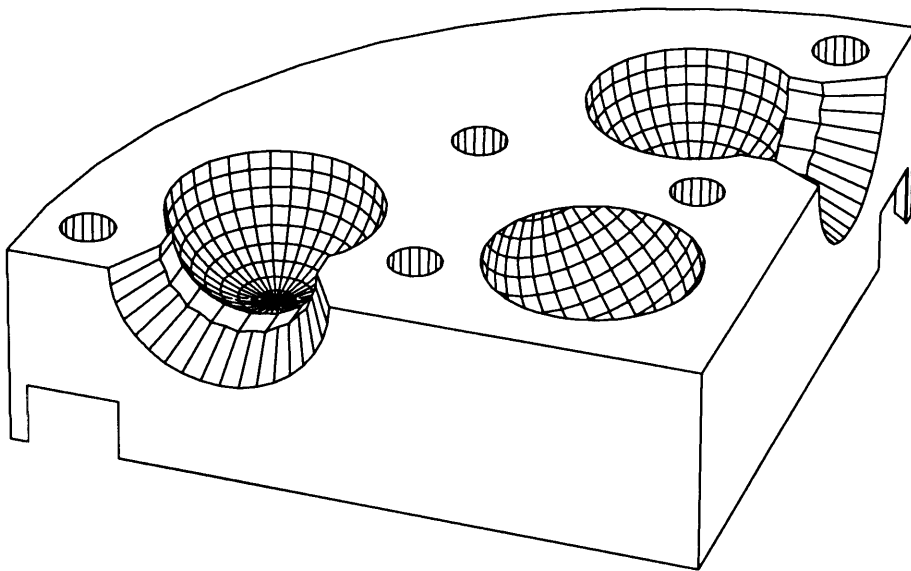
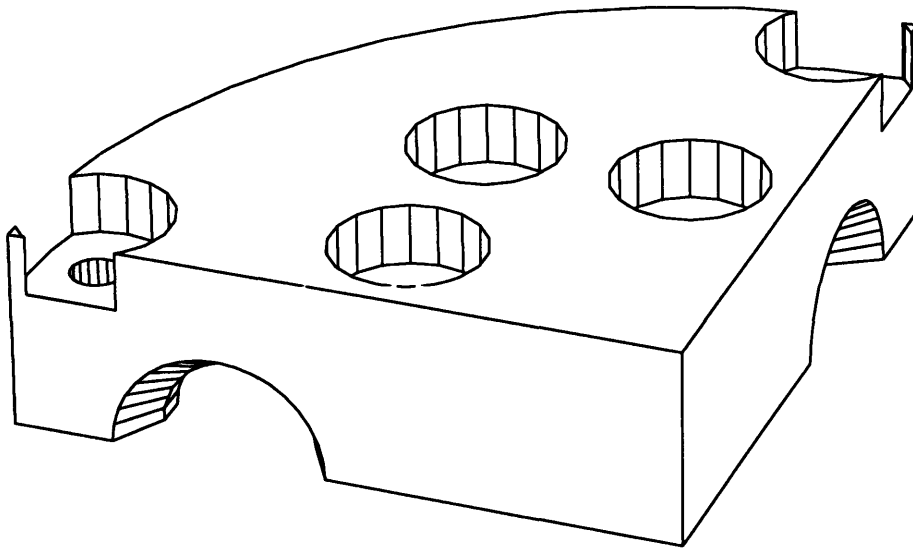
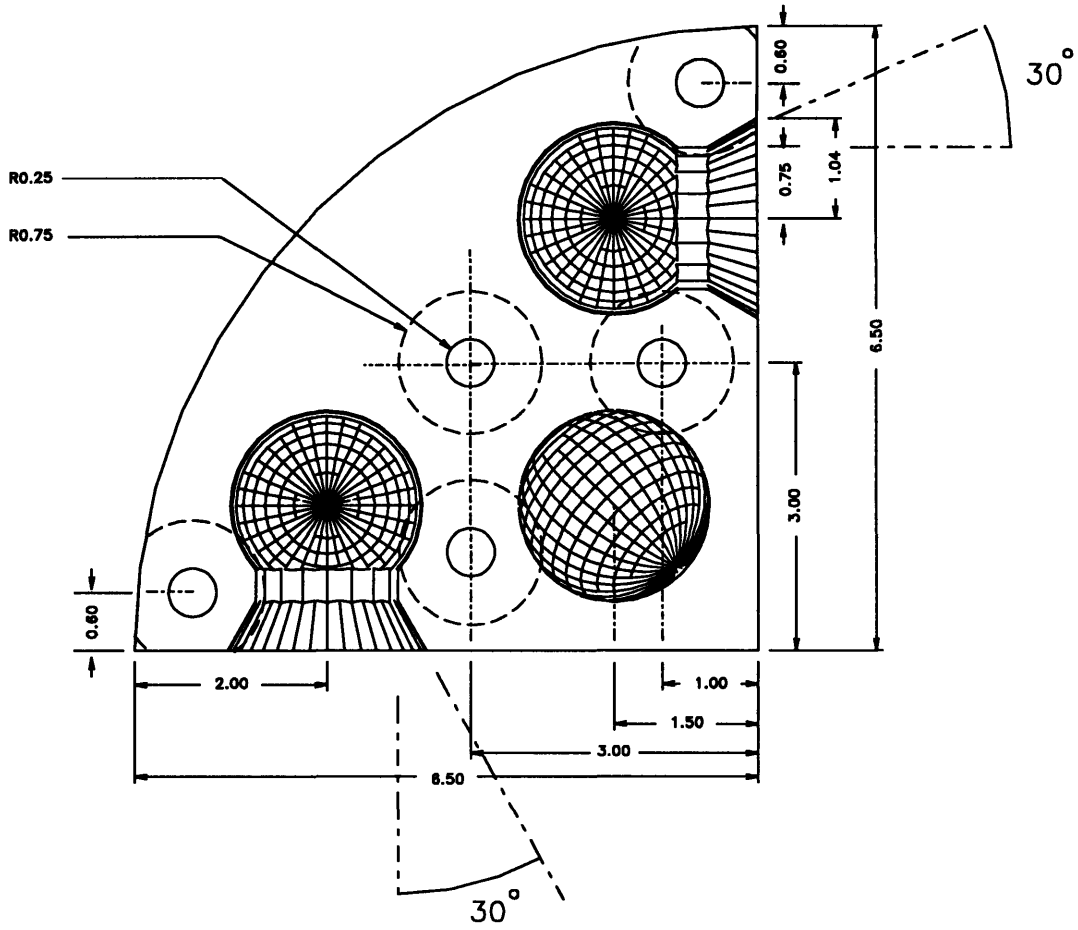


Figure B-7: Joint 'B' Bottom Section Upright (Oblique View).

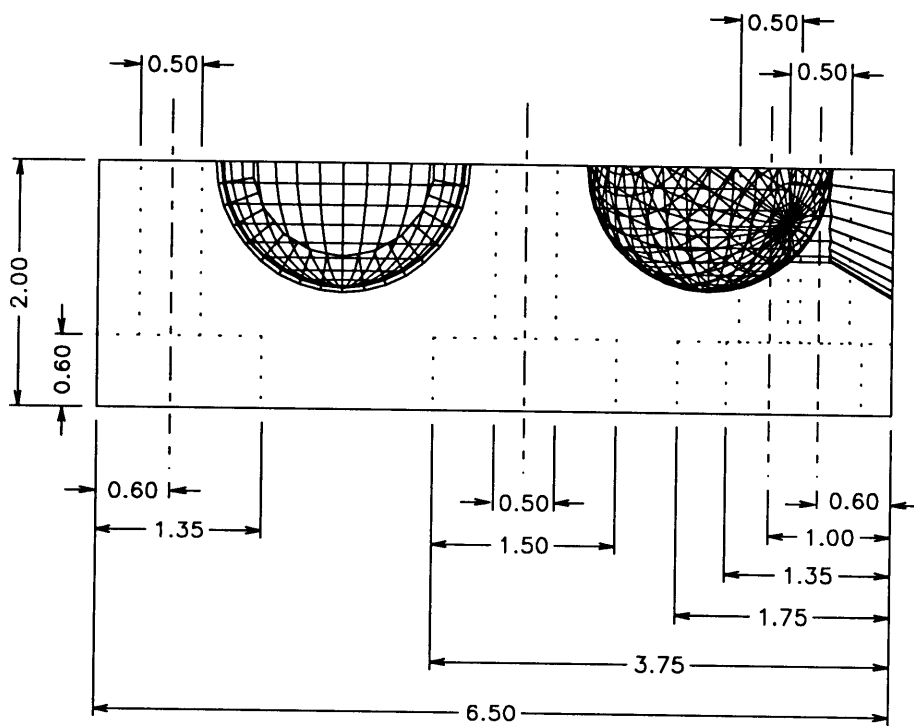


**Figure B-8: Joint 'B' Bottom Section Inverted (Oblique View).**



(Dimensions in Centimeters)

Figure B-9: Joint 'B' Bottom Section (Top View).



(Dimensions in Centimeters)

Figure B-10: Joint 'B' Bottom Section (Side View).

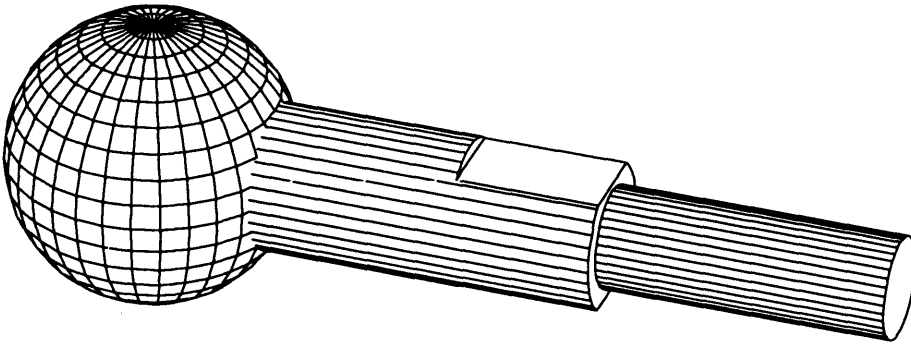
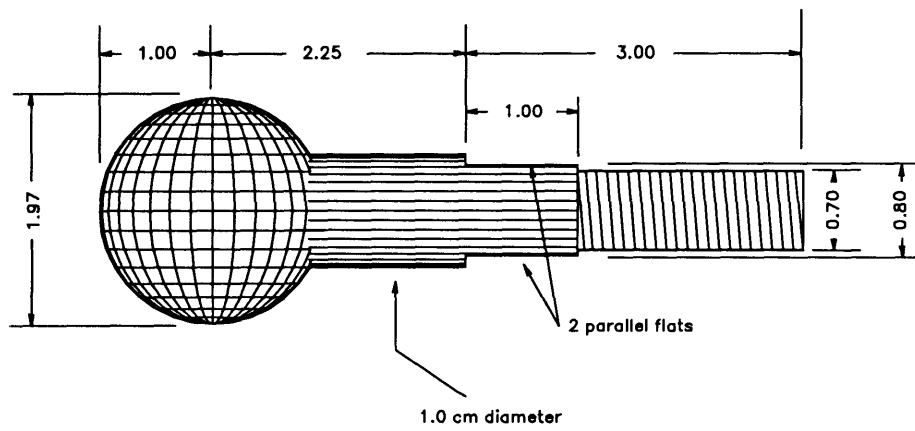
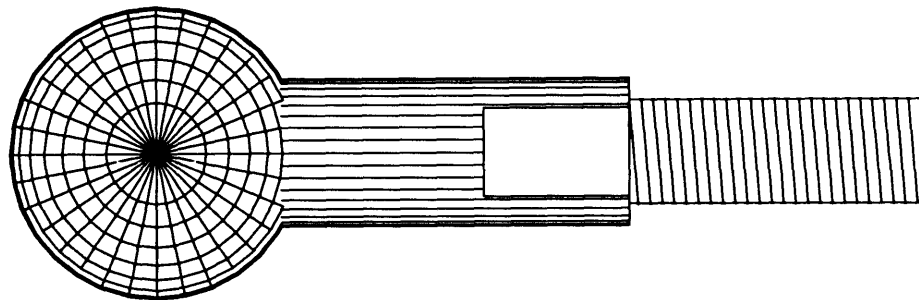


Figure B-11: Joint 'B' Spherical Male Leg (Oblique View).



(Dimensions in Centimeters)

Figure B-12: Joint 'B' Spherical Male Leg (Side View).



**Figure B-13: Joint 'B' Spherical Male Leg ( Top View).**



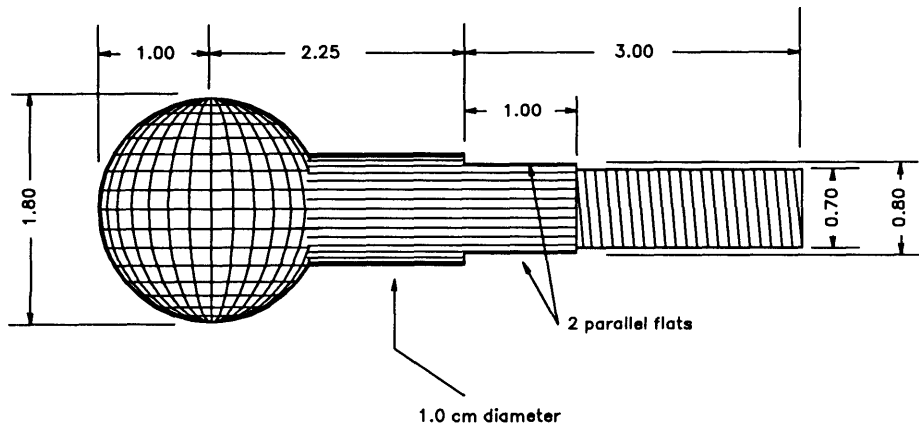
## **Appendix C**

### **Joint 'C' Design**

Joint 'C' is identical with respect to Joint 'B' with only three exceptions. First, the spherical male legs are machined to a diameter of 1.80 cm vice 1.97 cm. Second, the smaller diameter permits use of a visco-elastic interface of an approximate thickness of 1 mm. The material used for the visco-elastic interface is 'Plastic Dip Coating' which is very economical and commercially available. Third, the spherical recesses of the joint body are not coated with any material. In Joint 'B' both contact surfaces are coated with Teflon to obtain a surface possessing minimal friction. In the case of Joint 'C' only the male legs are coated.

The visco-elastic material was applied by dipping the male ends into the liquid coating. Once an appreciable thickness was achieved the joint body was used as a mold to create a uniform coating on the exterior surface. Without the use of the joint body to act as a mold it was not possible to achieve a uniform thickness around the male end. Several moldings are required because of the inherent shrinkage which occurs with each molding process. The diameter of the coating asymptotically approaches the diameter of the spherical recesses with each molding process.

Fig. C-1 illustrates the male spherical leg for Joint 'C'. All other dimensions of Joint 'C' are found in Appendix B.



(Dimensions in Centimeters)

Figure C-1: Joint 'C' Spherical Male Leg (Side View).

# Appendix D

## Matlab Code

*Typical M-file for calculating scattering matrix transmission functions..*

```
%b14.m: Rigid Joint Transmission Function Flexural
%(Leg 2 y-direction) Transmission Function (dB)
%vs. Frequency Log-scale depicting average, max,
%and min for 10 samples.
clear
load yleg1 %time gate matlab file for leg 1 (excitation leg)
load yleg2 %time gate matlab file for leg2 and leg3 (response legs)
load j11c11 %joint 1 (joint 'A', longitudinal excitation, test number 1 channel 11 test data
load j11c12
load j11c8
load j11c10
a=(j11c11-j11c12)/2; %output waveform calculation
a1=yleg2.*a; %timegated output waveform
a2=fft(a1,8192);
a3=abs(a2);
z=(j11c8+j11c10)/2; %longitudinal excitation waveform
z1=yleg1.*z; %time gated excitation waveform
z2=fft(z1,8192);
z3=abs(z2);
x1=a3./z3; %transmission function calculation for test one

load j12c11
load j12c12
load j12c8
load j12c10
a=(j12c11-j12c12)/2;
a1=yleg2.*a;
a2=fft(a1,8192);
a3=abs(a2);
z=(j12c8+j12c10)/2;
z1=yleg1.*z;
z2=fft(z1,8192);
z3=abs(z2);
x2=a3./z3; %transmission function calculation for test two

load j13c11
load j13c12
load j13c8
load j13c10
a=(j13c11-j13c12)/2;
a1=yleg2.*a;
a2=fft(a1,8192);
a3=abs(a2);
```

```

z=(j113c8+j113c10)/2;
z1=yleg1.*z;
z2=fft(z1,8192);
z3=abs(z2);
x3=a3./z3; %transmission function calculation for test three

```

```

load j114c11
load j114c12
load j114c8
load j114c10
a=(j114c11-j114c12)/2;
a1=yleg2.*a;
a2=fft(a1,8192);
a3=abs(a2);
z=(j114c8+j114c10)/2;
z1=yleg1.*z;
z2=fft(z1,8192);
z3=abs(z2);
x4=a3./z3; %transmission function calculation for test four

```

```

load j115c11
load j115c12
load j115c8
load j115c10
a=(j115c11-j115c12)/2;
a1=yleg2.*a;
a2=fft(a1,8192);
a3=abs(a2);
z=(j115c8+j115c10)/2;
z1=yleg1.*z;
z2=fft(z1,8192);
z3=abs(z2);
x5=a3./z3; %transmission function calculation for test five

```

```

load j116c11
load j116c12
load j116c8
load j116c10
a=(j116c11-j116c12)/2;
a1=yleg2.*a;
a2=fft(a1,8192);
a3=abs(a2);
z=(j116c8+j116c10)/2;
z1=yleg1.*z;
z2=fft(z1,8192);
z3=abs(z2);
x6=a3./z3; %transmission function calculation for test six

```

```

load j117c11
load j117c12
load j117c8
load j117c10
a=(j117c11-j117c12)/2;
a1=yleg2.*a;

```

```

a2=fft(a1,8192);
a3=abs(a2);
z=(j117c8+j117c10)/2;
z1=yleg1.*z;
z2=fft(z1,8192);
z3=abs(z2);
x7=a3./z3; %transmission function calculation for test seven

```

```

load j118c11
load j118c12
load j118c8
load j118c10
a=(j118c11-j118c12)/2;
a1=yleg2.*a;
a2=fft(a1,8192);
a3=abs(a2);
z=(j118c8+j118c10)/2;
z1=yleg1.*z;
z2=fft(z1,8192);
z3=abs(z2);
x8=a3./z3; %transmission function calculation for test eight

```

```

load j119c11
load j119c12
load j119c8
load j119c10
a=(j119c11-j119c12)/2;
a1=yleg2.*a;
a2=fft(a1,8192);
a3=abs(a2);
z=(j119c8+j119c10)/2;
z1=yleg1.*z;
z2=fft(z1,8192);
z3=abs(z2);
x9=a3./z3; %transmission function calculation for test nine

```

```

load j1110c11
load j1110c12
load j1110c8
load j1110c10
a=(j1110c11-j1110c12)/2;
a1=yleg2.*a;
a2=fft(a1,8192);
a3=abs(a2);
z=(j1110c8+j1110c10)/2;
z1=yleg1.*z;
z2=fft(z1,8192);
z3=abs(z2);
x10=a3./z3; %transmission function calculation for test ten
matr=[x1,x2,x3,x4,x5,x6,x7,x8,x9,x10]';
b14max=max(matr)';
b14min=min(matr)';
b14a=(x1+x2+x3+x4+x5+x6+x7+x8+x9+x10)/10;

```

*Typical M-file: Calculation of Transmission Functions c14 and c24 (Figure 6-1)*  
 %c14c24.m: Rigid Joint Transmission Function Flexural (Leg 3 y-direction  
 %and x-direction), Transmission Function (dB) vs. Frequency Log-Scale  
 %depicting average, max, and min for 10 samples.

```
clear
load c:\labwork\j1\c14a
load c:\labwork\j1\c14min
load c:\labwork\j1\c14max

load c:\labwork\j1\c24a
load c:\labwork\j1\c24min
load c:\labwork\j1\c24max

f= 65536*(0:4095)/8192;

c14b=20*log10(c14a);
c14maxa=20*log10(c14max);
c14mina=20*log10(c14min);

c24b=20*log10(c24a);
c24maxa=20*log10(c24max);
c24mina=20*log10(c24min);

y=8.77*10^(-4)*sqrt(2*pi*f); %aPredicted Function Calculation
t=(5*y+8*(y.^2))./(2+6*y+9*(y.^2));
t1=20*log10(t);

subplot(2,1,1), plot(f,c14b(1:4096),'k.',f,c14maxa(1:4096),'k- -',f,c14mina(1:4096),'k- -',f,t1(1:4096),'k:')
title('Scattering Matrix Element c14')
ylabel('Transmission Function (dB)')
xlabel('Frequency (Hz)')

axis([0 15000 -80 10])
hold on
grid on

subplot(2,1,2), plot(f,c24b(1:4096),'k.',f,c24maxa(1:4096),'k- -',f,c24mina(1:4096),'k- -',f,t1(1:4096),'k:')
title('Scattering Matrix Element c24')
ylabel('Transmission Function (dB)')
xlabel('Frequency (Hz)')

axis([0 15000 -80 10])
hold on
grid on

gtext('Predicted')
gtext('Predicted')
```

```

Typical M-file: Calculation of Reciprocity Transmission Functions b41 and b42 (Figure 6-13)
%b41b42.m: Rigid Joint Reciprocal Transmission Function Longitudinal Wave (Leg 2)
%for given Flexural Wave (y-direction and x-direction), Transmission Function (dB) vs.
%Frequency Log-Scale depicting average, max, and min for 10 samples.
clear
load c:\labwork\j1\b14a
load c:\labwork\j1\b14min
load c:\labwork\j1\b14max

load c:\labwork\j1\b24a
load c:\labwork\j1\b24min
load c:\labwork\j1\b24max

f= 65536*(0:4095)/8192;

%Reciprocity calculation
w=2*pi*f;
w=w';
b14a=b14a(1:4096);
b14max=b14max(1:4096);
b14min=b14min(1:4096);
b24a=b24a(1:4096);
b24max=b24max(1:4096)';
b24min=b24min(1:4096)';

b14a=(8.77E-04)*sqrt(w).*b14a;
b14max=(8.77E-04)*sqrt(w).*b14max;
b14min=(8.77E-04)*sqrt(w).*b14min;
b24a=(8.77E-04)*sqrt(w).*b24a;
b24max=(8.77E-04)*sqrt(w).*b24max;
b24min=(8.77E-04)*sqrt(w).*b24min;

b14b=20*log10(b14a);
b14maxa=20*log10(b14max);
b14mina=20*log10(b14min);

b24b=20*log10(b24a);
b24maxa=20*log10(b24max);
b24mina=20*log10(b24min);

y=8.77*10^(-4)*sqrt(2*pi*f); %Predicted Transmission Function Calculation
t=(3.8*i*y+3.8*(y.^2)+1.298*i*(y.^2)+1.298*y)/(2.667*y+2.667*i*y+1.8*(y.^2)+1.8*i);
t1=abs(t);
t2=20*log10(t1);

subplot(2,1,1), plot(f,b14b(1:4096),'k',f,b14maxa(1:4096),'k- -',f,b14mina(1:4096),'k- -',f,t2(1:4096),'k:')
title('Scattering Matrix Element b41')
ylabel('Transmission Function (dB)')
xlabel('Frequency (Hz)')

axis([0 15000 -80 10])
hold on
grid on

```

```

subplot(2,1,2), plot(f,b24b(1:4096),'k-',f,b24maxa(1:4096),'k--',f,b24mina(1:4096),'k--',f,t2(1:4096),'k:')
title('Scattering Matrix Element b42')
ylabel('Transmission Function (dB)')
xlabel('Frequency (Hz)')

axis([0 15000 -80 10])
hold on
grid on

gtext('Predicted')
gtext('Predicted')

```

*M-file for Windowing Process for a typical incident longitudinal waveform (Figure 5-1)*

```

clear

load c:\labwork\j1\j111c24.mat
load c:\labwork\j1\j111c25.mat
w=(j111c24+j111c25)/2;

%window function
nn=5;
n=105;
for i=1:n
    a=840;
    b=840+(i-1);;
    c=pi/2:pi/(2*nn):pi;
    d=cos(c).*cos(c);
    e=length(c);
    f=pi:pi/(2*nn):3*pi/2;
    g=cos(f).*cos(f);
    h=length(f);
    y=zeros(8192,1);
    y(a:b)=ones(b-a+1,1);
    y(a:a+e-1)=d(1:e);
    y(b-h+1:b)=g(1:h);

    z=y.*w;

end
t=0:1.52588*10^(-5):0.125;
subplot(7,1,1), plot(w(840:1100))
xlabel('Data Points')
title('Rigid Joint Non-Windowed Longitudinal Wave (Leg 3)')
axis([0 350 -8000 8000])

subplot(7,1,3), plot(z(840:1100))
xlabel('Data Points')
title('Windowed Longitudinal Wave')
axis([0 350 -8000 8000])

subplot(7,1,5), plot(y(840:1100))

```



```
title('Largest Window')
xlabel('Data Points of Window')
axis([0 350 0 2])
```

# Appendix E

## Data Collection and Organization

### *Data Collection*

Two experimental approaches were taken in collecting data for all joints. These were taken as an attempt to determine the scattering matrix elements for incident flexural and longitudinal waves. Successful attempts were completed in generating pure longitudinal waves in Leg 1. Unsuccessful attempts were made in creating pure incident flexural waves.

Several reasons exist for the inability to generate pure incident flexural waves. The problem in generating pure flexural waves arose from the difficulty in striking Leg 1 in the y-direction without generating a significant component in the x-direction. Likewise, difficulty was encountered in the effort to generate pure flexural waves in the x-direction without forming a significant component in the y-direction. Torsional wave contamination also resulted from the flexural contamination.

Another significant issue which stifled efforts to determine the flexural scattering matrix elements was the lack of adequate damping treatment and the presence of significant noise caused by transverse sensitivity from the accelerometers. Ideally, striking Leg 1 with a flexural impulse exactly in the y-direction will create only a pure flexural wave in the y-direction. But, since a flexural wave (x-direction) and a torsional wave are also formed, these waves need to be dissipated so that only a pure flexural wave (y-direction) is incident at the joint. In the case of the flexural wave there is no known damping treatment that is able to dissipate the orthogonal flexural wave and the torsional wave. The contamination by these waves, the transverse sensitivity (inability to accurately measure the extent of contamination) and the lack of adequate damping treatment prevented accurate assessment of the flexural scattering matrix elements.

This is not the case for the longitudinal impulse for which significant dissipation occurs for all wave types other than the longitudinal wave. For these experiments, Leg 1 was excited at the end, 7 feet from the location of the accelerometers on that leg.

Damping treatment was applied to five feet of Leg 1; the damping treatment started 6 inches from the end of the leg and continued to 1.5 feet below the position of the accelerometers. 1/8" thick neoprene was wrapped in a helical fashion along the length. Then, 3/16" diameter stainless steel balls were glued to the layer of neoprene. The density of the balls increased along the length of neoprene in a step-wise manner. The density began at 5 balls per inch for 10 inches and increased at a rate of 5 balls per inch for each 10 inch segment. The final placement consisted of 30 balls per inch for the last 10 inch segment. The 5 foot section was then wrapped, in a helical fashion, with 1/8" thick neoprene. This length of damping treatment offered significant dissipation of all wave types except the longitudinal wave.

#### *Data Organization*

Fig. E-1 illustrates the position, lead orientation and channel numbering of the accelerometers used for data collection of each leg. Of equal importance, Tables E.1 through E.3 prescribe the formulae used for deriving the acceleration for each wave type. This information is intended to facilitate further research by the acoustics group at MIT.

The data collected in the experimentation is maintained by the acoustics group at MIT. The data is organized in two broad categories: one for longitudinal impulse tests and one for flexural impulse tests (*y*-direction only). Ten impulse tests were taken for flexural excitation and ten impulse tests were taken for longitudinal excitation. The filenames permit quick determination of: the joint being tested, the type of impulse excitation, the test number, and the channel number. For example, filename 'j314c21.mat' (Matlab file) means that the data is: Joint 3 ('C'), longitudinal test #4, channel 21. Similarly, the filename 'j2a8c16.mat' means that the data is: Joint 2 ('B'), flexural test #8, channel 16. All data for the rigid joint (Joint 'A') is contained in files of the form 'j1xxxx.mat'.

Fig. E-1 does not depict Channels 1 and 9. Channel 1 is the impulse force channel and Channel 9 was not used.

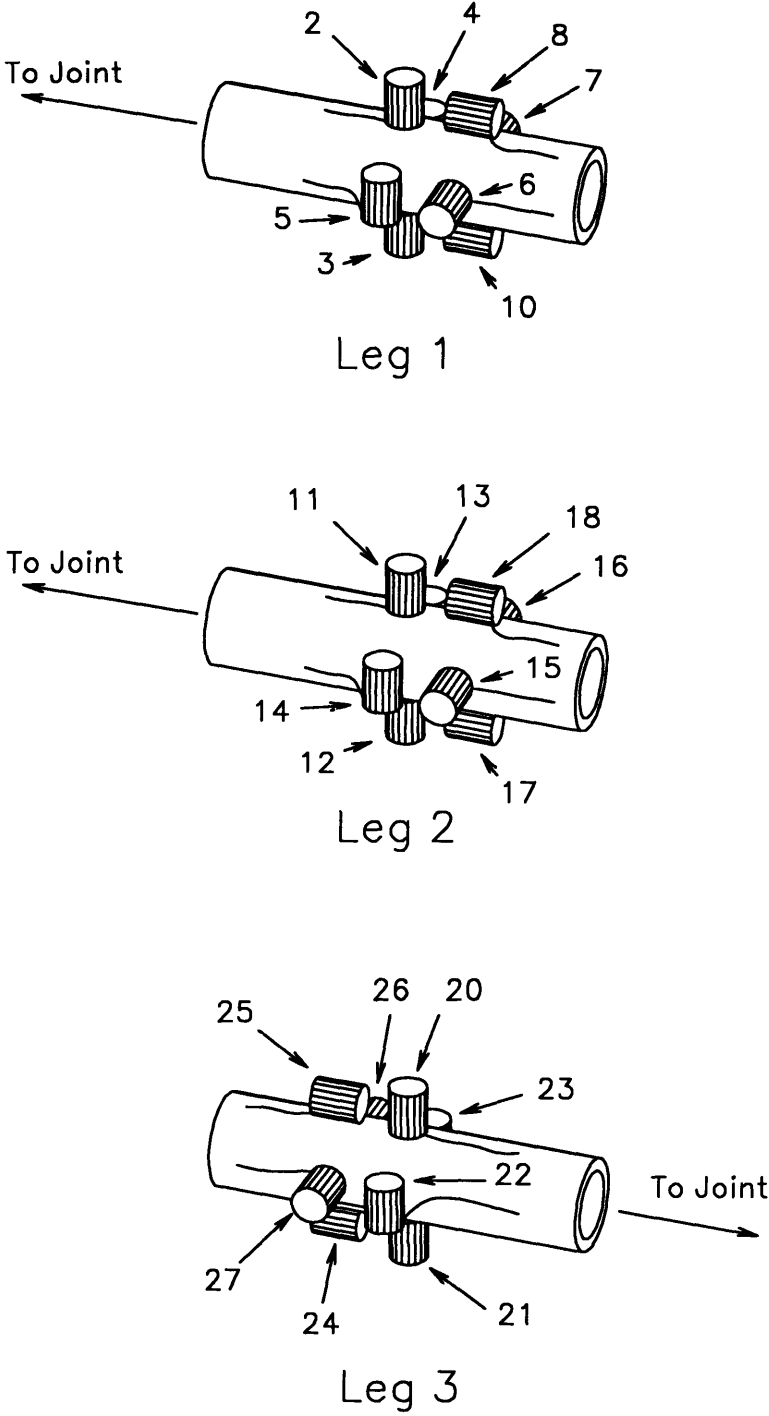


Figure E-1: Accelerometer position, lead orientation and channel numbering.

Table E.1: Leg 1 Wave Formulae

<b>Leg 1</b>	
Flexural (y-direction)	(Ch.2 - Ch.3)/2
Flexural (x-direction)	(Ch.6 - Ch.7)/2
Torsional	(Ch.4 - Ch.5)/2
Longitudinal	(Ch.8 + Ch.10)/2

Table E.2: Leg 2 Wave Formulae

<b>Leg 2</b>	
Flexural (y-direction)	(Ch.11 - Ch.12)/2
Flexural (x-direction)	(Ch.15 - Ch.16)/2
Torsional	(Ch.13 - Ch.14)/2
Longitudinal	(Ch.17 + Ch.18)/2

Table E.3: Leg 3 Wave Formulae

<b>Leg 3</b>	
Flexural (y-direction)	(Ch.20 - Ch.21)/2
Flexural (x-direction)	(Ch.26 - Ch.27)/2
Torsional	(Ch.22 - Ch.23)/2
Longitudinal	(Ch.24 + Ch.25)/2

## Bibliography

- [1] Duncan, Francis. 1990. Rickover and the Nuclear Navy. Annapolis, Maryland: Naval Institute Press.
- [2] Branthonne, Denis. 1994. Influence of Dynamic Absorbers on a Three Dimensional Truss. S.M. Thesis. Massachusetts Institute of Technology.
- [3] Guo, Yueping. 1993. Effects of Structural Joints on Sound Scattering. J. Acoustic Society of Am., 93(2) 857-863.
- [4] Cremer, Heckl, Ungar. 1988. Structure-Borne Sound, Second Edition. Springer-Verlag.
- [5] Lyon, Richard H. 1987. Machinery Noise and Diagnostics. Butterworth-Heinemann, Boston.
- [6] Rosenhouse, Ertel, and Mechel. 1981. Theoretical and Experimental Investigations of Structure-borne Sound Transmission through a T-Joint in a Finite System. J. Acoustic Society of Am., 70, 492-499.
- [7] Leung, R. C. N. and Pinnington, R. J. 1990. Wave Propagation through Right-Angled Joints with Compliance - Flexural Incidence Waves. J. Sound Vib. 142, 31-46.
- [8] Leung, R. C. N. and Pinnington, R. J. 1990. Wave Propagation through Right-Angled Joints with Compliance - Longitudinal Incidence Waves. J. Sound Vib. 142, 31-46.

- [9] Guo, Yueping. 1994. Diffraction of Flexural Waves at Structural Joints. J. Acoustic Society of Am., 95:1426-1434.
- [10] Guo, Yueping. 1995. Flexural Wave Transmission Through Angled Structural Joints. J. Acoustic Society of Am., 97(1):289-287.
- [11] Arciszewski, T. 1985. Spherical Joint in Space Structures. Patent Application. Wayne State University. Detroit.
- [12] Shackson, S. 1986. Development Analysis - Spherical Joint for Space Structures. Report prepared for Wayne State University, Detroit.
- [13] Tzou, H. S. and Rong, Y. 1991. Contact Dynamics of a Spherical Joint and a Jointed Truss-Cell System. AIAA Journal. 29, 81-88.
- [14] Gutkowski, L. J. and Kinzel, G. L. 1992. A Coulomb Friction Model for Spherical Joints. Robotics, Spatial Mechanisms and Mechanical Systems, ASME. DE-Vol. 45, 243-249.
- [15] Uduma, Olowokere, Arciszewski. 1989. Survey of Existing Studies on the Strength and Deformation of Spherical Joints in Steel Space Structures. American Institute of Steel Construction, Third Quarter, 102-109.
- [16] Heath, Marcus R. A. 1994. Dynamic Behavior of a Three Dimensional Aluminum Truss in Free Space. S.M. Thesis. Massachusetts Institute of Technology.
- [17] Strang, Gilbert. 1986. Introduction to Applied Mathematics. Wellesley-Cambridge Press.